Aging alters chromatin accessibility and transcriptional regulation in murine liver tissue

Inaugural-Dissertation

zur

Erlangung des Doktorgrades

der Mathematisch-Naturwissenschaftlichen Fakultät

der Universität zu Köln

vorgelegt von

Mihaela Bozukova

aus Sofia, Bulgarien

Köln 2021

Teile dieser Arbeit wurden in folgender Publikation veröffentlicht. / Parts of this work were published in the following scientific article.

Bozukova, M., Nikopoulou, C., Kleinenkuhnen, N., Grbavac, D., Goetsch, K., Tessarz, P. (2022). Aging is associated with increased chromatin accessibility and reduced polymerase pausing in liver. Mol Syst Biol. 18: e11002. 10.15252/msb.202211002.

Gutachter:	Dr. Peter Tessarz
	Prof. Dr. Andreas Beyer
Prüfungsvorsitzender:	Prof. Dr. Jan Riemer

Tag der mündlichen Prüfung: 08. Dezember 2021

Acknowledgments

I am certain that I will remember my time at the MPI Age as one of the most formative and intellectually stimulating experiences of my life. I am grateful for having had the opportunity to meet and interact with such kind, supportive and talented colleagues and friends throughout my PhD.

To begin with, I would like to express my sincere gratitude to Dr. Peter Tessarz for his unyielding support and encouragement, for his trust in my abilities and for the scientific freedom to explore the fascinating world of computational biology.

I would like to thank my thesis committee, Prof. Dr. Andreas Beyer and Prof. Dr. Dario Valenzano, for their constructive feedback and encouragement. I would also like to thank Prof. Dr. Jan Riemer for agreeing to be on my thesis examination committee.

I am also thankful to all current and past members of the Tessarz lab for the support, helpful advice and for creating such a fun working environment. Special thanks to Dr. Chrysa Nikopoulou for starting my recruitment process well in advance at a Christmas market and for generously sharing her extensive knowledge and wisdom.

I would also like to thank Dr. Jorge Bouças, Dr. Franziska Metge and Dr. Theodore Georgomanolis. It was an honor to learn from these bioinformatics experts.

I am deeply thankful to Prof. Dr. Argyris Papantonis. His passion for both science and literature motivates me to follow my passion with the same dedication and enthusiasm.

I would like to thank the Cologne Graduate School of Ageing Research for the incredible opportunities, as well as funding. Special thanks to the CGA coordinators for their tremendous support. Thanks also to CGA classmates who were always a great source of fun and joy.

I owe special thanks to Dany, Dora, Tona and Steph for their friendship, support and encouragement that kept me going. Thanks also to Susanna and Luca for bringing joy in the form of delicious pasta and tiramisu.

I am grateful to my family for incenting me to strive towards my goals. My gratitude for their unconditional love and support can hardly be expressed in words.

All this would not have been possible without the sweeter half of Team B – a never-ending source of love, inspiration and motivation.

Abstract

Regulation of gene expression is tightly linked to the organization of the mammalian genome. With age, chromatin alterations occur on all levels of genome organization, accompanied by changes in gene expression profiles. However, little is known about the detailed changes in transcriptional regulation with age. Here, we systematically characterize age-related changes in the local chromatin landscape of murine liver tissue and their link to transcriptional regulation. To the best of our knowledge, this is the first systematic inventory of the connection between aging, chromatin accessibility and transcriptional regulation *in vivo*, in a whole tissue. We observe that aging of murine liver tissue is accompanied by an increase in chromatin accessibility at promoter regions of protein-coding genes. Yet, although promoter accessibility is a requirement for transcription, the increased accessibility did not result in enhanced transcriptional output. Instead, aging is accompanied by a decrease of promoter-proximal pausing of RNA polymerase II (Pol II). We propose that these changes in transcriptional regulation are due to a reduced stability of the pausing complex and may represent a mechanism to compensate for the age-related increase in chromatin accessibility in order to prevent aberrant transcription.

Table of Contents

List of figures

1. Introduction

Eukaryotic transcription is the first step in gene expression and represents a focal point for cellular regulation. The transcription process is precisely regulated and tightly controlled to ensure maintenance of cell identity, fidelity and responsiveness to external stimuli and a changing environment. Transcriptional regulation occurs at multiple levels, with two tightly interconnected processes that majorly shape the process: chromatin and its regulators on the one hand and the transcription apparatus and its regulators on the other hand.

1.1 The local chromatin landscape

In eukaryotes, the two-meter-long DNA molecule is sequentially folded and compacted to fit the confined cellular nucleus (Figure 1). The compaction of chromosomal DNA involves the coordinated interplay between DNA and various protein factors to yield the dynamic nucleoprotein complex called chromatin. The basic structural and functional unit of chromatin, the nucleosome, comprises 147 base pairs (bp) of DNA wrapped around a histone octamer in a spool-like manner (Luger et al., 1997). The histone octamer consists of two molecules of each H2A, H2B, H3 and H4 (Burlingame et al., 1985).

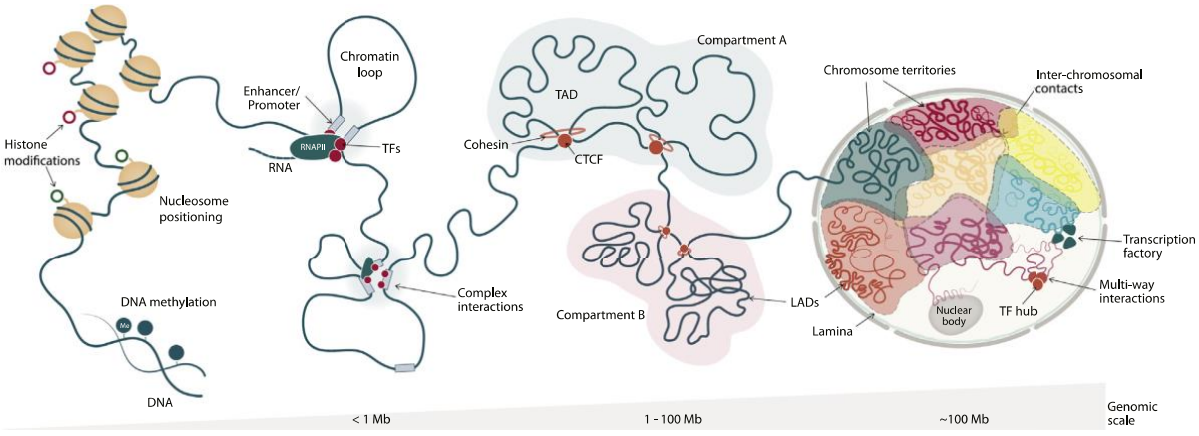

Figure 1. Levels of genome organization. DNA is sequentially compacted to fit the confined cellular nucleus. Figure retrieved without modifications from (Harabula and Pombo, 2021).

The histone tails are exposed on the surface of nucleosomes and are subject to a plethora of post-translational modifications that are involved in the recruitment of non-histone proteins to chromatin (Zhou et al., 2011). Many of these histone modifications are enriched over

regulatory elements in the genome and are associated with gene activation or repression. For example, trimethylation of H3K4 (H3K4me3) and H3K36 (H3K36me3) are highly enriched at the promoters and gene bodies of actively transcribed genes, respectively. H3K27ac and H3K4me1 are usually deposited at enhancer regions. Instead of directly regulating transcription, activating histone marks have been proposed to function as regulatory modules, which compete with and prevent the deposition of repressive histone marks (Zentner and Henikoff, 2013).

Thus, nucleosomes provide a lattice for the deposition of various epigenetic signals. However, nucleosomes are by no means static entities. The chromatin structure on nucleosomal level is regulated via assembly, complete or partial disassembly and repositioning of nucleosomes. For this, cells have evolved a wide variety of specialized ATP-dependent chromatin remodelers and chaperones. A collaboration between these is crucial for regulating nucleosome occupancy and stability and has a direct effect on the biological function of the DNA template, e.g. by preventing or enabling the recruitment of transcription factors.

1.2 Transcription

Transcription of protein-coding and many non-coding regions of the eukaryotic genome is carried out by RNA polymerase II (Pol II), which was isolated and characterized over 50 years ago (Roeder and Rutter, 1969). Pol II transcription follows a defined cycle of initiation, elongation and termination (Figure 2). Throughout this cycle, the coordinated binding and dissociation of various factors ensures tight regulation of the entire process. In the following, we will discuss our current understanding of transcriptional regulation by focusing on the initial stages of the transcription cycle (Figure 2).

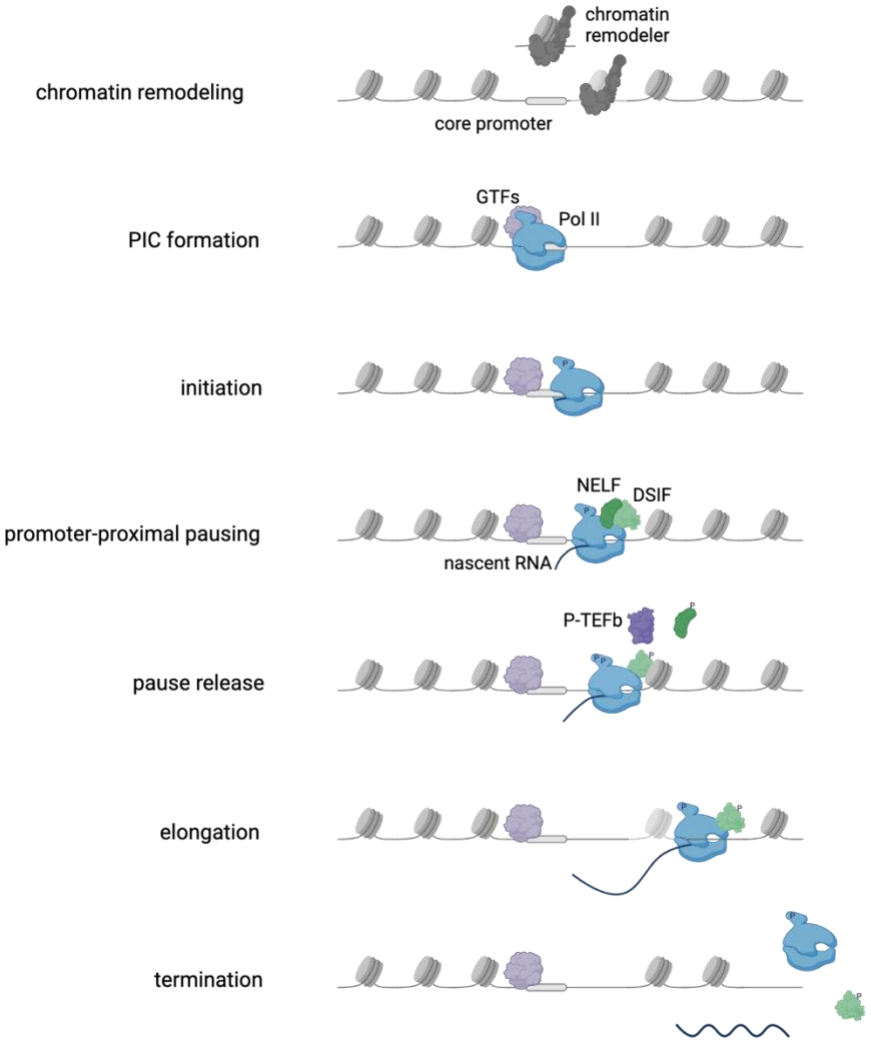

Figure 2. Pol II transcription cycle. Schematic of the main steps in the Pol II transcription cycle: initiation, elongation and termination. Phosphorylation is shown as “P”. Figure created with Biorender and inspired by (Core and Adelman, 2019).

1.2.1 Promoter accessibility

The local chromatin landscape directly impinges on transcription with nucleosomes creating physical barriers to Pol II and transcription factors. Thus, for transcription to initiate, the promoter region needs to be rendered accessible first (Figure 2). An “open” (i.e. accessible) promoter is the result of a dynamic and tightly regulated interplay between DNA sequence and ATP-dependent chromatin remodelers (Venkatesh and Workman, 2015). Poly(dA:dT) tracts in promoter regions intrinsically disfavor nucleosome formation due to their structural rigidity (Kaplan et al., 2009), resulting in the formation of nucleosome-depleted regions (NDRs). These NDRs are maintained by chromatin remodelers that displace nucleosomes away from

the region, selectively creating an NDR that is flanked by two strongly positioned nucleosomes – the +1 and -1 nucleosome (the numbering is with respect to the NDR) (Kubik et al., 2018). This localized chromatin accessibility at promoter regions is a pre-requisite for transcription and the size of the nucleosome-free region positively correlates with TF binding and subsequent gene activation (Scruggs et al., 2015).

1.2.2 Transcription initiation

Pol II is recruited to the accessible promoter region through the concerted action of general transcription factors (GTFs), resulting in the sequential formation of the preinitiation complex (PIC) (Figure 2). In the first step of PIC assembly, the GTF TFIID recognizes and binds to core promoter elements (Nogales et al., 2017). Subsequent binding of TFIIA and TFIIB (Buratowski et al., 1989) results in the recruitment of Pol II in complex with TFIIF to the promoter (Muhlbacher et al., 2014). TFIIF stimulates TFIIH binding, whose helicase subunit XPB unwinds the DNA duplex, resulting in the formation of the transcription bubble (Holstege et al., 1996). In the PIC, Pol II is bound to the promoter, but has not yet initiated RNA synthesis. Promoter escape and nascent RNA synthesis are triggered by the phosphorylation of Ser5 and Ser7 of the C-terminal domain (CTD) of Pol II by the CDK7 kinase domain of TFIIH (Wong et al., 2014).

1.2.3 Promoter-proximal pausing

After elongating 20-60 nt, Pol II stalls (Figure 2). The first *in vivo* evidence of this promoter-proximal Pol II pausing emerged from nuclear run-on experiments at the β-globin locus in mature hen erythrocytes (Gariglio et al., 1981). A similar accumulation of Pol II at the 5' end of genes was later observed on mammalian c-myc (Bentley and Groudine, 1986), the HIV long terminal repeat (Kao et al., 1987) and uninduced Drosophila heat shock protein (Hsp) genes (Gilmour and Lis, 1986; Rougvie and Lis, 1988). Two decades later, genome-wide studies demonstrated that promoter-proximal pausing, which until then had been observed only at a handful of loci, was a ubiquitous step in the transcription cycle of Drosophila and mammalian genes (Core et al., 2008; Muse et al., 2007; Zeitlinger et al., 2007). The appreciation or promoter-proximal Pol II pausing as an additional regulatory layer following transcription initiation caused a paradigm shift in our understanding of transcriptional regulation.

Functions of promoter-proximal pausing

Promoter-proximal pausing might have a variety of functions for different classes of genes. Four common overarching functions have been proposed (Adelman and Lis, 2012) (Core and Adelman, 2019):

Maintenance of nucleosome-depleted regions around promoters. The promoter regions of uninduced *Hsp* genes in Drosophila are devoid of nucleosomes. On a genome-wide scale, highly paused genes have been observed to exhibit low nucleosome occupancy in the promoter region (Gilchrist et al., 2010). Removal of the pause-inducing factor NELF in Drosophila results in decreased pausing and increased nucleosome occupancy particularly at promoters that favor nucleosome assembly (Gilchrist *et al.*, 2010). This suggests that paused Pol II competes with nucleosomes at promoter regions to maintain a permissive chromatin structure. This function can explain the seemingly contradictory observation that ablation of NELF leads to a decrease rather than an increase in transcriptional output (Gilchrist *et al.*, 2010).

Rapid and synchronous gene activation. Paused Pol II is ready for rapid entry into productive elongation upon a stimulus. Thus, pausing allows for rapid gene activation by circumventing potentially stochastic steps during transcription initiation like the recruitment of GTFs. Furthermore, pausing allows for the synchronous and coordinated activation of genes, which is important for instance during early embryonic development in Drosophila (Zeitlinger *et al.*, 2007).

Integration of signals. In addition to initiation, pausing provides another regulatory layer for fine-tuning transcription. This allows for the integration of signals affecting recruitment and initiation with those regulating pausing and pause release.

Checkpoint for elongation and RNA processing. Pausing represents a kinetic window of opportunity facilitating proper coordination of nascent RNA synthesis and co-transcriptional processing.

Mechanism and main regulators of promoter-proximal pausing

Stable promoter-proximal Pol II pausing is facilitated by the binding of the pause-inducing factors NELF (negative elongation factor) and DSIF (DRB sensitivity-inducing factor) to Pol II (Figure 2) (Lee et al., 2008; Wada et al., 1998; Wu et al., 2003). Recent advances in structural biology have allowed a more comprehensive understanding of the mechanistic details of promoter-proximal Pol II pausing, thereby enhancing our understanding of gene regulation.

The eukaryotic DSIF complex, consisting of the two subunits SPT4 and SPT5, plays multiple roles during transcription. DSIF is globally required for productive transcription elongation (Shetty et al., 2017) and functions by enhancing the processivity of the Pol II elongation

complex (Fitz et al., 2018; Henriques et al., 2018). Specifically, SPT5 enhances processivity by binding to the DNA exit tunnel of Pol II, aiding in re-winding of upstream DNA and preventing backtracking of Pol II. Furthermore, SPT5 was very recently shown to play a central role in safeguarding Pol II by preventing the degradation of its major subunit RPB1 (Aoi et al., 2021).

Structural studies of a DSIF-Pol II elongation complex revealed that DSIF contacts all nucleic acid elements within the elongation complex – the non-template DNA in the transcription bubble, the upstream DNA and the nascent RNA (Bernecky et al., 2017). These close contacts are achieved via DNA and RNA clamps around the upstream DNA and exiting RNA, respectively (Bernecky *et al.*, 2017). The DNA clamp maintains a closed Pol II active-center cleft by restricting the non-template DNA strand in the transcription bubble and positioning upstream DNA. Thus, the DNA clamp ensures the stability and processivity of the elongation complex; DNA clamp opening is associated with Pol II pausing. The RNA clamp, on the other hand, maintains the nascent RNA in the Pol II exit tunnel, which is also important for the stability and processivity of the elongation complex. Of central importance for this function are several arginine residues in the RNA clamp, which, when methylated, decrease the affinity of DSIF for Pol II (Kwak et al., 2003). Mutations of these residues shifted the site of pausing in *in vitro* transcription assays using Drosophila nuclear extracts (Qiu and Gilmour, 2017). This emphasizes the central regulatory role of the RNA clamp in promoter-proximal pausing either by preventing or assisting in extrusion of the nascent RNA.

The second important player in establishing promoter-proximal pausing is NELF, which binds to the Pol II-SPT5 interface. Thus, NELF binding occurs after DSIF binding: DSIF binds around the DNA and nascent RNA, followed by NELF binding to the so-called Pol II funnel on the opposite side (Vos et al., 2018b). NELF stabilizes Pol II pausing in an allosteric manner through multiple potential mechanisms (Vos *et al.*, 2018b): NELF binding stabilizes the tilted state of the DNA-RNA hybrid in the active site of paused Pol II. Additionally, NELF contacts the Pol II funnel that leads to the active site, which blocks the entry of NTP substrates. Furthermore, NELF sterically inhibits binding of positive elongation factors, further stabilizing the paused state. Finally, NELF binding prevents TFIIS binding and reactivation of backtracked Pol II.

Importantly, DSIF and NELF binding requires the presence of the exiting RNA transcript (Missra and Gilmour, 2010). This is corroborated by the fact that multiple DSIF and NELF contacts on Pol II overlap with GTF binding sites, indicating that a paused Pol II state can be established only after promoter escape and dissociation of the GTFs (Bernecky *et al.*, 2017; Vos *et al.*, 2018b).

Pause release

The duration of pausing is dictated by the recruitment and activity of P-TEFb (positive transcription elongation factor b) (Figure 2) (Marshall and Price, 1995). P-TEFb is a heterodimer of cyclin T and CDK9 (cyclin-dependent kinase). CDK9 phosphorylates many proteins, including NELF, the DSIF subunit SPT5 as well as Ser2 of the CTD of Pol II. SPT5 phosphorylation transforms DSIF from an inhibitory to a stimulating elongation factor (Bernecky *et al.*, 2017) and triggers the dissociation of NELF (Figure 2). This causes a Pol II conformation change from the tilted DNA-RNA hybrid characteristic for paused Pol II towards an active conformation that allows addition of new NTPs to the nascent RNA chain (Vos et al., 2018a).

1.2.4 Transcription elongation

Following pause release, a multitude of elongation factors and histone chaperones are recruited to the Pol II elongation complex facilitating nucleosome passage and productive elongation (Farnung et al., 2018). Dissociation of the pausing factor NELF frees a binding site for the PAF (polymerase associated factor) complex (Vos *et al.*, 2018a), which binds and travels with elongating Pol II. PAF allosterically stimulates Pol II (Vos et al., 2020) and further functions as a recruitment platform for histone modifying enzymes and chaperones. PAF is required for H2B monoubiquitination at lysine 120 (H2BK120). This histone modification, together with the histone chaperones SPT6 and FACT (facilitates chromatin transcription), aids in Pol II transcription through nucleosomes (Pavri et al., 2006).

SPT6 and FACT facilitate the disassembly and reassembly of nucleosomes as Pol II passes through, thereby maintaining the chromatin landscape during transcription elongation. In yeast, depletion of these transcription-coupled histone chaperones leads to histone loss and mislocalization of histone modifications (Jeronimo et al., 2019). In contrast, knockdown of FACT in Drosophila S2 cells (Tettey et al., 2019) and acute depletion of SPT6 in mammalian cells (Zumer et al., 2021) had little effect on global nucleosome occupancy. However, both FACT and SPT6 depletion in these systems exhibited a strong effect on the early stages of elongation: In Drosophila, FACT knockdown resulted in alterations in the +1 nucleosome (Ramachandran et al., 2017) and a decrease in promoter-proximal Pol II assessed by ChIP-nexus upon inhibiting transcription initiation (Tettey *et al.*, 2019). In mammalian cells, acute depletion of SPT6 led to an accumulation of Pol II at the +1 nucleosome (Zumer *et al.*, 2021). These findings highlight the central role of the histone chaperones FACT and SPT6 in overcoming the major Pol II barrier that is the +1 nucleosome. This is consistent with the emerging model, in which Pol II faces two barriers in early elongation: the promoter-proximal

pause site (1st barrier) and the +1 nucleosome (2nd barrier) (Aoi et al., 2020) (Zumer *et al.*, 2021).

1.3 Enhancer regions of the mammalian genome

In addition to the effects of local chromatin structure on transcription, long-range interactions between *cis*-regulatory elements (enhancers) and their target promoters are important for fine-tuning transcriptional programs. Enhancers are short DNA segments that regulate cell-type specific gene expression programs in response to internal and external cues. Enhancers serve as binding platforms for transcription factors and cofactors, thereby increasing the local concentration of the transcription machinery in the close proximity of the target promoters upon looping. A key study underpinning the tight structure-to-function relationship of the genome demonstrated that experimentally forced chromatin looping between the murine β-globin promoter and the respective enhancer results in the expression of the β-globin gene (Deng et al., 2012). More specifically, transcription factors or cofactors recruited by enhancers interact with the transcription machinery at promoters, affecting either PIC formation and initiation (Figure 3A) (Eychenne et al., 2016) or pause release (Figure 3B) (Boija et al., 2017; Chen et al., 2017).

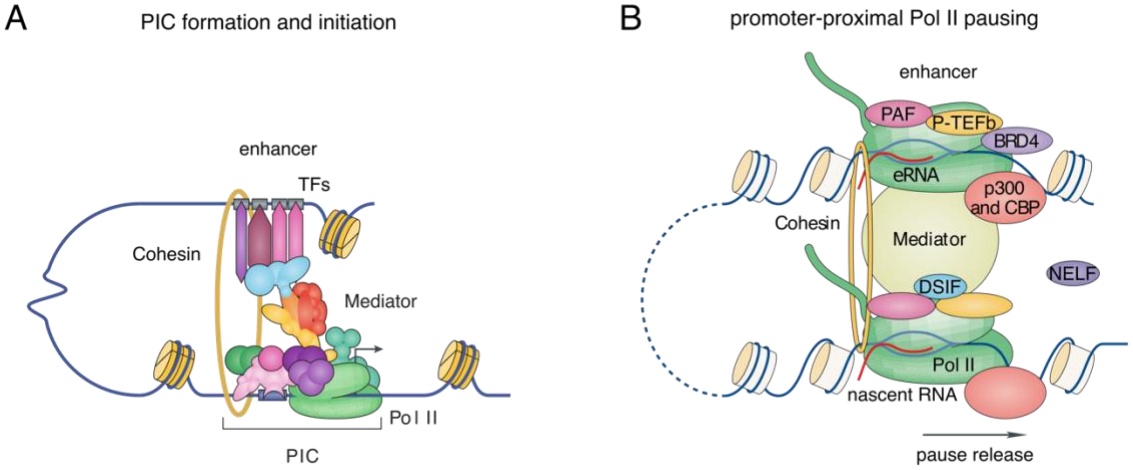

Figure 3. Regulation of transcription by enhancers. Transcription factors and cofactors are recruited to enhancers and interact with the transcription machinery at promoters upon enhancer-promoter looping. This impacts either PIC formation and transcription initiation (A) or promoter-proximal Pol II pausing and pause release (B). Figures A and B adapted from (Soutourina, 2018) and (Chen et al., 2018), respectively.

Additionally, enhancers may regulate their target genes through transcripts produced from the enhancer regions themselves. A surprising discovery revealed that enhancer transcription is widespread (De Santa et al., 2010; Kim et al., 2010) and positively correlates with enhancer activity and the expression level of the target gene (Andersson et al., 2014; Henriques *et al.*, 2018). Thus, enhancer transcription does not appear as a byproduct of random Pol II activity, but is rather a hallmark of active enhancers. Initially, the process of enhancer transcription itself was suggested to be important for enhancer function by creating a permissive chromatin landscape (Kaikkonen et al., 2013; Mousavi et al., 2013). These studies observed that enhancer transcription, but not the enhancer RNA (eRNA), was required for enhancer function. However, emerging evidence places eRNAs more centrally in transcriptional regulation of target genes. Several potential mechanisms of action have been suggested, which are not mutually exclusive and can be grouped into two major categories (Figure 4).

Altering the chromatin landscape. Most eRNAs are chromatin-associated and not free in the nucleoplasm and may, therefore, exert their function through interacting with chromatin-associated proteins. Indeed, eRNA knockdown resulted in decreased chromatin accessibility of the respective enhancer regions (Mousavi *et al.*, 2013; Tsai et al., 2018), suggesting a role of eRNAs in creating or maintaining permissive chromatin. Supporting this idea, eRNAs were shown to increase H3K27ac at the respective enhancer and target promoter regions through direct interactions with the histone acetyltransferase CBP and p300 (Figure 4A) (Bose et al., 2017). H3K27 hyperacetylation in turn results in recruitment of BRD4, which can also directly interact with eRNAs themselves (Rahnamoun et al., 2018) (discussed below, Figure 4C). This feed-forward loop contributes to additional eRNA production and the maintenance of an active enhancer state. Furthermore, eRNAs have been implicated in stabilizing enhancer-promoter interactions (Figure 4B) (Kim et al., 2015; Li et al., 2013) by interacting with cohesin (Cajigas et al., 2018; Pezone et al., 2019; Tsai *et al.*, 2018) and the Mediator complex (Hsieh et al., 2014).

Regulating the transcriptional machinery. eRNAs possess the inherent ability to interact with the transcriptional machinery and chromatin regulators, thereby increasing the recruitment and occupancy of these factors at promoters and enhancing transcription (Mousavi *et al.*, 2013). It has been proposed that this occurs through “transcription factor trapping”, in which nascent RNA from both enhancers and promoters increases the affinity of transcription factors for DNA, thereby creating a transcription factor sink around sites of active transcription (Figure 4C) (Huang et al., 2018; Sigova et al., 2015; Spurlock et al., 2017). In addition to regulating Pol II recruitment, eRNAs have also been implicated in regulating promoter-proximal Pol II pausing through activation of P-TEFb and by acting as a decoy for

NELF (Figure 4D) (Gorbovytska et al., 2021; Schaukowitch et al., 2014; Shii et al., 2017; Zhao et al., 2016). This stimulates pause release and the transition of Pol II to productive elongation. The eRNA-NELF interaction is hypothesized to be mediated through enhancer-promoter looping, emphasizing the tight structure-to-function relationship of the genome (Gorbovytska *et al.*, 2021).

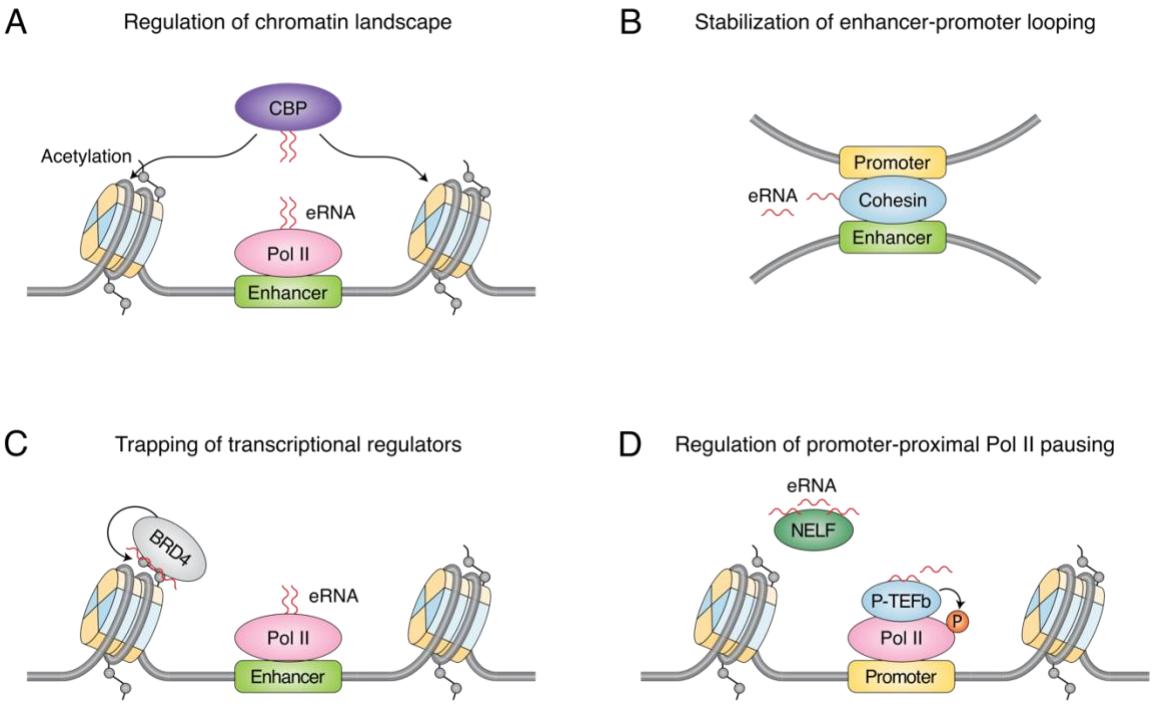

Figure 4. Role of eRNAs in transcriptional regulation. eRNAs can alter the chromatin landscape by interacting with chromatin modifying enzymes (A). Furthermore, eRNAs control gene expression by stabilizing enhancer-promoter loops (B) and by interacting with transcriptional regulators to increase their local concentrations (C). Additionally, eRNAs have been implicated in directly regulating promoter-proximal Pol II pausing by acting as a decoy for NELF and aiding in P-TEFb activation. Figure adapted from (Sartorelli and Lauberth, 2020).

1.4 Epigenetic hallmarks of aging

Aging, which is broadly defined as the time-dependent deterioration of physiological functions, is a multifaceted process driven by a complex network of factors. A growing body of evidence highlights the contribution of epigenetic alterations to the aging process (Booth and Brunet, 2016) and places epigenetic deregulation among the nine hallmarks of aging (Lopez-Otin et al., 2013). Importantly, aging is accompanied by epigenetic alterations on all levels of genome organization (Figure 5).

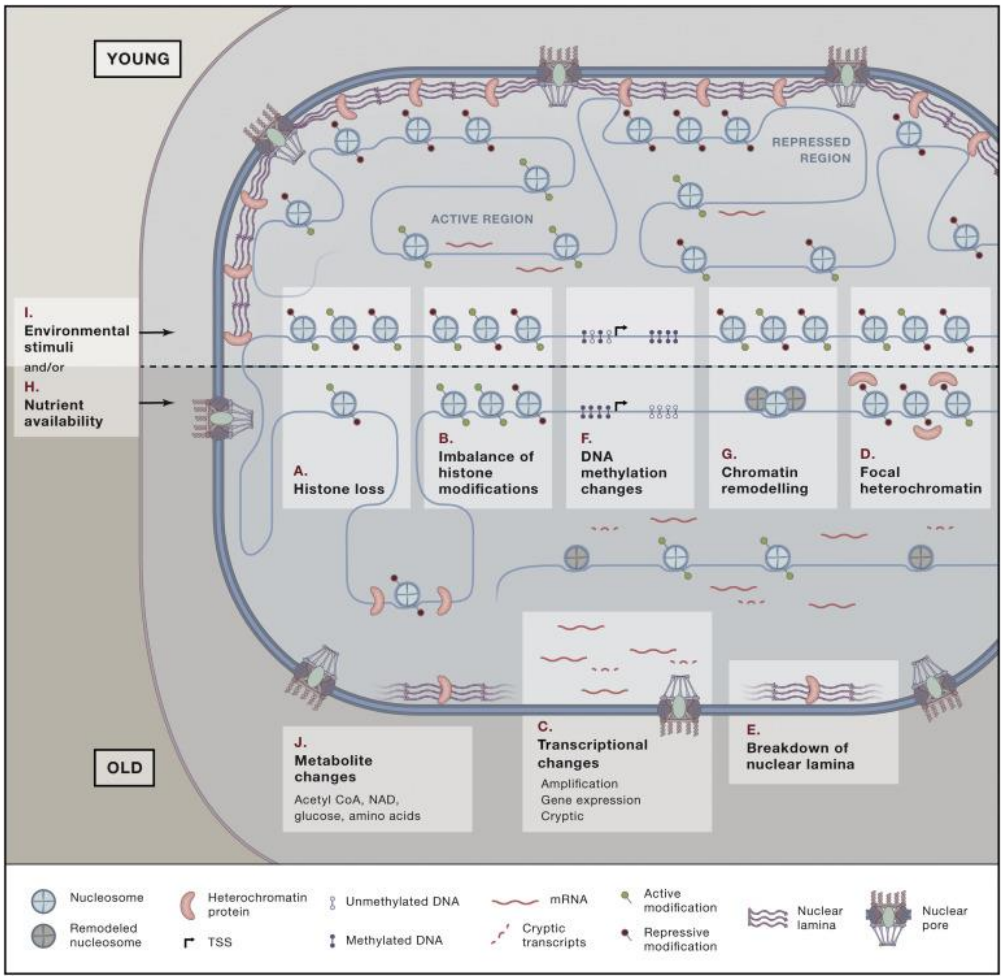

Figure 5. Epigenetic hallmarks of aging. Aging is accompanied by epigenetic alterations at all levels of genome organization. Figure retrieved without modifications from (Sen et al., 2016).

Altered DNA methylation patterns. The pattern of DNA methylation, which is generally associated with transcriptional silencing, is altered with age. In general, aging is accompanied by a global hypomethylation and a region-specific hypermethylation (Ciccarone et al., 2018; Cruickshanks et al., 2013). Rather than a programmed phenomenon, the changes are consistent with an (epigenetic) drift, in which DNA methylation levels progressively diverge due to increased rates of stochastic methylation changes across the genome during aging. Nonetheless, a number of GC sites exhibit reproducible methylation changes and provide the basis for epigenetic clocks that have been used to accurately predict biological age in a large number of tissues (Horvath, 2013).

Altered nucleosome occupancy. During replicative aging in yeast, histone expression is globally decreased (Feser et al., 2010), resulting in a global reduction of nucleosome occupancy by ~50 % and a global upregulation of transcription (Hu et al., 2014). Depletion of

histones has also been observed in senescent human fibroblasts (Ivanov et al., 2013; O'Sullivan et al., 2010) and quiescent skeletal muscle stem cells from aged mice (Liu et al., 2013). In contrast, no global loss of histones was observed in multiple murine tissues (heart, liver, cerebellum, olfactory bulb) (Chen et al., 2020). Instead, aging was accompanied by local changes of both increased and decreased nucleosome occupancy. Thus, in contrast to replicative aging in yeast or senescent mammalian cells, chronological aging in mammalian tissues does not seem to be accompanied by drastic changes in histone expression.

Accumulation of histone variants. Canonical histones are incorporated into chromatin in a DNA replication-dependent fashion. In contrast, histone variants are expressed throughout the cell cycle and can replace (canonical) histones in existing nucleosomes, thereby endowing chromatin with unique properties (Buschbeck and Hake, 2017). With age, canonical histones are gradually exchanged for histone variants. For example, aging is accompanied by increased deposition of macro H2A (mH2A) in murine liver and lung, as well as muscle of baboons (Kreiling et al., 2011). Deposition of the histone variant H3.3 also exhibits an age-related increase in several mouse somatic tissues such as liver, kidney, brain and heart (Tvardovskiy et al., 2017). In fact, by the age of 18 months, the canonical H3 isoforms were almost completely replaced by H3.3 (Tvardovskiy *et al.*, 2017). Furthermore, H2A.Z has recently been reported to accumulate in the hippocampus of aged mice (Stefanelli et al., 2018). Thus, the replacement of canonical histones with histone variants appears to be a common theme in aging.

Altered histone modifications patterns. Another epigenetic feature of aging is the alteration in post-translational modifications of histone proteins, which are crucial for regulating the accessibility and expression of the underlying genes.

H3K4me3. Replicative aging in yeast is accompanied by an increase in the activating mark H3K4me3 in both promoter and non-promoter regions of the genome, with the latter resulting in an increase in cryptic transcription (Cruz et al., 2018). A modest increase in H3K4me3 levels has also been observed in aged hematopoietic stem cells (Sun et al., 2014). In contrast, H3K4me3 is decreased in aged muscle satellite cells (Liu *et al.*, 2013). Thus, H3K4me3 appears to have different effects on lifespan in different organisms and cell types.

H3K36me3. In yeast and *C. elegans*, an age-related decrease in the activating H3K36me3 and a concomitant increase in cryptic transcription at a subset of genes has been reported (Sen et al., 2015). This has been confirmed by observations in Drosophila, where experimental reduction of H3K36me3 levels through methyltransferase inhibition resulted in reduced lifespan (Pu et al., 2015).

H3K27me3. In *C. elegans*, aging is accompanied by reduced levels of the repressive mark H3K27me3 and ectopically increasing it increases lifespan (Jin et al., 2011; Maures et al., 2011). In contrast, decreasing H3K27me3 levels by depleting components of the Polycomb repressive complex 2 (PRC2) homolog in Drosophila resulted in lifespan extension (Siebold et al., 2010). Consistent with this, an age-related increase in H3K27me3 levels has been reported for killifish brain tissues (Baumgart et al., 2014), quiescent mouse muscle stem cells (Liu *et al.*, 2013) and aging hematopoietic stem cells (Greer et al., 2010). Thus, H3K27me3 influences lifespan in higher organisms in a manner opposing that in worms.

Histone acetylation. Members of the sirtuin (SIRT) family of NAD^+-dependent deacetylases have been implicated in the regulation of lifespan in a variety of model organisms (Lee et al., 2019). In yeast, Sir2 levels decrease with age, which is accompanied by increased levels of H4K16ac and compromised silencing of subtelomeric regions (Dang et al., 2009). Consistent with this, *sir2* yeast mutants exhibited a shortened lifespan (Kaeberlein et al., 1999). In mammals, the chromatin-associated SIRT6 suppresses gene expression by deacetylating H3K9 in telomeric regions (Michishita et al., 2008). SIRT6 deficiency in mice caused a premature aging-like phenotype (Mostoslavsky et al., 2006), while SIRT6 overexpression increased lifespan of male mice (Kanfi et al., 2012). Thus, sirtuins may have a pro-longevity role by promoting increased genomic stability.

Overall, data from multiple model organisms provides compelling evidence that altered histone modification patterns contribute to the aging process. An imbalance of activating and repressive marks can cause changes in transcriptional programs. The exact effects, however, seem to be highly organism- and context-dependent.

Altered higher-order genome organization. The higher-order genome organization is also affected by aging. For instance, the global loss of histone proteins in yeast is manifested in a decreased nucleosome occupancy (Hu *et al.*, 2014), which contributes to a progressive, global loss of constitutive heterochromatin. This has been explained in the heterochromatin loss theory of aging as leading to genomic instability and aberrant gene expression profiles (Villeponteau, 1997). Besides the global loss of constitutive heterochromatin, senescent human fibroblasts exhibit local formation of heterochromatic regions, referred to as senescence-associated heterochromatic foci (SAHF) (Chandra et al., 2015; Chandra et al., 2012).

In general, aging is characterized by changes in DNA methylation, nucleosome occupancy, deposition of histone variants, histone modifications and higher-order genome organization. Often, the observed trends cannot be generalized but rather appear to be highly cell-type- and organism-specific.

1.5 Transcriptional signatures of aging

Considering the tight structure-to-function relationship of the genome, it is not surprising that the age-related epigenetic changes cause alterations in transcriptional programs (Figure 5). Studies in yeast and *C. elegans* have linked enhanced cryptic transcription to the age-related decrease of H3K36me3 (Sen *et al.*, 2015) and increase of H3K4me3 (Cruz *et al.*, 2018). Recently, an increase in cryptic transcription with age was also reported in aged mammalian stem cells (murine hematopoietic and neural stem cells, human mesenchymal stem cells) (McCauley et al., 2021). This was accompanied by a more permissive chromatin state characterized by decreased H3K36me3 and increased H3K4me1, H3K4me3 and H3K27ac levels.

The histone loss observed during yeast replicative aging is accompanied by a decrease in nucleosome occupancy and a global transcriptional upregulation of gene expression (Hu *et al.*, 2014). In contrast, studies in flies, mice or humans do not report a global deregulation of gene expression during aging, with only 2-4 % of genes showing age-related changes (Stegeman and Weake, 2017). Although these genes vary among different tissues and organisms, some common patterns have emerged. For example, inflammatory and stress response pathways are induced with age (Benayoun et al., 2019; Kimmel et al., 2019; Schaum et al., 2020). The enhanced expression of these genes has been proposed to serve a protective role in aging and is the defining hallmark of “inflammaging”, which refers to a low-level, chronic state of inflammation with age (Franceschi and Campisi, 2014). In contrast, genes, whose expression is downregulated with age, are functionally more heterogenous and include tissue-specific genes. In general, there is an age-related decrease in the expression of metabolic genes as well as genes involved in DNA repair and chromatin remodeling (Sun *et al.*, 2014). Interestingly, machine-learning analysis was able to predict transcriptional changes based on epigenomic changes (Benayoun *et al.*, 2019), underscoring the central link between chromatin structure and the regulation of gene expression. The latter is essential for almost all aspects of cellular function. This is illustrated by the fact that expression of a small set of transcription factors is sufficient to alter cellular fate by converting differentiated cells into pluripotent stem cells. Additionally, gene regulation acts as a control center of the cell, thereby coordinating and processing cytoplasmic and extracellular signals and orchestrating the appropriate response. Considering this central role of transcription regulation for cellular and organismal function, it is tempting to propose that epigenomic changes are among the first to occur during aging and that these changes consequently trigger the emergence of other hallmarks of aging (Booth and Brunet, 2016).

2. Research aims

Accumulating evidence in the extant literature has highlighted the contribution of epigenetic alterations to the aging process. The chromatin landscape plays a central role in the spatiotemporal regulation of gene expression by controlling the accessibility of the transcriptional machinery and its regulators to DNA. Considering the tight functional interrelationship between chromatin landscape and transcription, it appears logical that age-related chromatin changes are accompanied by changes in gene expression profiles. Importantly, however, a systematic investigation of the relationship between transcriptional regulation and age-dependent changes in the chromatin landscape is still lacking.

In this project, we set out to characterize age-related changes in the chromatin landscape and their link to transcriptional regulation on a global, organ-wide scale by addressing the following questions:

1. How does aging affect the local chromatin landscape?
2. How do age-related chromatin changes influence transcriptional output?
3. How does aging affect transcriptional regulation?

For this, we performed different next generation sequencing-based experiments with freshly isolated whole liver tissue from young (3-month-old), middle-aged (12-month-old) and aged (18-month-old) mice. Integration of these high-resolution data sets provides a genome-wide view of age-related changes in the chromatin and transcription landscape of murine liver tissue. The liver is a complex organ involved in central functions important for whole-body homeostasis. Hepatocytes comprise 70-80 % of the liver volume, making it a quite homogenous tissue.

To the best of our knowledge, this is the first global investigation of age-related changes in transcriptional regulation *in vivo*. Along with insights into age-related changes in gene expression and chromatin landscape, integration of these high-resolution datasets illuminates fundamental molecular principles of transcriptional regulation and their link with chromatin organization.

3. Results

3.1 A sizeable fraction of the genome undergoes age-related changes in accessibility

To investigate how genome accessibility changes on a local scale with age, we performed ATAC-seq using liver tissue from young (3-month-old) and aged (18-month-old) mice (Corces et al., 2017). ATAC-seq allows for investigating the local chromatin landscape by mapping accessible genomic sites on a genome-wide scale (Buenrostro et al., 2013). For each age group of young and aged mice, we performed three to four independent biological replicates. The resulting plots of read-length distributions displayed characteristic ATAC-seq features with a high density of short read fragments (< 100 bp) (Figure 6A). These short reads originate from nucleosome-free regions and the periodic fragment size distribution is indicative of nucleosome-bound fragments. The high quality of the ATAC-seq data was corroborated by the high alignment rates (> 97 %), whereby the majority of aligned reads passed the filtering criteria (53-64 %) (Figure 6B). We identified over 38,000 accessible regions (peaks) per sample (Figure 6C). The high peak numbers, representing regions of signal enrichment, further confirm the high quality of the ATAC-seq data. Additionally, we employed the Fraction of Reads in Peaks (FRiP) score as a quantitative measure of the signal-to-noise ratio (Figure 6D). Here, reads falling within peak regions indicate accessible chromatin, while reads outside peak regions represent background noise (Landt et al., 2012). All ATAC-seq samples passed the FRiP standard of 0.2 defined by the ENCODE project for ATAC-seq (Figure 6D) (ENCODE, 2021).

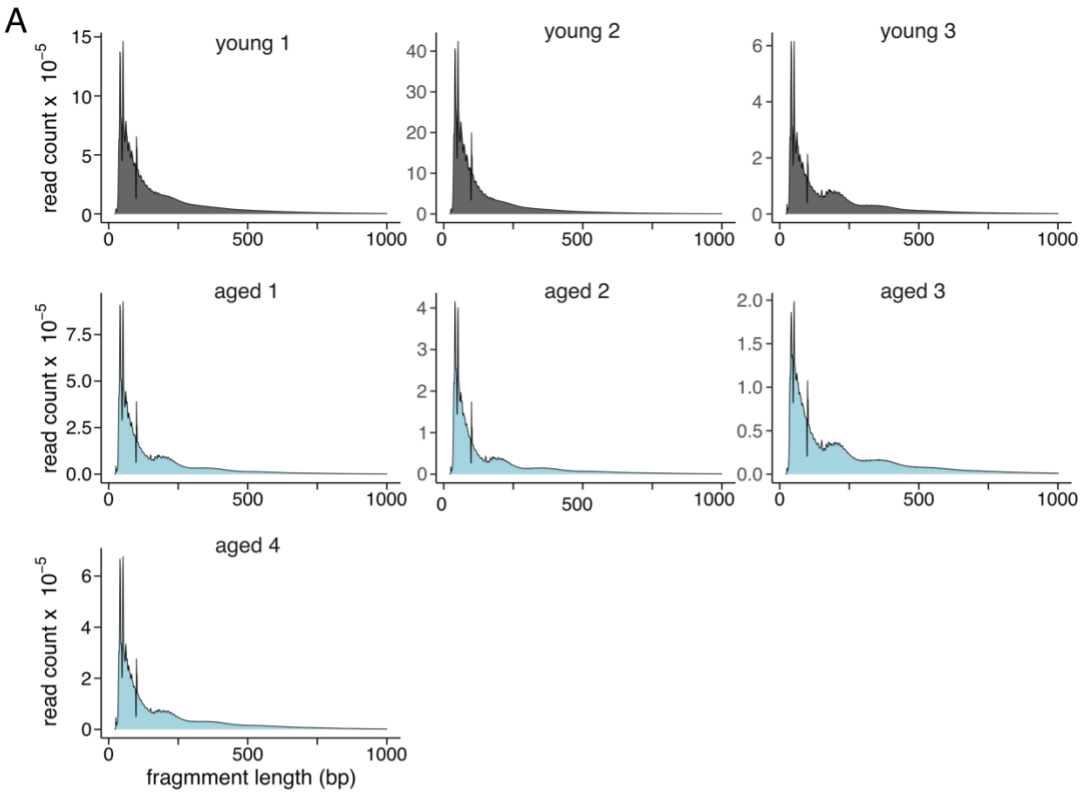
A
young 1
young 2
young 3
aged 1
aged 2
aged 3
aged 4
read count x 10^-5
fragmment length (bp)

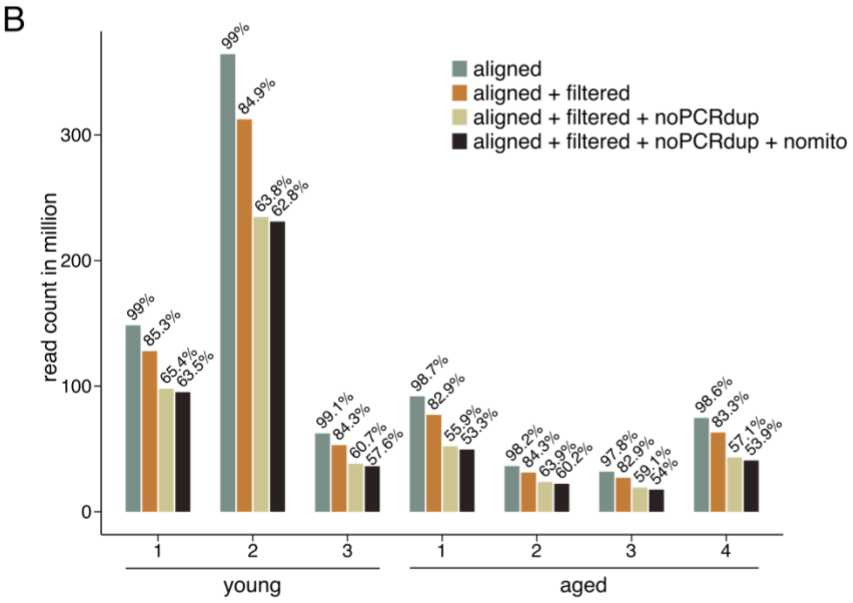
B
aligned
aligned + filtered
aligned + filtered + noPCRdup
aligned + filtered + noPCRdup + nomito
read count in million
young
aged

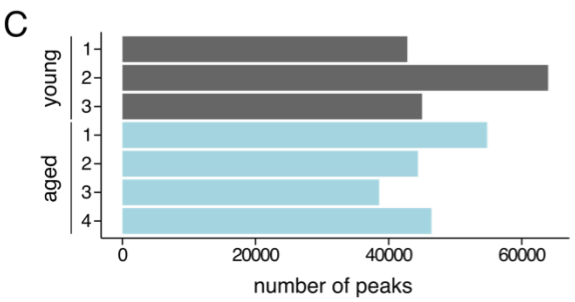
C
young
aged
number of peaks

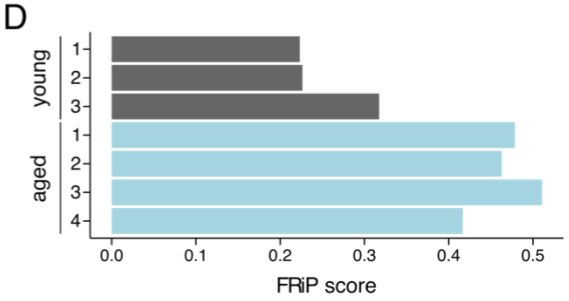
D
young
aged
FRiP score

Figure 6. (previous page) ATAC-seq libraries prepared from liver tissue of young and aged mice are of high quality. A. Fragment size distribution of reads passing filtering criteria for each ATAC-seq library. Each curve represents one biological replicate (n = 3 and 4 young and aged mice, respectively). B. Number of ATAC-seq reads successfully aligned and passing filtering criteria. Aligned reads were filtered for high quality (MAPQ > 10) and PCR duplicates and mitochondrial reads were removed. C. Number of peak regions identified in each ATAC-seq library. D. Signal-to-noise ratio assessed by the fraction of reads in peaks (FRiP).

As a first-level analysis to evaluate the similarity of our datasets, we performed principal component analysis (PCA) of the regions identified by ATAC-seq. PCA revealed that samples from the same age group (young or aged) formed two distinct clusters mostly distinguishable by the first two principal components, which explain more than 70 % of the variance in the data (Figure 7A). This analysis provided the first indication that in murine liver tissue the chromatin landscape is altered by age.

To further characterize the age-related changes in chromatin accessibility, we performed differential accessibility analysis. Notably, the accessibility of the majority of assessed genomic regions did not significantly change with age (Figure 7B). We found that 8.43 % of analyzed regions (4,691 out of 55,669) were differentially accessible with age (Figure 7B). Of these, 2,760 sites became more accessible, while for 1,931 sites the accessibility decreased with age. This slight trend towards an overall increased accessibility prompted us to further zoom into the differentially accessible sites by investigating their genomic location.

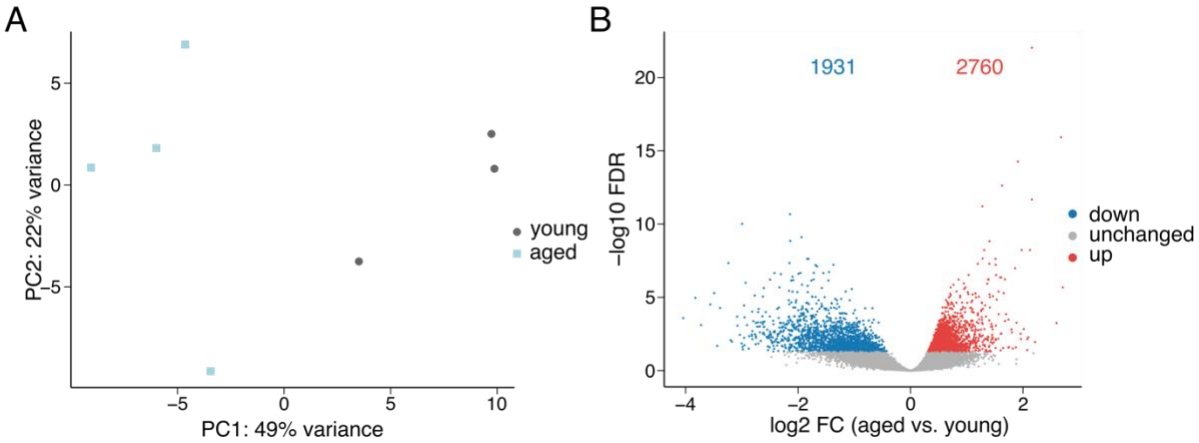

Figure 7. Chromatin accessibility exhibits age-related alterations. A. Principal component analysis of chromatin accessibility profiles. Rlog-normalized read counts (DESeq2) in consensus peak regions identified by ATAC-seq are depicted. Percentage of variance accounted for by each principal component is indicated. B. Volcano plot of differentially accessible genomic regions comparing liver tissue of aged relative to young mice (FDR < 0.05, Wald test). Increased accessibility: 2,760 regions (red), decreased accessibility: 1,931 regions (blue), regions with unchanged accessibility: 50,978 (grey).

3.2 Promoter regions are more accessible with age

To characterize the genomic locations of the differentially accessible sites, we annotated them in relation to the nearest genomic feature. We observed that the sites with increased accessibility in aged liver were on average closer to annotated TSSs compared to less accessible sites, suggesting an age-related increase in the accessibility of promoter regions (Figure 8A). Indeed, promoter regions and 5' UTRs became more accessible with age, while the accessibility of distal intergenic and genic sites decreased (Figure 8B). In fact, the majority of regions (63.4 %), for which we detected an increased accessibility, were located within annotated promoter regions (Figure 8C). In contrast, only 15.0 % of regions with decreased accessibility in aged animals overlapped promoter regions (Figure 8C). This age-related increase in chromatin accessibility at promoter regions was detectable both on a metagene (Figure 8D) and single-gene level (Figure 8E).

Gene ontology (GO) enrichment analysis revealed that genes with more accessible promoters in liver from aged animals were involved in metabolic processes such as amino acid and nucleoside metabolism (Figure 9A). Additionally, multiple genes with an age-related increase in promoter accessibility were involved in lysine acetylation (Figure 9A). Of note, histone acetylation at lysine residues directly affects chromatin structure by neutralizing the positive charge of the lysine side chain of histone tails. This charge neutralization weakens the contact between histones and DNA, resulting in a more open chromatin conformation (Gorisch et al., 2005). In contrast, genes with decreased promoter accessibility with age were associated with functions related to nucleosome assembly and organization (Figure 9B).

Overall, our ATAC-seq data reveal that a sizeable fraction of the murine genome undergoes age-related changes in chromatin accessibility. Importantly, the accessibility at promoter regions increases with age.

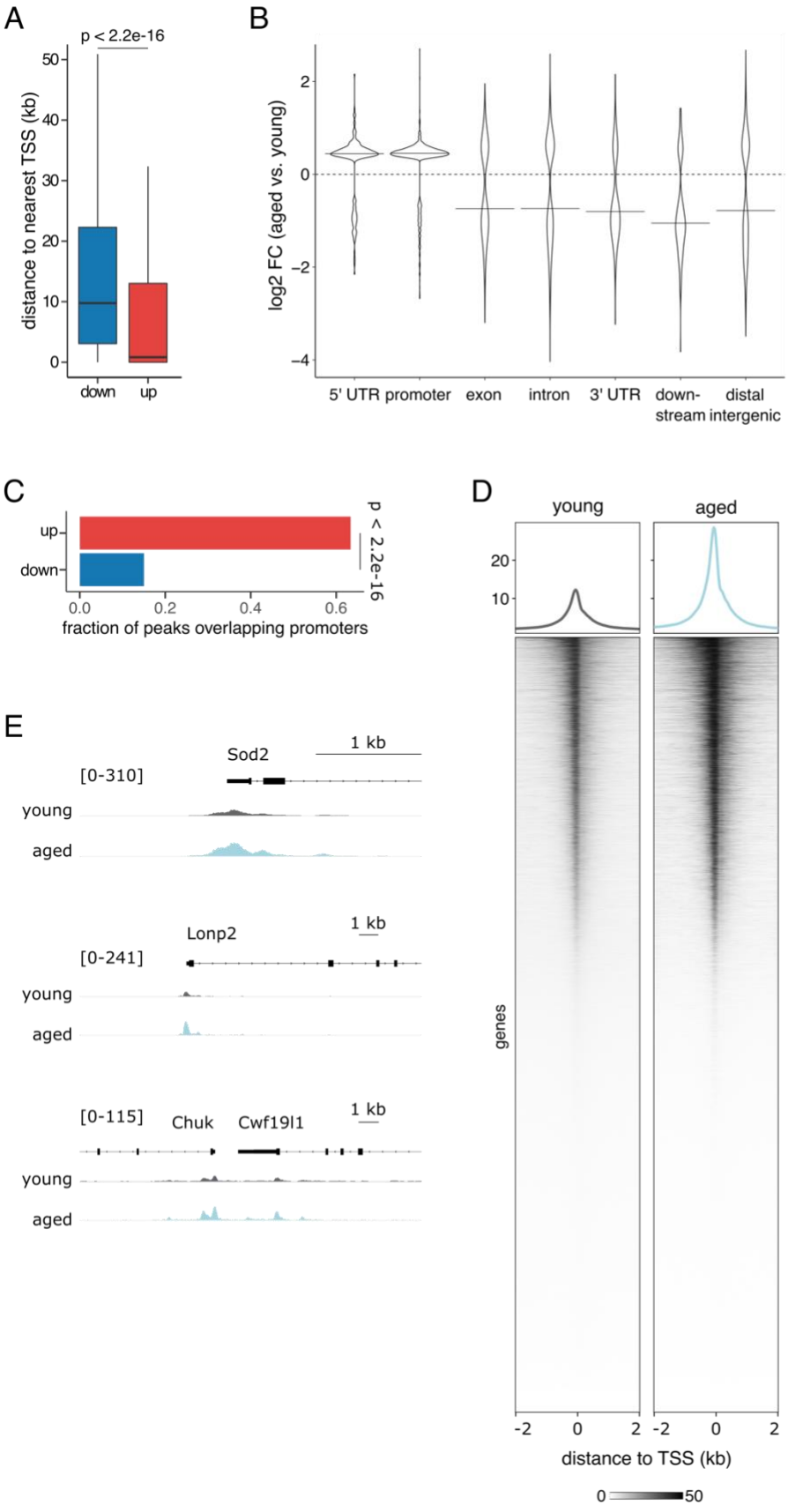
A
p < 2.2e-16
distance to nearest TSS (kb)
50
40
30
20
10
0
down
up
B
log2 FC (aged vs. young)
2
0
−2
−4
5' UTR
promoter
exon
intron
3' UTR
down-stream
distal intergenic
C
up
down
p < 2.2e-16
0.0
0.2
0.4
0.6
fraction of peaks overlapping promoters
D
young
aged
20
10
genes
-2
0
2
distance to TSS (kb)
0
50
E
Sod2
1 kb
[0-310]
young
aged
Lonp2
1 kb
[0-241]
young
aged
[0-115]
Chuk
Cwf19l1
1 kb
young
aged

Figure 8. (previous page) Chromatin accessibility at promoter regions increases with age in murine liver tissue. A. Distance of differentially accessible sites to the nearest annotated TSS. P-value was calculated using a two-sided Wilcoxon rank-sum test. B. Genomic locations of differentially accessible sites. Y-axis represents the log2-fold change (log2 FC) in accessibility in the liver of aged versus young animals. C. Proportion of differentially accessible sites overlapping promoters (defined as TSS $\pm$ 200 bp). P-value was calculated using a two-sided, two proportion z-test. D. Heatmap and average intensity profiles of promoter accessibility over all annotated TSSs in the mouse genome. Read densities of merged biological replicates were normalized to 1x coverage. E. Representative genome browser views of promoters with increased accessibility in aged mice. Peak intensity range is indicated in brackets. Reads from biological replicates were merged.

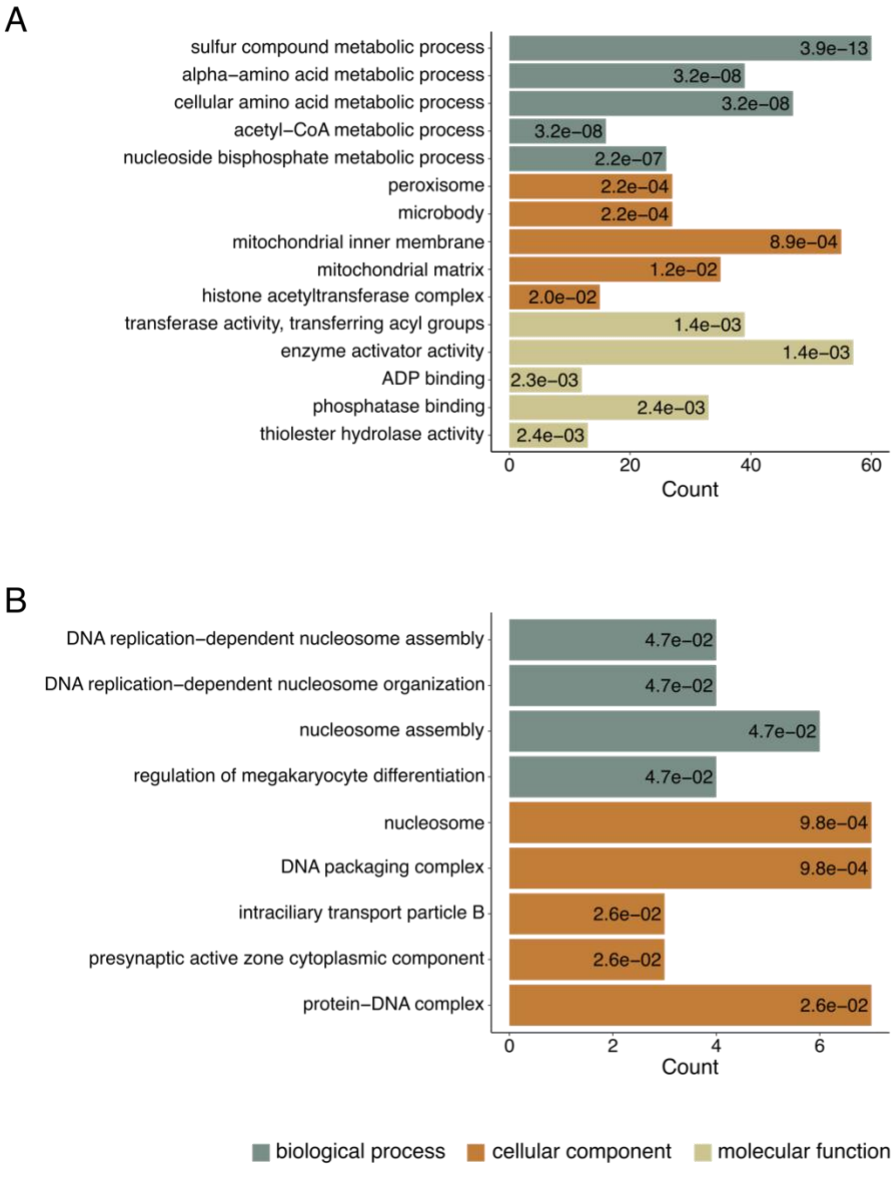

Figure 9. (previous page) GO term enrichment analysis of differentially accessible promoter regions. A, B. Enriched GO terms for genes with increased (A) and decreased (B) accessibility in the liver of aged mice. Only genes with a differentially accessible TSS were included in the analysis (n = 1,945 genes in total; 1,704 with increased and 241 with decreased promoter accessibility). Only the top five enriched GO terms ranked by adjusted p-value (Benjamini-Hochberg (BH) procedure, FDR < 0.05) are displayed. BH-adjusted p-values are reported for each GO term inside the respective bar.

3.3 Aging has a modest effect on transcriptional output

Given the central role of promoter accessibility for transcription, we next asked whether the observed age-related increase in promoter accessibility affects transcriptional output. For this, we assessed steady-state transcription using publicly available liver RNA-seq data from the Tabula Muris Senis Consortium (Schaum *et al.*, 2020). Here, we exploited the availability of gene expression data from multiple age groups and included, in addition to young and old (3- and 18-months of age, respectively), also middle-aged (12-month-old) mice. This enables a more detailed investigation into the temporal dynamics of gene expression changes with age. Gene expression patterns in aged liver were clearly distinct from those of young and middle-aged animals as observed by PCA (Figure 10A). Here, the first two principal components captured slightly more than 50 % of the sample variance (Figure 10A), which is lower than the variance explained by the two first components for chromatin accessibility (i.e. 73 %, Figure 7A).

Differential expression analysis revealed that the expression of the majority of genes did not significantly change with age (Figure 10B, C). We identified less than 500 differentially expressed genes in pairwise comparisons of middle-aged and aged relative to young mice. Thus, gene expression in the liver appears to be relatively resistant to aging. This is consistent with observations from single-cell RNA-seq data from the Tabula Muris Consortium (Tabula Muris, 2020), where aged liver hepatocytes exhibited no drastic changes in transcriptional programs in contrast to for instance immune and stem cells (Zhang et al., 2021).

To directly assess the effect of promoter accessibility on transcriptional output, we integrated the ATAC-seq with the RNA-seq data. Interestingly, the age-related increase in promoter accessibility is not directly reflected in increased transcriptional output (Figure 10D). Thus, an increase in promoter accessibility does not automatically yield an increase in steady-state transcription.

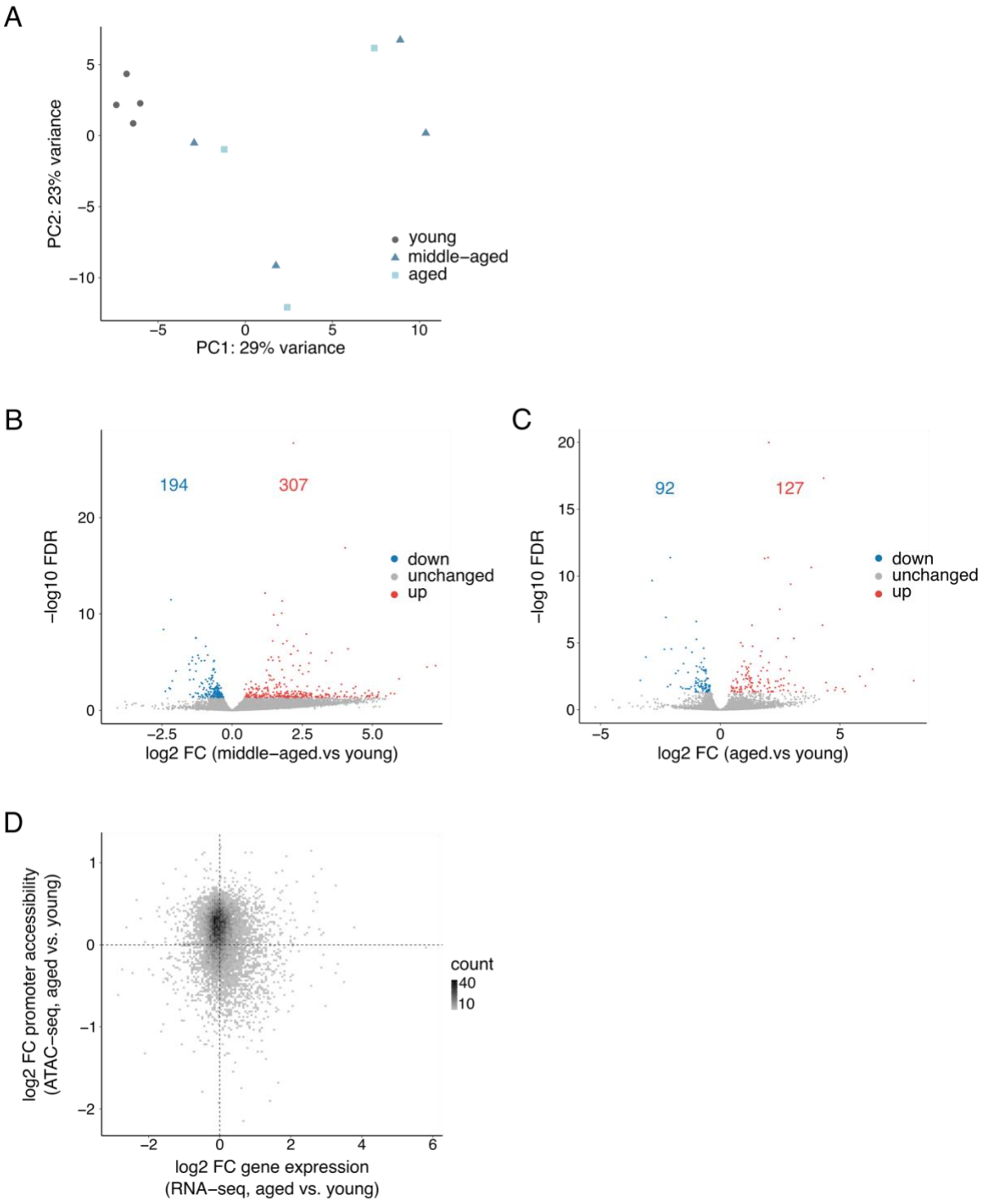

Figure 10. Modest changes in gene expression accompany liver aging. A. PCA scatter plot of gene expression profiles. Percentage of variance accounted for by each principal component is indicated. B. Volcano plot of differentially expressed genes comparing middle-aged relative to young animals (FDR < 0.05, Wald test). 307 genes were up-regulated (red) and 194 down-regulated (blue). C. Volcano plot of differentially expressed genes in the liver of aged versus young animals (FDR < 0.05, Wald test). 127 genes were up-regulated (red) and 92 down-regulated (blue). D. Scatter plot of the change in gene expression (RNA-seq) and promoter accessibility (ATAC-seq) in aged versus young mice. Promoter region defined as TSS +/- 200 bp.

3.4 Establishing tissue NET-seq to capture nascent transcription in murine liver tissue

Of note, standard RNA-seq measures steady-state mRNA levels, which are determined by both synthesis and degradation rates. To exclude the contribution of mRNA degradation, we next focused exclusively on nascent transcription reporting solely on synthesis. To evaluate nascent transcription on a genome-wide level, we employed native elongating transcript sequencing (NET-seq) (Mayer and Churchman, 2016). NET-seq quantitatively maps the position of transcriptionally engaged Pol II with single-nucleotide resolution and strand specificity. In brief, actively transcribing Pol II together with the nascent RNA is quantitatively purified from cells by cellular fractionation. To prevent run-on transcription, fractionation is performed in the presence of the potent Pol II inhibitor α-amanitin, which prevents NTP recognition and catalysis by the Pol II trigger loop (Brueckner and Cramer, 2008; Kaplan et al., 2008). Then, the isolated nascent RNA is fragmented, converted into cDNA and processed into a sequencing library employing a minimal number of PCR cycles. The library preparation method is designed in a way that upon random fragmentation of the nascent transcripts, only the 3' ends of nascent transcripts carrying a free hydroxy-group are sequenced. This reveals the position of transcriptionally engaged Pol II at nucleotide resolution.

NET-seq has been successfully applied to multiple cell culture systems (Mayer and Churchman, 2016; Mylonas and Tessarz, 2018). For application in murine liver tissue, we modified the protocol to include efficient tissue homogenization and nuclei isolation in one single step (for details see 6. Materials and Methods). We named this new twist of the original protocol tissue NET-seq (tNET-seq). We performed tNET-seq using freshly isolated liver tissue from three independent biological replicates from young (3-month-old), middle-aged (12-month-old) and aged (18-month-old) mice. These age groups match those of the RNA-seq data, enabling direct integration of the two datasets. tNET-seq libraries showed high reproducibility when comparing biological replicates (Figure 11A, B), indicating the high robustness of the approach.

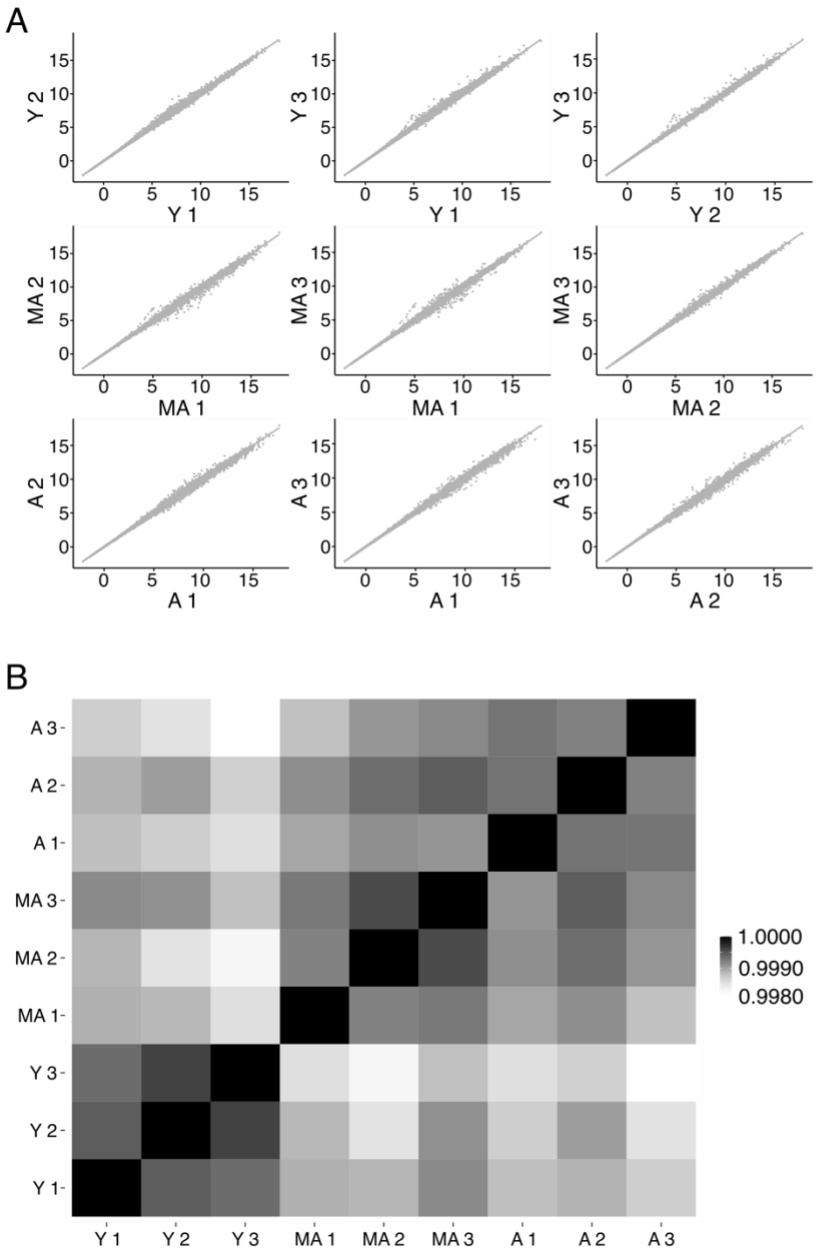

Figure 11. tNET-seq libraries prepared from young, middle-aged and aged liver are highly reproducible. A. Pairwise comparison of tNET-seq samples. Normalized read counts (rlog transformation, DESeq2) in non-overlapping, protein-coding genes above 2 kb in size are reported. B. Heatmap of replicate correlations using normalized read counts as in A. The color code represents Pearson correlation coefficient. Y, young; MA, middle-aged; A, aged.

3.5 Aging has a modest effect on nascent transcription

Having established tNET-seq, we then assessed how nascent transcription is affected by age. For this, we stringently defined a set of protein-coding genes that do not overlap with other transcription units within 2.5 kb of the TSS and TES and are longer than 2 kb (n = 12,460 genes). We further included only genes with sufficient coverage taking RPKM > 1 as an arbitrary cut-off value (n = 3,280 genes). All subsequent analyses were performed using this gene set, hereafter referred to as tNET genes.

Using these tNET genes, we assessed Pol II density at TES as a proxy for nascent transcriptional output. Consistent with the modest changes we observed in steady-state expression levels as quantified by RNA-seq (Figure 10), the nascent transcriptional output beared the same signature of being modestly affected with age (Figure 12A). Yet, there were clear differences between the nascent transcriptome profiles of young and aged liver, assessed by PCA (Figure 12B). The three age groups formed distinct clusters, with the first two principal components explaining more than 60 % of the variance among samples.

To further dissect age-related changes in nascent transcription, we quantified the nascent transcript levels by assessing Pol II density within the gene bodies of the tNET gene set. Compared to young animals, we found 11 % (367 out of 3,278) and 22 % (717 out of 3,278) of the tNET genes to be differentially transcribed in middle-aged and aged liver, respectively (Figure 12C, D). There was an equal distribution between up- and down-regulated nascent transcripts, highlighting the fact that there is no global unidirectional shift (i.e., increase or decrease) in the nascent transcription with age. Together, these results demonstrate that while promoter accessibility is a requirement for transcription, its increased accessibility does not automatically result in elevated nascent transcription.

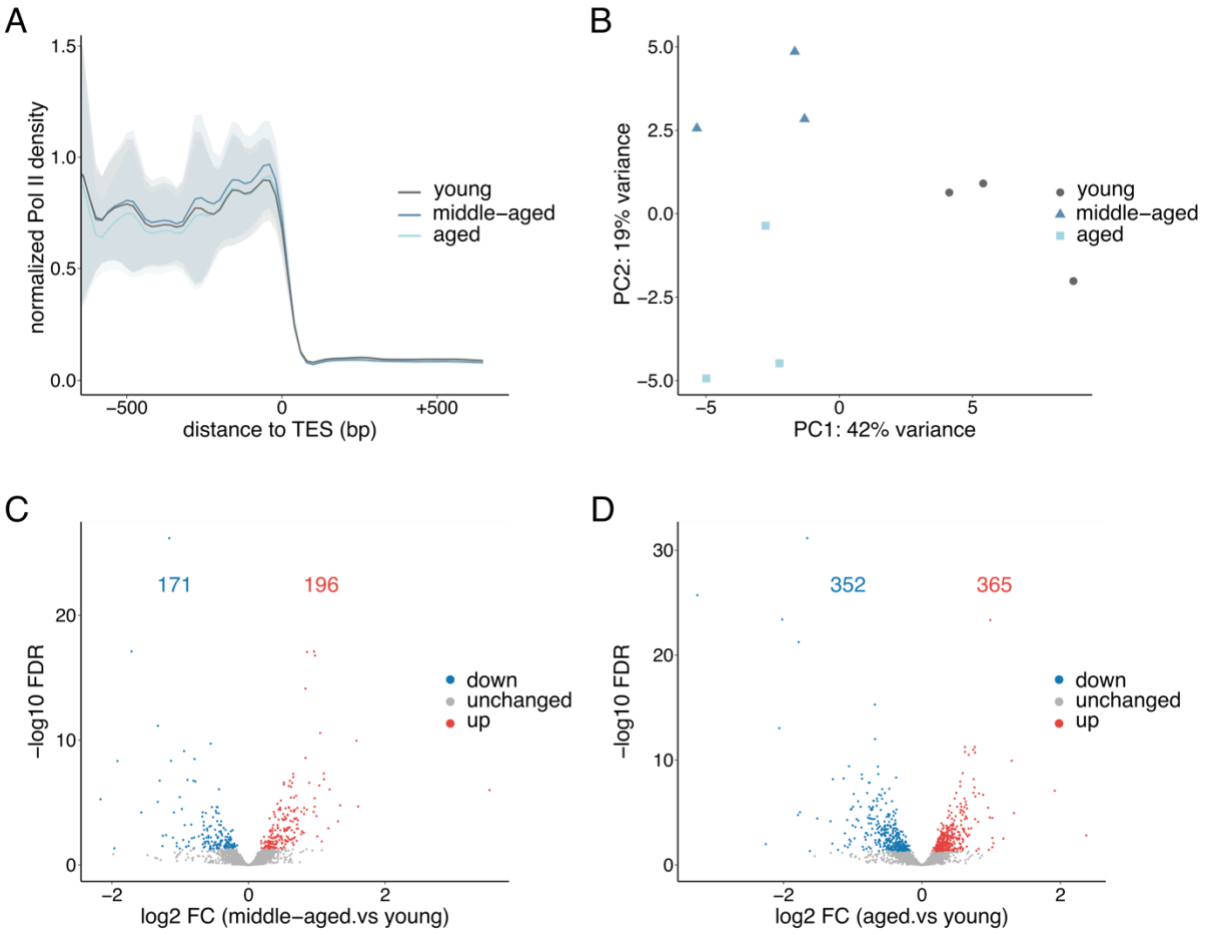

Figure 12. Aging has a modest effect on nascent transcription. A. Metagene profile showing normalized Pol II densities (tNET-seq) at TESs of tNET genes. Read densities were normalized to 1x coverage. Solid lines represent mean values and shading indicates the 95 % confidence interval. B. Principal component analysis of nascent transcription assessed by tNET-seq. PCA was performed with the normalized read counts (rlog transformation, DESeq2) in gene bodies of non-overlapping, protein-coding genes above 2 kb in size. The percentage of variance accounted for by each principal component is indicated. C. Volcano plot of differentially transcribed genes (gene-body Pol II density) in middle-aged relative to young animals (FDR < 0.05, Wald test). 196 genes were up-regulated (red) and 171 down-regulated (blue). D. Volcano plot of differentially transcribed genes (gene-body Pol II density) in aged relative to young animals (FDR < 0.05, Wald test). 365 genes were up-regulated (red) and 352 down-regulated (blue).

3.6 Age-related changes in nascent transcription are not directly mirrored in steady-state mRNA levels

To link nascent with steady-state transcription, we directly compared tNET-seq and RNA-seq data sets. The moderate positive correlation between the normalized signal indicated an overall agreement between the two data sets (Figure 13A). Furthermore, we observed a weak positive correlation between age-related changes in nascent and steady-state transcription (Figure 13B). However, the age-related changes in nascent transcription did not directly mirror the alterations in mRNA abundance. In fact, only 18 genes were found to be both differentially transcribed (tNET-seq) and differentially expressed (RNA-seq) with age (Figure 14A). Of these, only 14 genes showed concordant changes (up- or down-regulated in both tNET-seq and RNA-seq). Despite the low gene number, we still performed a GO enrichment analysis, which should be considered here as an orientation rather than for the selection of any functional categories. Concordantly up-regulated genes (n = 5 genes) were implicated in nuclear processes such as nuclear transport (Figure 14B). Concordantly down-regulated genes (n = 9 genes) were linked to the structural organization of organelles (Figure 14C). Yet, the number of genes in both groups is very low to clearly assign these functional categories. Together, these results demonstrate that age-related changes in nascent transcription do not necessarily reflect the steady-state mRNA levels. These findings highlight the important contribution of post-transcriptional regulatory processes (e.g. degradation) to steady-state mRNA levels.

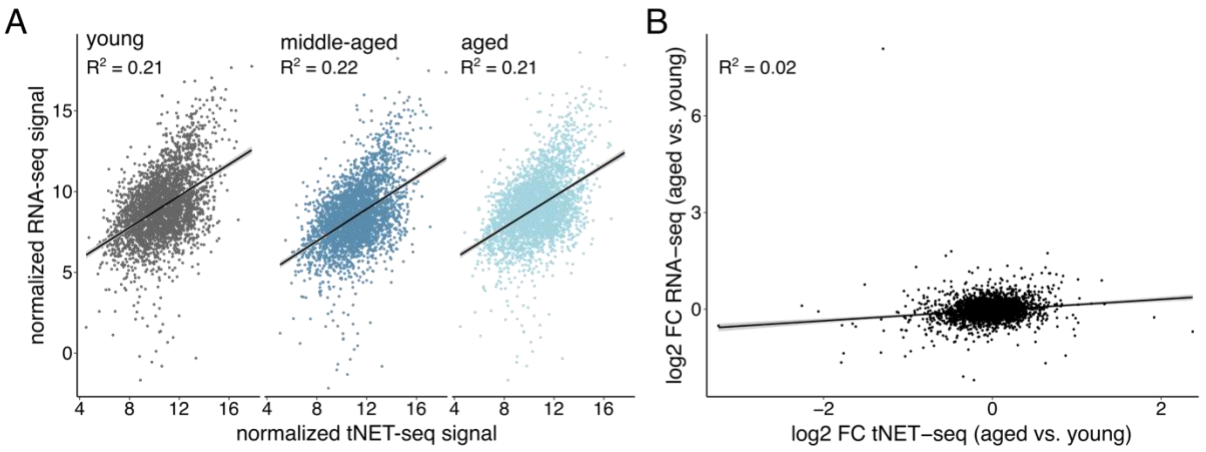

Figure 13. Relationship between changes in nascent and steady-state transcription associated with aging. A. Correlation between nascent (gene-body Pol II density, tNET-seq) and steady-state transcription (RNA-seq). Mean normalized read counts (rlog transformation, DESeq2) of merged biological replicates from young, middle-aged and aged animals are reported. B. Correlation between changes in nascent (gene-body Pol II density, tNET-seq) and steady-state transcription (RNA-seq) of aged versus young animals.

A

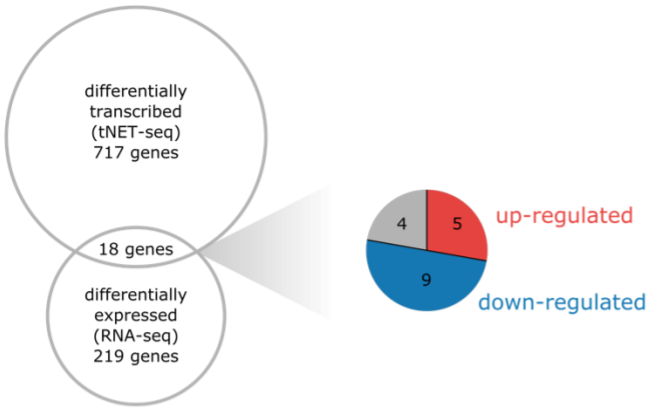

B up-regulated

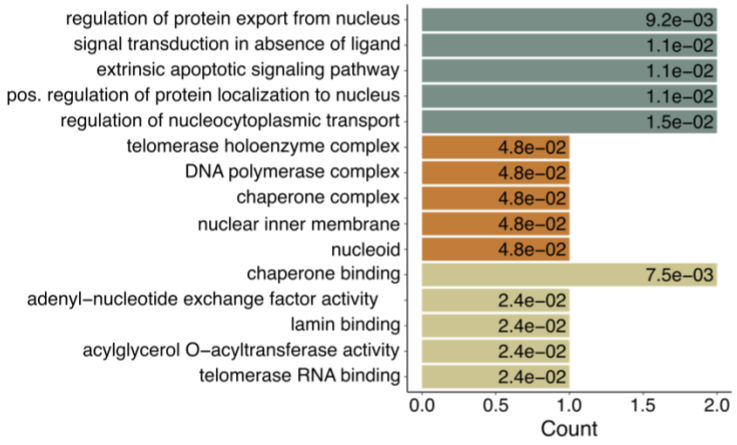

C down-regulated

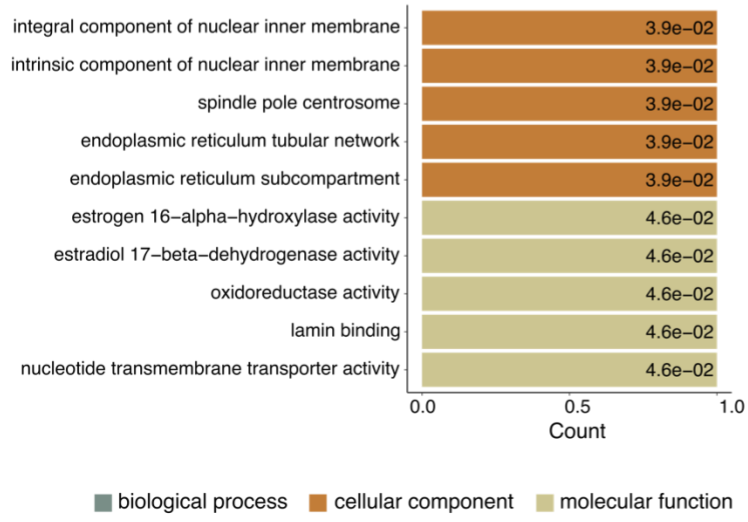

Figure 14. (previous page) Characterization of genes with concordant age-related changes in nascent and steady-state transcription. A. Venn diagram of differentially transcribed (gene-body Pol II density, tNET-seq) and differentially expressed genes (RNA-seq) in aged versus young mice. Only significantly changed genes (FDR < 0.05, Wald test) were included. Up- or down-regulated genes in both datasets are indicated in red and blue, respectively. Genes exhibiting divergent changes are indicated in grey. B, C. GO term analysis for concordantly upregulated (B) or downregulated genes (C) in both datasets (n = 5 and 9 genes, respectively). Only the top five enriched GO terms ranked by adjusted p-value (Benjamini-Hochberg (BH) procedure, FDR < 0.05) are displayed. BH-adjusted p-values are reported for each GO term inside the respective bar.

3.7 Age-related changes in nascent transcription lack a clear signature

Considering the limited number of genes overlapping in the tNET-seq and RNA-seq datasets, we next focused our attention exclusively on the nascent transcription. We asked whether genes that were differentially transcribed with age exhibit a specific signature in their gene structure and features. For this, we assessed whether gene characteristics are related to the observed age-related changes in nascent transcription. We found no considerable relationship between age-related changes in nascent transcription and gene length (Figure 15A), exon length (Figure 15B) or the number of exons per gene (Figure 15C).

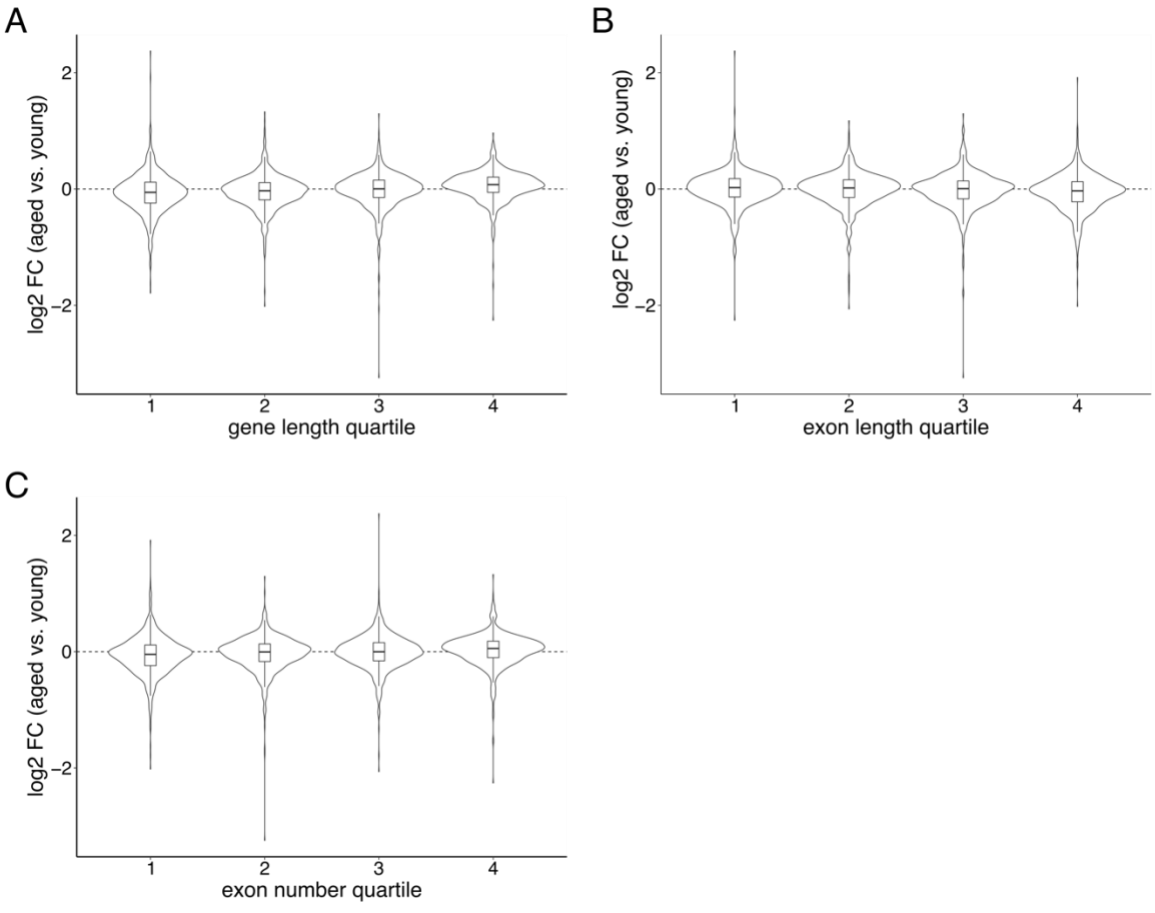

Figure 15. (previous page) Relationship between gene features and age-related changes in nascent transcription. Changes in nascent transcription (gene-body Pol II density, tNET-seq) in aged versus young animals in relationship to gene length (A), median exon length (B) or exon number per gene (C). The gene length was calculated as the total exonic length after reducing a gene's exons to a non-overlapping set. Number of genes per quartile: 819.

Next, we added further nuance to our nascent transcription analysis by assessing the temporal trajectories of change. For this, in addition to the standard Wald test for pairwise comparison (Figure 12C, D), we performed differential testing using a likelihood ratio test. Considering young, middle-aged and aged animals, we found 29 % of genes (953 out of 3,278) to be differentially transcribed. Trajectory analysis of these differentially transcribed genes (for details see 6. Materials and Methods) resulted in four distinct clusters of genes exhibiting similar patterns (Figure 16).

To gain a more detailed insight into the functional categories of these gene clusters, we performed GO enrichment analysis. The four gene clusters we identified exhibited distinct and specific functional enrichment (Figure 16): Genes in cluster 1, which showed an overall increase in nascent transcription with age, were linked to mRNA processing and splicing (Figure 16A). In contrast, genes in clusters 2 and 3 were implicated in lipid metabolism (Figure 16B, C). While genes from these two clusters are involved in the same biological function, they displayed distinct temporal trajectories (Figure 16B, C). This contrasting behavior of genes involved in the same biological function likely captures the variety of changes in lipid metabolic processes occurring in the highly metabolic liver tissue. The smallest gene cluster (cluster 4) contains genes linked to the interferon gamma response (Figure 16D).

To further dissect whether the differentially transcribed genes are implicated in murine aging, we cross-referenced them to a recently published resource of "global aging genes" defined both on a tissue and organismal level based on single-cell RNA-seq data from the Tabula Muris Senis Consortium (Zhang *et al.*, 2021). Of the hepatocyte-specific aging genes, a large fraction of 45 % (1,158 out of 2,569) was present in our tNET-seq dataset that we used for differential transcription testing and trajectory analysis. 34 % of these (396 out of 1,158) were differentially transcribed with age, which is in the same order of magnitude as the overall genes found to be differentially transcribed (29 %, 953 out of 3,278). These differentially transcribed "aging genes" were not enriched in any particular cluster of differentially transcribed genes, but rather comparably spread over all four clusters (Figure 16), suggesting no common pattern in the changes of their nascent transcription.

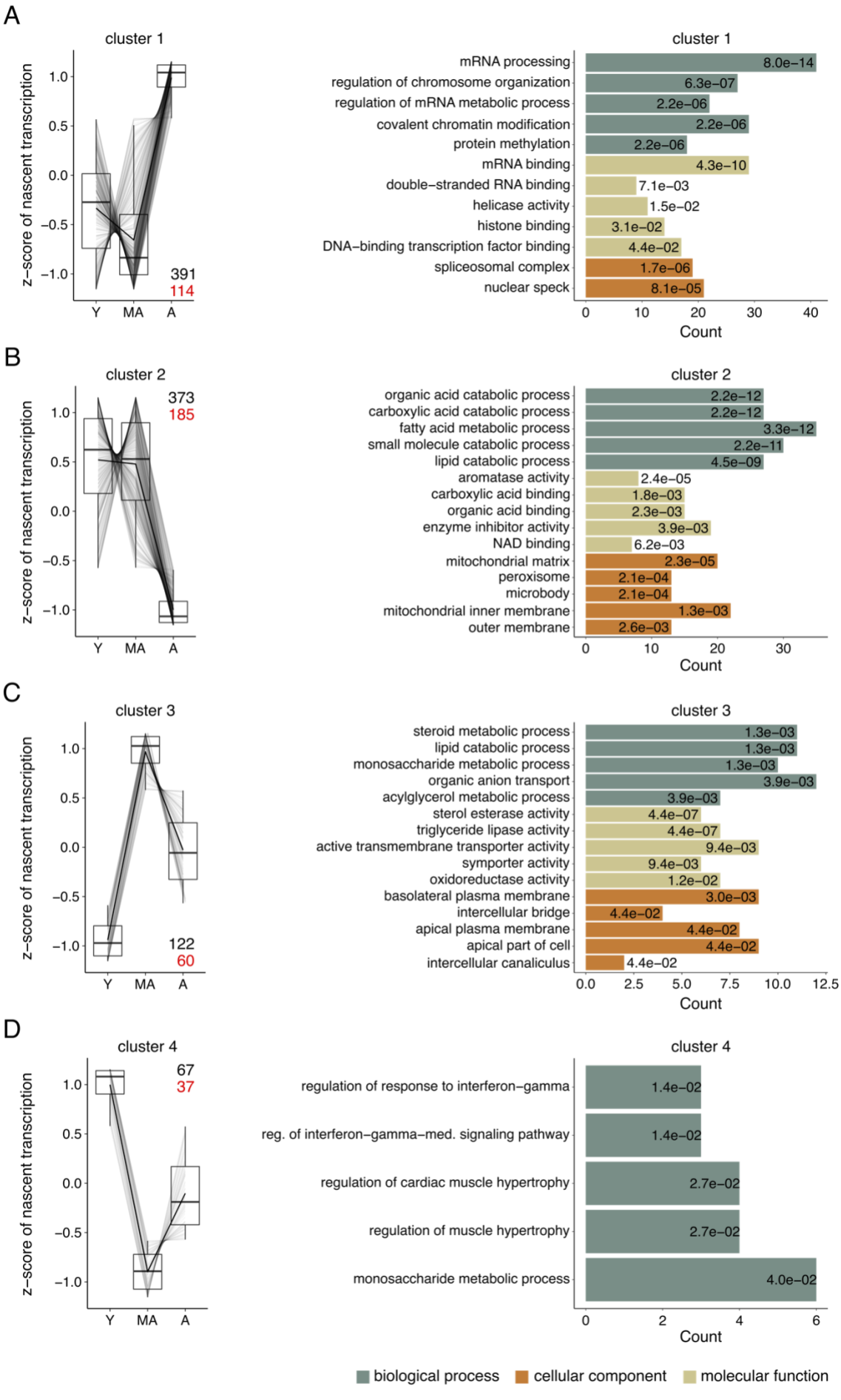
A
cluster 1
z−score of nascent transcription
1.0
0.5
0.0
−0.5
−1.0
391
114
Y
MA
A
cluster 1
mRNA processing
regulation of chromosome organization
regulation of mRNA metabolic process
covalent chromatin modification
protein methylation
mRNA binding
double−stranded RNA binding
helicase activity
histone binding
DNA−binding transcription factor binding
spliceosomal complex
nuclear speck
8.0e−14
6.3e−07
2.2e−06
2.2e−06
2.2e−06
4.3e−10
7.1e−03
1.5e−02
3.1e−02
4.4e−02
1.7e−06
8.1e−05
0
10
20
30
40
Count
B
cluster 2
z−score of nascent transcription
373
185
cluster 2
organic acid catabolic process
carboxylic acid catabolic process
fatty acid metabolic process
small molecule catabolic process
lipid catabolic process
aromatase activity
carboxylic acid binding
organic acid binding
enzyme inhibitor activity
NAD binding
mitochondrial matrix
peroxisome
microbody
mitochondrial inner membrane
outer membrane
2.2e−12
2.2e−12
3.3e−12
2.2e−11
4.5e−09
2.4e−05
1.8e−03
2.3e−03
3.9e−03
6.2e−03
2.3e−05
2.1e−04
2.1e−04
1.3e−03
2.6e−03
0
10
20
30
Count
C
cluster 3
z−score of nascent transcription
122
60
cluster 3
steroid metabolic process
lipid catabolic process
monosaccharide metabolic process
organic anion transport
acylglycerol metabolic process
sterol esterase activity
triglyceride lipase activity
active transmembrane transporter activity
symporter activity
oxidoreductase activity
basolateral plasma membrane
intercellular bridge
apical plasma membrane
apical part of cell
intercellular canaliculus
1.3e−03
1.3e−03
1.3e−03
3.9e−03
3.9e−03
4.4e−07
4.4e−07
9.4e−03
9.4e−03
1.2e−02
3.0e−03
4.4e−02
4.4e−02
4.4e−02
4.4e−02
0.0
2.5
5.0
7.5
10.0
12.5
Count
D
cluster 4
z−score of nascent transcription
67
37
cluster 4
regulation of response to interferon−gamma
reg. of interferon−gamma−med. signaling pathway
regulation of cardiac muscle hypertrophy
regulation of muscle hypertrophy
monosaccharide metabolic process
1.4e−02
1.4e−02
2.7e−02
2.7e−02
4.0e−02
0
2
4
6
Count
biological process
cellular component
molecular function

Figure 16. (previous page) Trajectory analysis of differentially transcribed genes in aged liver. A-D. Trajectory analysis of differentially transcribed genes in aged versus young mice (n = 953 genes, likelihood ratio test, DESeq2) resulted in four distinct gene clusters. In each cluster, the total number of genes and the number of "aging genes" (Zhang *et al.*, 2021) are designated in black and red, respectively. Nascent transcript levels are reported in the parallel coordinate plot on the left as z-scores of gene-body Pol II density. GO term analysis for each gene cluster is depicted on the right. Only the top five enriched GO terms ranked by adjusted p-value (Benjamini-Hochberg (BH) procedure, FDR < 0.05) are displayed. BH-adjusted p-values are reported for each GO term inside the respective bar. Y, young; MA, middle-aged; A, aged.

Taken together, these analyses reveal age-related alterations in the nascent transcriptome with a large fraction of the previously defined "aging genes" being altered. Yet, the changes in nascent transcription were not congruent and unidirectional, suggesting that nascent transcription alone does not control the coordinated global aging behavior at tissue and organismal level reported earlier (Zhang *et al.*, 2021). Overall, this corroborates the modest correlation between tNET-seq and RNA-seq we observed (Figure 13), implying that the other processes that determine transcript half-life may shape the coordinated gene expression signature detected within and across tissues (Zhang *et al.*, 2021).

3.8 Connection between promoter accessibility and transcriptional output

Chromatin accessibility at promoter regions is a pre-requisite for transcription and the size of the nucleosome depleted region positively correlates with gene activation (Scruggs *et al.*, 2015). To directly assess the effect of promoter accessibility on transcriptional output, we integrated the ATAC-seq with the tNET-seq and RNA-seq datasets. Here, we interrogated the promoter accessibility, nascent and steady-state transcription of tNET genes present in all three datasets (Figure 17). The age-related increase in promoter accessibility at these genes was not accompanied by increased nascent or steady-state transcription (Figure 17). These results demonstrate that while promoter accessibility is a requirement for transcription, increased accessibility does not automatically result in increased transcriptional output.

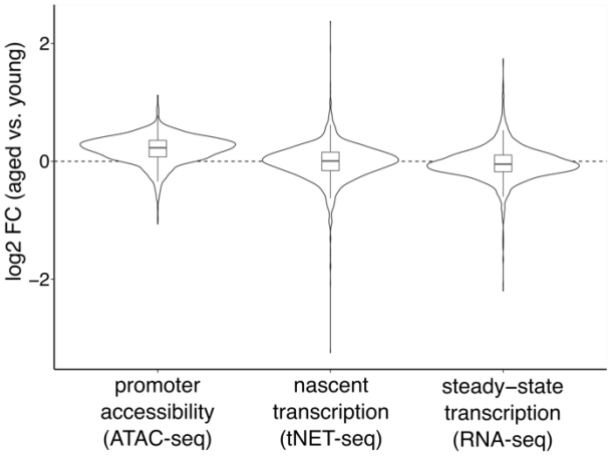

Figure 17. The age-related increase in promoter accessibility is not directly reflected in increased nascent or steady-state transcription. Violin and boxplots of changes in promoter accessibility (ATAC-seq), nascent transcription (gene-body Pol II density, tNET-seq) and steady-state transcription (RNA-seq) in aged versus young mice. Only tNET genes present in all three datasets are included here (n = 2,693 genes). Promoter defined as TSS +/- 200 bp.

3.9 Promoter-proximal Pol II pausing decreased with age

The discrepancy between the increased promoter accessibility and the overall modest change in transcriptional output with age, together with the lack of a clear signature in terms of common functionalities, led us to focus on the initial stages of transcription at the promoter region, which is where much of the transcriptional regulation occurs. Promoter-proximal Pol II pausing is of particular interest in the context of transcriptional regulation since emerging evidence places it central to transcriptional regulation (Core and Adelman, 2019). (t)NET-seq is a powerful approach for investigating Pol II pausing since increased Pol II density at a specific nucleotide is indicative of polymerase pausing at that site (Mayer et al., 2015). To quantify promoter-proximal pausing, we calculated the pausing index (PI), which is the ratio of the average Pol II density in the promoter region (defined here as TSS +/- 200 bp) to that in the gene body (defined here as TSS + 200 bp to TES - 200 bp) (Rahl et al., 2010; Zeitlinger *et al.*, 2007). The PI provides a measure of the magnitude of promoter-proximal Pol II density relative to that in the gene body. Based on the PI values in young animals, we classified the tNET genes into three pausing categories with high (PI ≥ 3), moderate (1.5 < PI < 3) or low (PI ≤ 1.5) pausing. 69.7 % of the analyzed genes were either highly or moderately paused in young animals (Figure 18A). This corroborates promoter-proximal pausing as a wide-spread phenomenon in liver, consistent with previous reports in other organisms and cell types (Adelman and Lis, 2012).

To investigate alterations in promoter-proximal Pol II pausing with age, we generated metagene profiles of a 1-kb region around the TSSs of tNET genes (Figure 18B). Notably, we observed an age-related decrease in promoter-proximal Pol II pausing, which was, however, not accompanied by a change in Pol II density in the immediate 5’ gene bodies (Figure 18B)

or at the TES as a proxy for transcriptional output (Figure 12A). The age-related decrease in promoter-proximal pausing is also reflected in a progressive decrease in PI (Figure 18C). Interestingly, highly paused genes (PI > 3 in young mice) experienced the highest decrease in promoter-proximal Pol II pausing with age (Figure 18D).

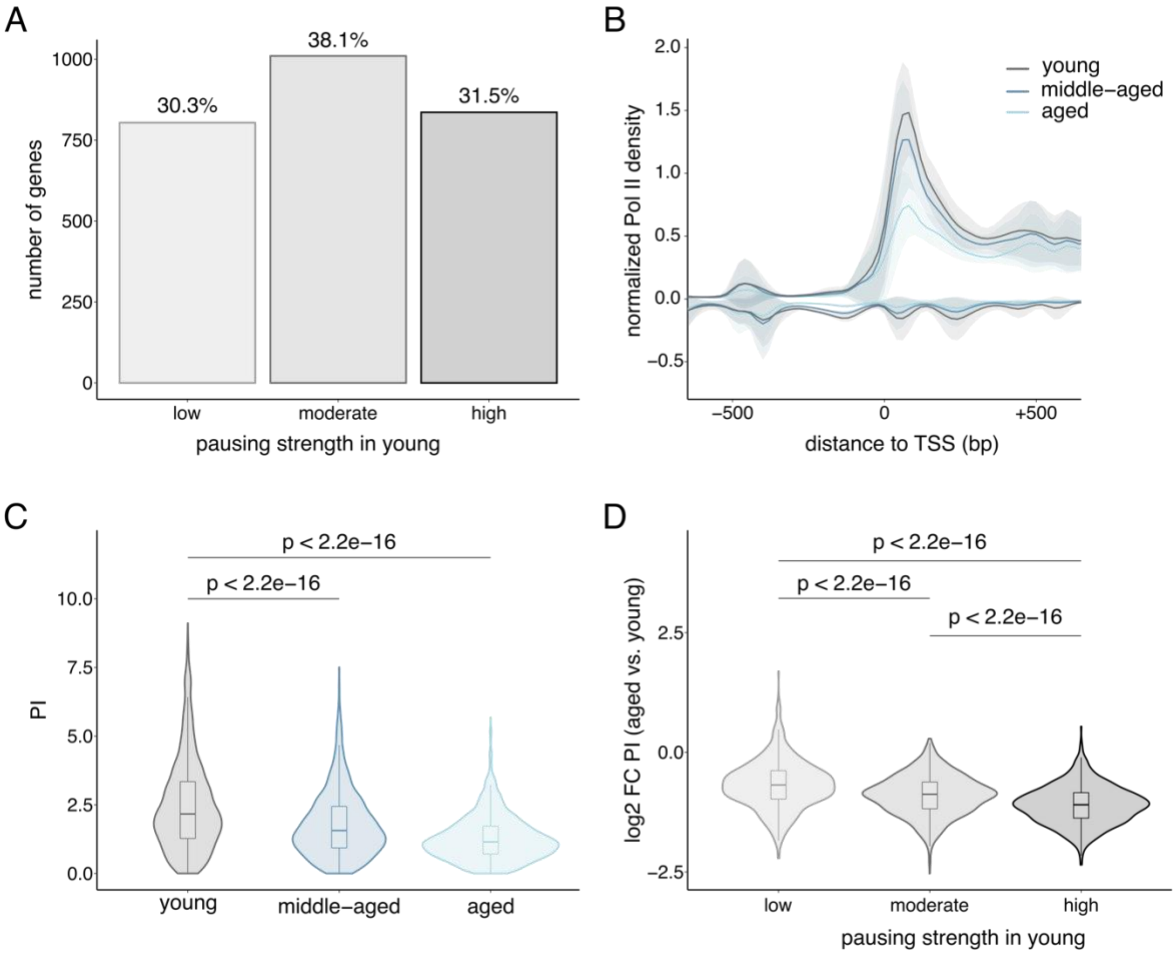

Figure 18. Promoter-proximal Pol II pausing decreases with age. A. Bar plot of the pausing index (PI) quantifying the extent of promoter-proximal pausing in young mice. PI is the ratio of the averaged Pol II density in the promoter region (defined as TSS +/- 200 bp) to the density in the gene body (defined as TSS + 200 bp to TES - 200 bp). The 2,650 genes were divided into three groups based on the PI in young animals: highly paused (PI ≥ 3; n = 836), moderately paused (1.5 ≤ PI < 3; n = 1,010), and lowly paused (PI < 1.5; n = 804). B. Average profile of normalized Pol II densities (tNET-seq) at the promoter-proximal region of all tNET genes. Read densities were normalized to 1x coverage. Solid lines represent mean values and shading indicates the 95 % confidence interval. The increased Pol II density at those regions compared to the gene body is indicative of paused Pol II. C. Violin and box plots of PI values in young, middle-aged and aged animals. D. Violin and box plot of log2-fold change in PI of aged versus young liver. Genes were grouped by PI as in A. p-values in C and D were calculated using a two-sided Wilcoxon rank-sum test.

Changes in the PI depend on both changes in the numerator (promoter-proximal Pol II) and denominator (gene-body Pol II). Therefore, we considered the possibility that the age-related decrease in PI may be related to the levels of nascent transcription. Hence, we grouped the tNET gene set into equal-sized groups based on their level of nascent transcription in young mice (Figure 19A). The fold changes in PI between all groups were similar, indicating that the age-related decrease in PI occurs irrespective of the gene's expression level. This was further confirmed by the observation that differentially transcribed genes consistently exhibited a lower PI in aged animals (Figure 19B). This is true even for the down-regulated genes, corroborating that the observed effect with age was specific to the promoter-proximal region (numerator of PI) and not linked to transcription levels (denominator of PI). Overall, these findings reveal an age-related decrease in promoter-proximal Pol II pausing affecting the majority of the analyzed genes.

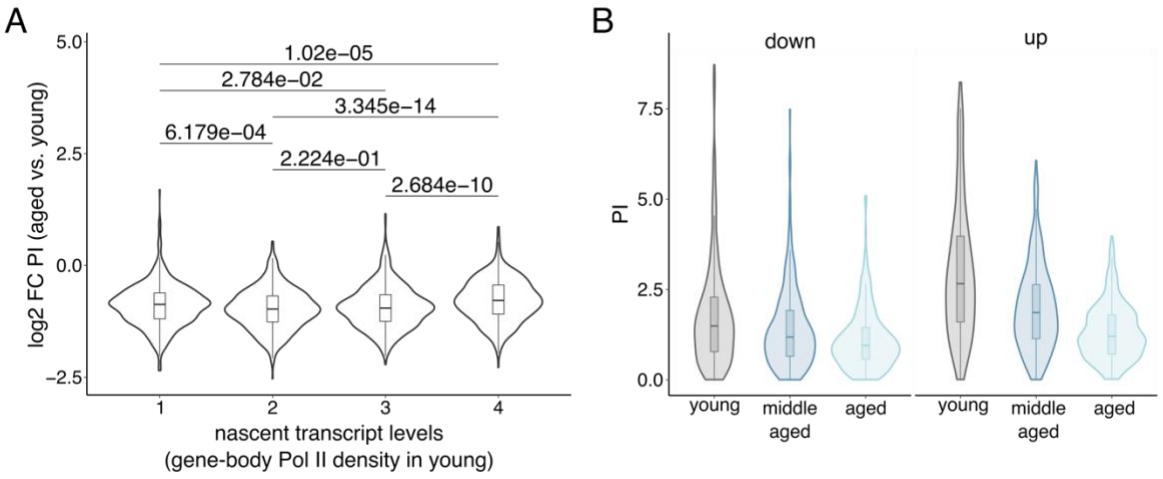

Figure 19. The age-related decrease in promoter-proximal pausing is independent of nascent transcription levels. A. Violin and box plots of PI change in aged versus young animals. Genes were divided into four equal-sized groups based on their level of nascent transcription (gene-body Pol II density) in the liver of young mice. p-values were calculated using a two-sided Wilcoxon rank-sum test. B. Violin and box plots showing the PI in young, middle-aged and aged animals. Only genes found to be differentially transcribed in aged versus young mice are included and grouped by the direction of change (down-regulated, left panel; up-regulated, right panel).

3.10 Assessing age-related changes in transcription factor expression and recruitment

To investigate the causal effects behind the age-related decrease in promoter-proximal Pol II pausing, we assessed the expression levels of important transcriptional regulators involved in the early stages of transcription. Notably, we observed no change in the expression of these factors with age (Figure 20A). However, while the expression of these transcription regulators was not affected by age, their recruitment to chromatin might have been altered. To assess this, we performed ChIP-seq for the DSIF component SPT4. We observed a decreased occupancy of SPT4 at TSSs of tNET genes in aged animals (Figure 20B). Due to handling difficulties, biological replicates were separately processed, resulting in batch effects. Nonetheless, the observed trends were detectable in both batches (replicates 1 and 2, Figure 20B). Thus, while their expression does not seem to be affected with age, the recruitment and binding of important pausing factors to chromatin might be altered, resulting in changes in promoter-proximal Pol II pausing. This is consistent with the decreased level of promoter-proximal Pol II pausing we observed using tNET-seq (Figure 18B, C). These results suggest that the age-related decrease in promoter-proximal Pol II pausing might be explained by an altered stability of the pausing complex in aged animals. The dissociation of Pol II from chromatin at this early stage of transcription might antagonize the effect of the age-related increase in promoter accessibility, leading to an overall unchanged transcriptional output.

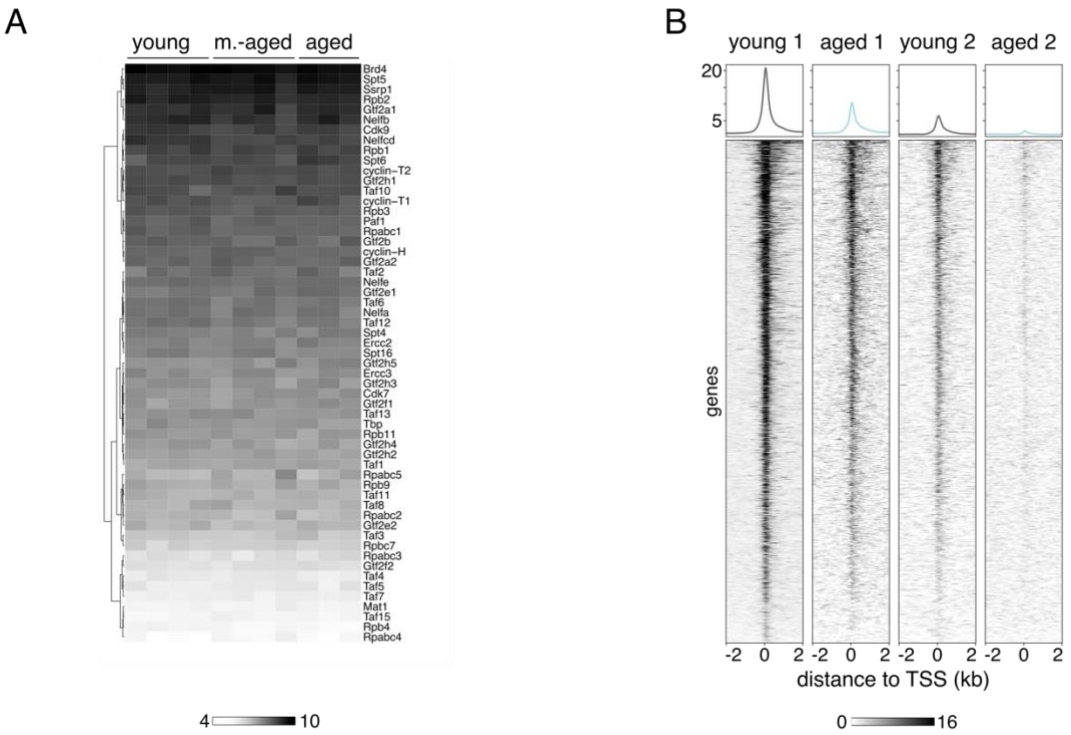

Figure 20. (previous page) Expression levels and chromatin binding of relevant transcription regulators. A. Steady-state mRNA levels (RNA-seq) of relevant transcription regulators in young, middle-aged and aged mice. Normalized read counts (rlog transformation, DESeq2) are reported. B. Heatmaps and average intensity profiles of SPT4 ChIP-seq signal at TSSs of tNET genes in young and aged animals. Read densities were normalized to 1x coverage.

3.11 Assessing age-related changes in enhancer activity

Enhancers are important regulatory elements determining cell type-specific transcription. As previously mentioned, these regulatory elements exert their function through multiple mechanisms affecting either transcription initiation or the early stages of elongation. Considering the central role of enhancers in fine-tuning transcription, we were interested in investigating how enhancer activity is affected by aging.

3.11.1 Identification of active enhancers in murine liver

Active enhancers are characterized by accessible chromatin regions marked with H3K27ac and H3K4me1, but not H3K4me3, on the flanking nucleosomes (Creyghton et al., 2010; Heintzman et al., 2007). For identifying active enhancers in murine liver, we analyzed publicly available histone ChIP-seq data from liver tissue of young (3 month), middle-aged (12 months) and aged (29 months) mice (Benayoun *et al.*, 2019). The ChIP-seq data sets are of high quality, which was corroborated by the high alignment rates and the high number of reads passing the filtering (Figure 21A), as well as the high signal-to-noise ratio (Figure 21B). The high numbers of peaks, representing regions of signal enrichment (Figure 21C), and the high FRiP scores (Figure 21D) further confirmed the high quality of the data. Assessing the distribution of identified peak regions in relation to annotated features provided further validation of the dataset. As expected, H3K4me3 marks were predominantly found in promoter regions, while H3K27ac marks were located mainly in intronic or intergenic regions (Figure 21E).

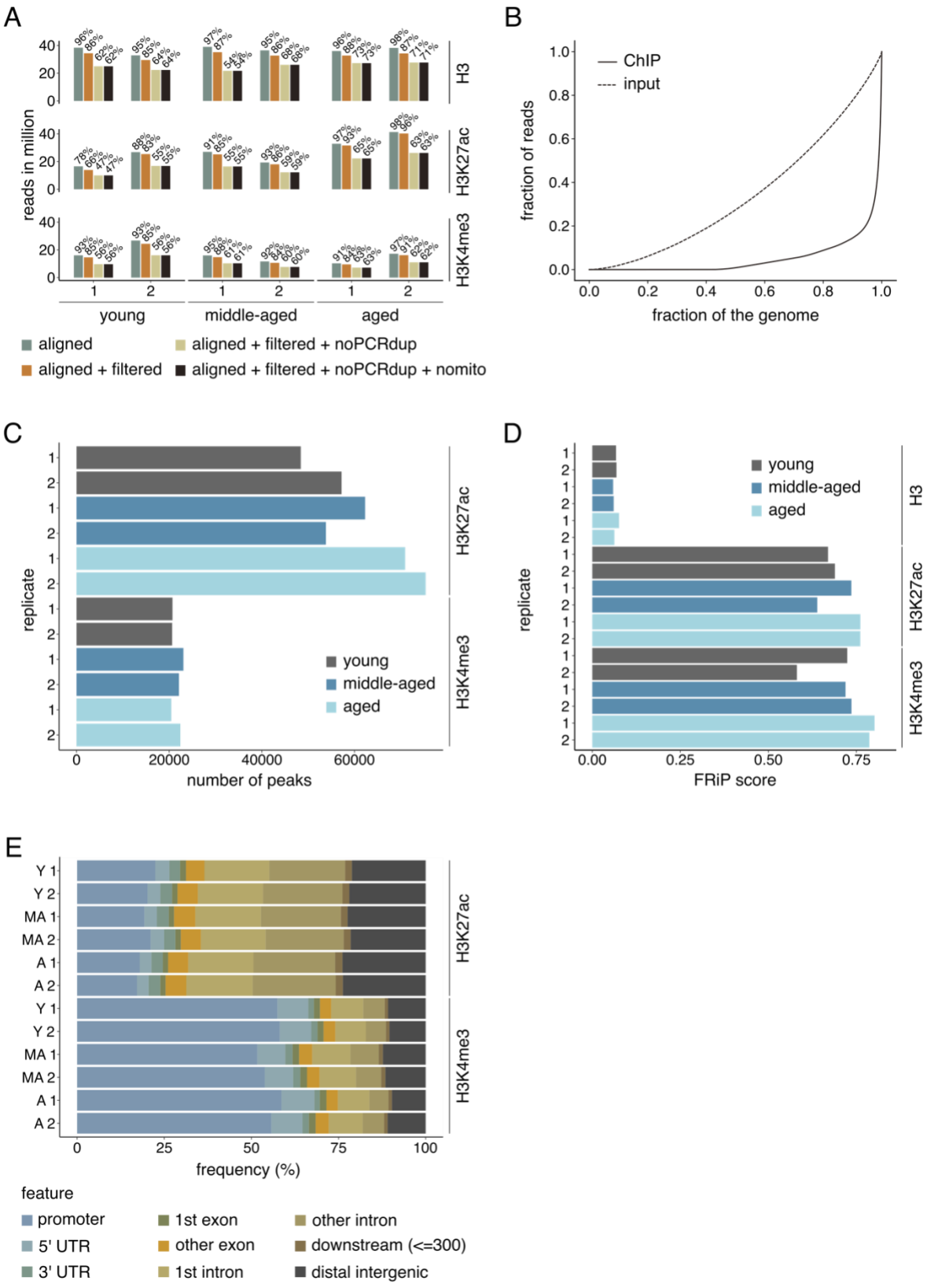
A
reads in million
young
middle-aged
aged
H3
H3K27ac
H3K4me3
aligned
aligned + filtered
aligned + filtered + noPCRdup
aligned + filtered + noPCRdup + nomito
B
ChIP
input
fraction of reads
fraction of the genome
C
replicate
number of peaks
young
middle-aged
aged
D
FRiP score
E
frequency (%)
feature
promoter
5' UTR
3' UTR
1st exon
other exon
1st intron
other intron
downstream (<=300)
distal intergenic

Figure 21. (previous page) Quality control of histone ChIP-seq data. A. Number of ChIP-seq reads unambiguously aligned and passing filtering criteria. Aligned reads were filtered for high quality (MAPQ > 10). PCR duplicates and reads of mitochondrial origin were removed. B. Signal enrichment of a representative ChIP-seq library (H3K27ac) and input sample (H3) of aged replicate 1. The cumulative sum of read counts for equal-sized genomic bins is plotted. C. Number of peak regions identified in the ChIP-seq samples. D. Fraction of reads in peaks (FRiP). E. Genomic distribution of annotated peaks. Y, young; MA, middle-aged; A, aged.

After validating the high quality of the ChIP-seq data, we identified enhancer regions by integrating histone marks with the chromatin accessibility information obtained from our ATAC-seq dataset (for details see 6. Materials and Methods). This resulted in the identification of 8,855 high-confidence, putative enhancers, that were present in all three age groups. Comparison of these active enhancer regions with published enhancer annotations from the Enhancer Atlas (Gao and Qian, 2020) revealed a fairly small overlap with the datasets from mice embryos (E14.5), neonates or liver hepatocytes (i.e. less than 900 regions), likely because of the highly tissue- and context-specific mode of action of enhancers. The high tissue specificity is further corroborated by the genomic location of the identified enhancers: The majority are located in intronic regions compared to intergenic regions (Figure 22), consistent with a recent report highlighting the predominantly intronic location of tissue-specific enhancers (Borsari et al., 2021).

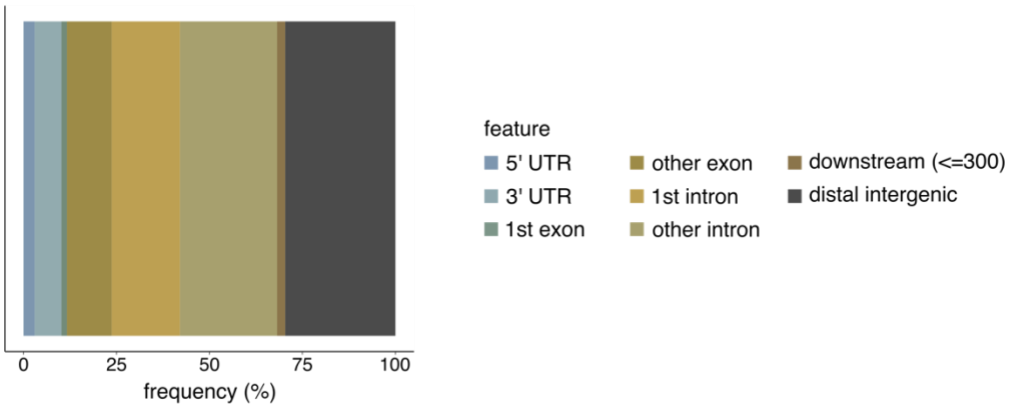

Figure 22. Liver-specific enhancers are predominantly located in intronic regions. Genomic distribution of identified active enhancers.

3.11.2 Enhancer activity is not decreased in aged liver

Having identified active, liver-specific enhancers, we then assessed enhancer activity using chromatin accessibility as a proxy. We observed an increased enhancer accessibility in aged compared to young animals (Figure 23A), resembling the age-related increase in promoter accessibility (Figure 8). In fact, 21.3 % (587 out of 2,760) of the genomic regions that were more accessible with age were located within enhancer regions (Figure 23B). In contrast, only 6.7 % (129 out of 1,931) of sites that exhibited a significant decrease in accessibility with age were found within enhancer regions (Figure 23B). This trend of more enhancer sites becoming more accessible with age compared to those with decreased accessibility mirrors the accessibility changes at promoters (Figure 23B).

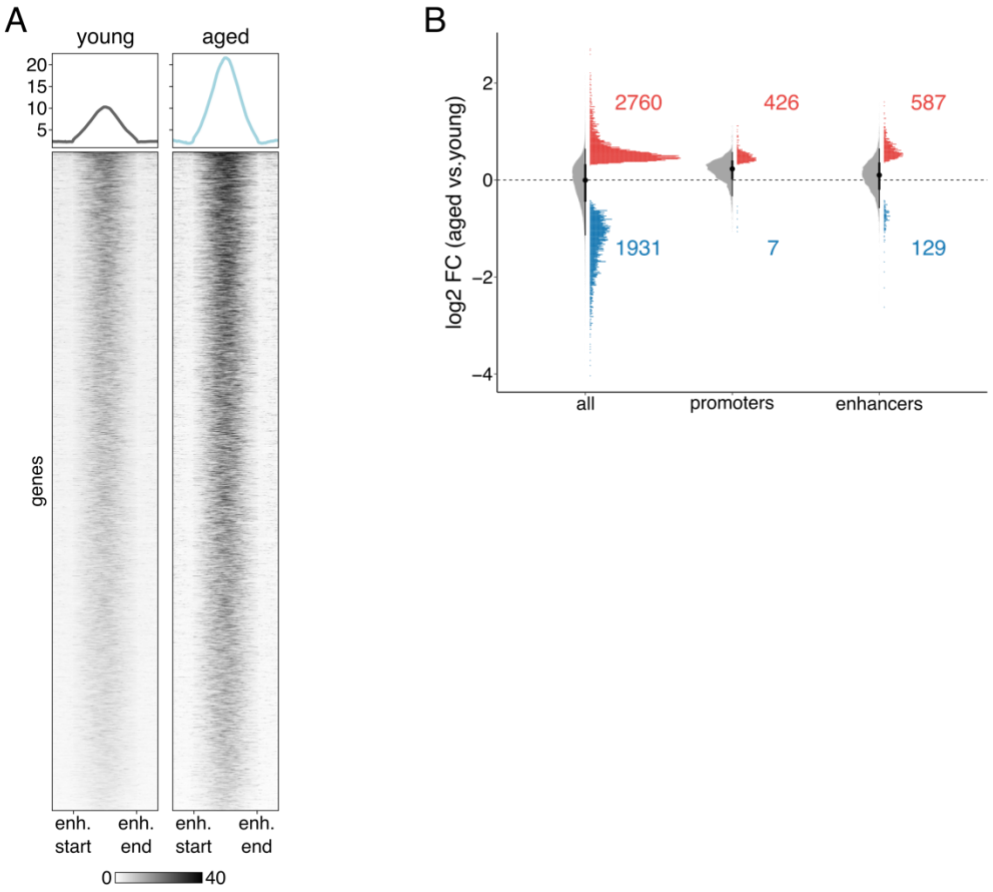

Figure 23. Enhancer accessibility increases with age. A. Heatmap and intensity profiles of promoter accessibility over active enhancers in liver (n = 8,855). B. Raincloud plots of changes in accessibility in aged versus young liver assessed by ATAC-seq. Raincloud plots are hybrid plots. Here, the violin and boxplots visualize the log2-fold change for all accessible genomic sites (“all”) or accessible sites overlapping tNET promoters or enhancers. The dot plot highlights regions significantly changed with age in each category (FDR < 5 %). The numbers in the plot denote significantly up- or down-regulated regions in each category.

Enhancer regions of the genome are actively transcribed (De Santa *et al.*, 2010; Kim *et al.*, 2010) and eRNA production and enhancer activity are highly correlated on a genome-wide scale (Andersson *et al.*, 2014; Henriques *et al.*, 2018). Therefore, we used eRNA levels as a second proxy for enhancer activity. (t)NET-seq captures nascent RNAs as they are being synthesized and before post-transcriptional processes that determine transcript stability take place. Therefore, the method allows for capturing short-lived RNA species like eRNAs, which are not detected with sufficient coverage by RNA-seq. We quantified eRNA production by assessing Pol II levels at the identified enhancer regions. We observed no age-related change in eRNA production (Figure 24). Overall, the unaltered eRNA production and the increased enhancer accessibility suggest that enhancer activity is not impaired with age.

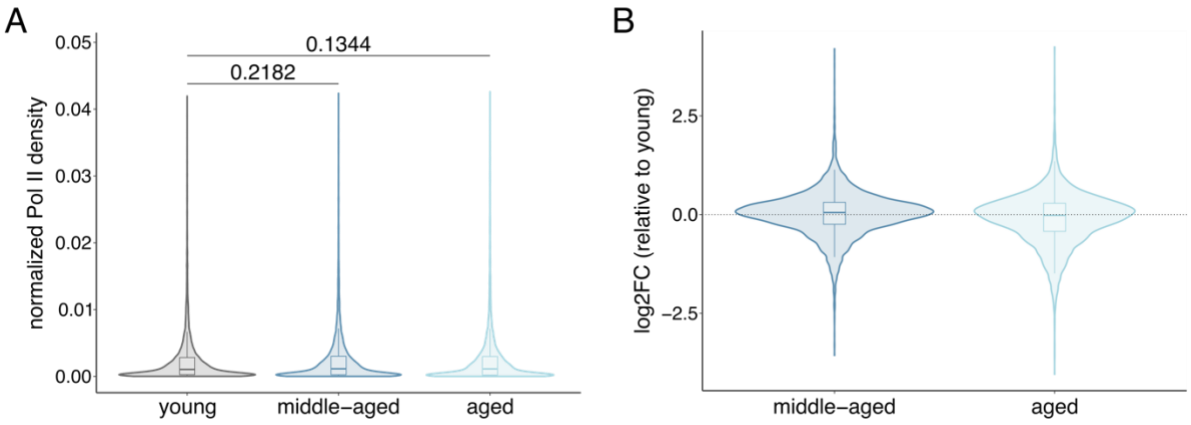

Figure 24. eRNA production is not altered with age. A. Violin and boxplots of Pol II density at enhancer regions. p-values were calculated using a two-sided Wilcoxon rank-sum test. B. Violin and box plots of log2-fold changes in Pol II density at enhancer regions of middle-aged and aged animals relative to young ones.

3.12 Connection between promoter-proximal Pol II pausing and the local chromatin landscape

The local chromatin landscape at promoter regions directly modulates transcriptional regulation and progression of Pol II by regulating the accessibility of the region. To investigate the relationship between promoter accessibility and promoter-proximal pausing, we integrated the ATAC-seq and tNET-seq datasets. With age, the majority of investigated promoters (96%) exhibited an increased chromatin accessibility with a concomitant decrease in promoter-proximal Pol II pausing (Figure 25). In light of the modest age-related changes in

transcriptional output (Figure 17), this points towards a compensatory mechanism, in which alterations at the step of promoter-proximal pausing might counteract the increased accessibility of the promoter regions, thereby maintaining transcriptional fidelity. This might be achieved through an altered stability of the Pol II pausing complex, consistent with the age-related decrease in SPT4 occupancy at tNET promoters (Figure 20).

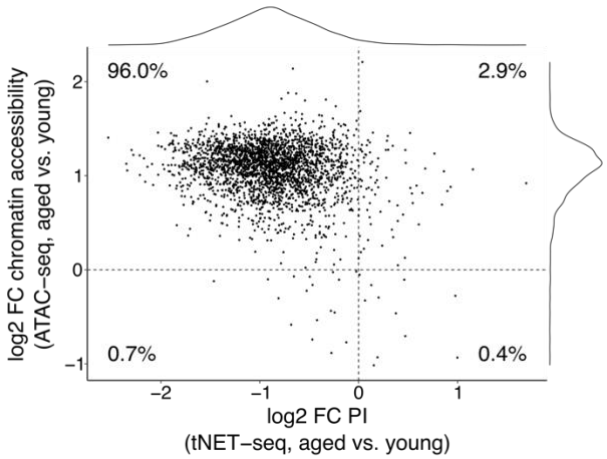

Figure 25. Aging leads to increased promoter accessibility with a concomitant decrease in promoter-proximal Pol II pausing. Scatter plot of the change in PI (tNET-seq) and promoter accessibility (ATAC-seq) in aged versus young mice. Promoter region defined as TSS +/- 200 bp.

Besides a nucleosome depleted region, active promoters are characterized by precisely positioned and phased downstream nucleosomes. The +1 nucleosome, which is the first nucleosome downstream of a TSS, has been suggested to influence promoter-proximal Pol II pausing (Jimeno-Gonzalez et al., 2015; Weber et al., 2014). To investigate whether the observed age-related decrease in promoter-proximal Pol II pausing can be linked to changes in nucleosome occupancy, we exploited the characteristic feature of ATAC-seq to generate fragments of varying sizes with clear periodicity, with longer fragments corresponding to nucleosome-associated regions. To quantify nucleosome abundance, we leveraged NucleoATAC (Schep et al., 2015) to compute nucleosome occupancy scores. We observed a higher median nucleosome occupancy in aged compared to young animals (Figure 26A). The higher nucleosome occupancy was also detectable specifically around TSSs of tNET genes (Figure 26B). Additionally, the inter-dyad distance between nucleosomes of aged mice was shorter when compared to young animals (Figure 26C). Finally, we observed higher nucleosome fuzziness in aged mice (Figure 26D). The fuzziness is an indicator of the precise positioning of a nucleosome, suggesting compromised precision in nucleosome positioning with age. These changes in both nucleosome occupancy and nucleosome fuzziness point towards altered local chromatin dynamics with age including both nucleosome deposition and nucleosome sliding. Importantly, the increased promoter accessibility cannot be attributed to

decreased nucleosome occupancy in the surrounding regions. In fact, promoters in aged liver tissue were characterized by both increased accessibility (Figure 8) and increased nucleosome occupancy (Figure 26). Together, these findings highlight that promoter accessibility and nucleosome occupancy are not mutually exclusive and are controlled by distinct mechanisms.

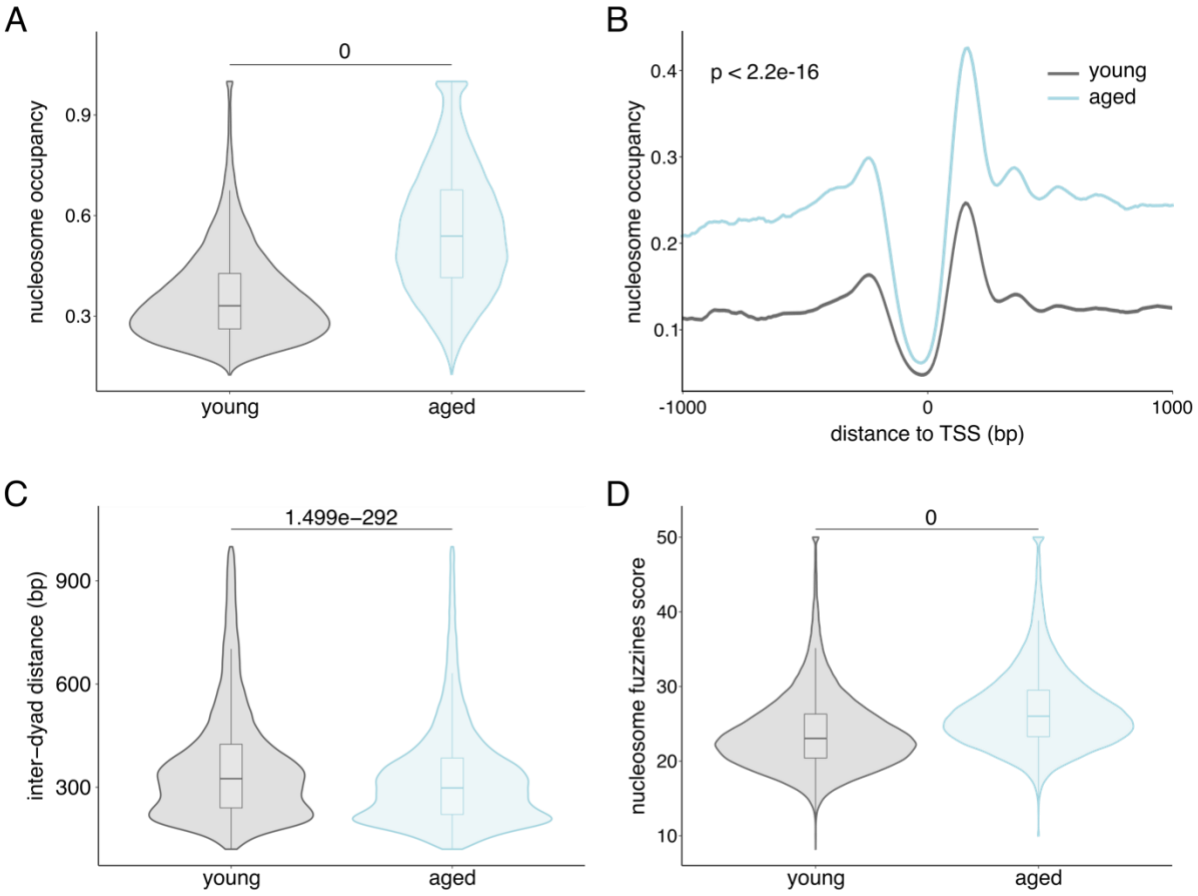

Figure 26. Nucleosome occupancy is altered with age. A. Violin and box plots of nucleosome occupancy genome-wide. B. Metaplot of average nucleosome occupancy at TSSs of tNET genes. Significance between average occupancy profiles was assessed using a two-sided Kolmogorov-Smirnov goodness-of-fit test C. Violin and box plots of inter-dyad distance quantifying the distances between neighboring nucleosomes. D. Violin and box plots of nucleosome fuzziness to assess how well positioned a nucleosome is. All nucleosome parameters were calculated using NucleoATAC (Schep *et al.*, 2015). p-values in A, C and D were calculated using a nonparametric two-sided Wilcoxon rank-sum test.

4. Discussion

The rapid developments of omics technologies in recent years have significantly advanced our understanding of the epigenome and its role in transcriptional regulation. Using freshly isolated liver tissue from young, middle-aged and aged mice, we provide a comprehensive analysis of age-related changes in the local chromatin landscape and the nascent transcriptome. The combination of multiple genome-wide techniques (tNET-seq, ATAC-seq, RNA-seq, ChIP-seq) creates a framework for investigating the interrelation between chromatin and transcriptional regulation and the age-related changes thereof.

We find that in murine liver tissue, a sizeable fraction of the genome undergoes age-related changes. In recent years, several studies have interrogated age-related changes in the chromatin landscape of different tissues and cell systems. Chromatin accessibility analysis of aged CD8+ T-cells from human donors revealed a decrease in promoter accessibility (Moskowitz et al., 2017; Ucar et al., 2017). Recently, an overall more compacted chromatin architecture has also been observed in aged murine neutrophils (Lu et al., 2021). Contrasting these observations of decreased chromatin accessibility, a study reports no major changes in accessibility in aged murine B precursor cells (Koohy et al., 2018). Likely, age-related chromatin accessibility alterations are highly tissue- and cell-type specific, which may, at least in part, explain these contrasting observations.

Interestingly, we observed that healthy aging in murine liver is accompanied by increased chromatin accessibility at promoter regions. Chromatin opening at promoter regions might be due to aging-related loss of histone proteins resulting in more DNA regions being accessible to the Tn5 transposase, which would be in line with observations in yeast (Feser *et al.*, 2010) (Hu *et al.*, 2014). Such scenario, however, seems unlikely: We observed an increase in nucleosome occupancy, arguing against a global loss of histone proteins. This is supported by a recent report that aging in four different murine tissues (liver, heart, cerebellum, olfactory bulb) is not accompanied by drastic changes in H3 expression levels (Chen *et al.*, 2020). Thus, the changes in nucleosome occupancy we observed are most likely due to altered deposition patterns rather than changes in the core histone expression. In support of this, no global changes in nucleosome occupancy (assessed using H3 occupancy as a proxy) have been reported in aged murine liver tissue; only at a subset of loci either increased or decreased occupancy was observed (Chen *et al.*, 2020). This is also consistent with another report, in which MNase-seq of aged mouse liver revealed no global changes in nucleosome occupancy (Bochkis et al., 2014). Here also, local changes at only a subset of loci with either increased or decreased occupancy were observed. Interestingly, these age-related changes in

nucleosome occupancy occurred predominantly in distal regions of the genome (50-500 kb from TSSs) (Bochkis *et al.*, 2014). In contrast, we observed an increased nucleosome occupancy around TSSs of tNET genes (i.e. protein-coding, non-overlapping genes with sufficient coverage in our tNET-seq data). Important to note here is the difference between the assays employed: ATAC-seq maps accessible regions, while MNase-seq traces regions protected by nucleosomes. Thus, using ATAC-seq for nucleosome calling is inherently limited to nucleosomes flanking accessible regions and does not allow for drawing convincing conclusions about nucleosomes in distal regions of the genome.

Local chromatin dynamics are determined by two different modes of action for establishing permissive chromatin: nucleosome disassembly and nucleosome sliding. The former would involve full nucleosome disassembly in front of the elongating Pol II and reassembly in the wake of it. Such dynamic nucleosome eviction has been associated with highly transcribed genes (Lee et al., 2004; Schwabish and Struhl, 2004). Nucleosome sliding, on the other hand, is characterized by transcription through a remodeled nucleosome without full histone eviction. This has been observed both *in vitro* (Bintu et al., 2011; Kuryan et al., 2012) and *in vivo* (Gutierrez et al., 2017) and mechanistically linked to Pol II backtracking (Gaykalova et al., 2015). We observed an age-related increase in both nucleosome occupancy and nucleosome fuzziness. The former points towards alterations in nucleosome eviction, while the latter suggests changes in nucleosomal sliding.

How can this be reconciled with the increased promoter accessibility we observed at tNET genes in aged animals? Nucleosome occupancy and accessibility to DNA are not necessarily mutually exclusive. In fact, increased NDR accessibility does not automatically equate a decreased nucleosome occupancy in the surrounding regions. Promoters of genes activated by the unfolded protein response (UPR) in Drosophila S2 cells showed, as expected, increased accessibility upon activation. However, this was not accompanied by changes in nucleosome occupancy (Mueller et al., 2017). This lack of correlation between chromatin accessibility and nucleosome occupancy has been observed also in unperturbed Drosophila S2 cells using the same MNase titration approach (Mieczkowski et al., 2016). Another example of differential effects on nucleosome occupancy and chromatin accessibility was recently provided for polycomb group (PcG) proteins in mouse ESCs (King et al., 2018). PcG-bound promoters are characterized by low accessibility and high nucleosome occupancy. Expectedly, PRC1 depletion resulted in reduced nucleosome occupancy at target promoters (King *et al.*, 2018). On the other hand, PRC1 depletion did not influence chromatin accessibility at these promoters – they still exhibited lower levels of accessibility (King *et al.*, 2018). These observations further confirm that accessibility and nucleosome occupancy are not directly coupled and are controlled by distinct mechanisms. Thus, promoters often do not follow an

intuitively expected scenario of exhibiting high accessibility and low nucleosome occupancy. In fact, promoters are often characterized by both high nucleosome occupancy and high accessibility (Mieczkowski *et al.*, 2016; Voong et al., 2016). Salt fractionation to explore nucleosome stability revealed that promoter sites are enriched in the low-salt fraction, indicative of less stable nucleosomes (Mieczkowski *et al.*, 2016). Such differences in stability may be explained by differences in nucleosome composition. For instance, incorporation of the histone variants H3.3 and H2A.Z is known to destabilize nucleosomes (Jin and Felsenfeld, 2007). Hence, we would propose that the nucleosomes that are increasingly deposited with age are less stable.

Together, our data confirm that increased promoter accessibility cannot be simply attributed to decreased nucleosome occupancy. What, then, causes the age-related increase in promoter accessibility? Digestion of liver chromatin with restriction enzymes found ~45 % of promoter NDRs to be accessible, while the remaining promoter NDRs were protected (Chereji et al., 2019). What is the source of this protection of NDRs from restriction enzymes if not canonical nucleosomes? One possibility are fragile nucleosomes, which are highly dynamic, partially unwrapped nucleosomes in promoter regions (Chereji et al., 2016; Kubik et al., 2015). However, ChIP-exo and MNase-ChIP-seq experiments in yeast revealed that promoter NDRs are indeed histone-free (Rhee et al., 2014) and that the majority of promoters are occupied by MNase-sensitive, non-histone protein complexes (Chereji et al., 2017), challenging the existence of fragile nucleosomes (Kubik et al., 2017). Instead, so-called barrier complexes have been proposed to protect NDRs from restriction enzyme digestion (Chereji *et al.*, 2019). Candidates for these barrier complexes are chromatin remodelers or transcription factors like the TFIIIB-TFIIIC complex at tRNA genes (Nagarajavel et al., 2013). Unlike the uniform protection of DNA by canonical nucleosomes, barrier complexes could dynamically expose stretches of accessible DNA that would be digested. The stability of these complexes could be affected with age, yielding the age-related increase in promoter accessibility we observe in aged murine liver.

Consistent with our observations, promoter accessibility has been reported to poorly correlate with transcriptional activity (King *et al.*, 2018). Furthermore, digestion of liver chromatin with restriction enzymes found 58 % of the active and 32 % of the inactive promoters (defined by DNase I hypersensitivity) to be accessible (Chereji *et al.*, 2019). Thus, consistent with our observations, while promoter accessibility is required for transcription, an increase does not automatically enhance transcriptional output. Despite the increase in promoter accessibility, we observe only modest effects on both the nascent and steady-state transcriptome with age. This highlights that the expression levels of most genes are generally preserved in aged liver,

consistent with the notion that liver tissue seems to be more refractory to aging (Zhang *et al.*, 2021). To assess the sensitivity of cells within a tissue to aging, the authors computed aging scores based on scRNA-seq data from the Tabula Muris Consortium (Tabula Muris, 2020). Hepatocytes from different age groups exhibited similar aging scores, suggesting that their transcriptional programs are marginally affected by age (Zhang *et al.*, 2021). This is in contrast, for instance, to immune and stem cells that exhibited a stronger increase in aging scores, reflecting the higher turnover rates of these cell types.

We observed only a small overlap between differentially expressed and differentially transcribed genes upon aging, with more widespread changes identified in the nascent transcriptome. A similar discordance has been observed in total versus nuclear RNA-seq analyses of young and aged murine B precursor cells (Koohy *et al.*, 2018). Thus, changes in the nascent transcriptome might be buffered through post-transcriptional mechanisms affecting RNA stability. On the other hand, nascent transcription of other genes might not be altered by age; instead, altered post-transcriptional processes might result in the age-related differential expression of this second group of genes. This is consistent with complementary, unpublished single-cell data from our laboratory, highlighting the important contribution of post-transcriptional processes.

Despite the modest age-related effects on transcriptional output, we observed a strong decrease in promoter-proximal Pol II pausing. How can this age-related decrease in promoter-proximal Pol II pausing be explained? Focusing solely on the transcription process, we can envision three possible scenarios: A decrease in promoter-proximal Pol II pausing can be a consequence of a decreased initiation rate, or a decreased duration of pausing, or a combination of both.

Alterations in transcription initiation, including decreased Pol II loading or PIC assembly at the initiation site, would be detected as decreased promoter-proximal Pol II pausing. If less Pol II molecules are being loaded at the promoter, there will be less pausing. (t)NET-seq does not allow for directly quantifying initiating Pol II, since the nascent RNA needs to be at least 20 bp long for adapter ligation and unambiguous read alignment to the genome. Therefore, we adopted a different approach to assess transcription initiation. We focused on enhancer regions, which regulate transcription initiation levels by recruiting and stabilizing components of the PIC to the core promoter (Larke et al., 2021). Similar to the promoters, the enhancers also exhibited an age-related increase in accessibility, suggesting no decrease in enhancer activity with age. Consistent with this, eRNA production, which was the second proxy we used for enhancer activity, was not decreased with age. While we cannot directly assess initiation rates, our data point towards unaltered or increased, but not decreased initiation rates.

Alternatively, we can envision causal changes at the step of promoter-proximal Pol II pausing, i.e. an age-related decrease in Pol II dwell time. This could be caused by a more efficient pause release or a decreased stability of the pausing complex.

Assuming unaffected Pol II elongation speed, a more efficient pause release would be detectable as higher Pol II levels within gene bodies. However, we observed such an increase in gene-body Pol II only in a small subset of genes; in contrast, the decrease in pausing occurs on the majority of the analyzed genes. Furthermore, the decrease in pausing occurs even for genes that are downregulated with age, pointing towards an effect specific to the promoter-proximal region. Importantly, however, we cannot exclude the possibility of age-related changes in Pol II elongation speed. A faster Pol II elongation would result in shorter dwell times over any segment in the gene body, which would not be detected as increased Pol II levels in the gene body.

In addition to pause release, the stability of the pausing complex is crucial and is determined by the recruitment and association of NELF and DSIF with Pol II on the one hand and the dissociation of the pausing complex from chromatin on the other. We observed an age-elated decrease in the occupancy of the DSIF component SPT4 at tNET promoters. Hereby, we cannot distinguish between a reduced recruitment to or an increased dissociation from chromatin. How DSIF is recruited to Pol II remains enigmatic. A recent mass spectrometry analysis revealed that the proto-oncogene MYC recruits SPT5 to promoters, thereby promoting the assembly of SPT5 with Pol II and controlling the processivity of Pol II elongation complexes (Baluapuri et al., 2019). Furthermore, MYC also regulates pause release by recruiting the P-TEFb subunit CDK9 to promoters (Rahl *et al.*, 2010). Considering the link of MYC to inflammation and cancer (Greten and Grivennikov, 2019), it would be interesting to further explore its role in the context of aging and promoter-proximal Pol II pausing.

Besides an altered recruitment of the pausing factors, aging might affect the dissociation of the pausing complex from chromatin. SPT5 depletion using RNAi in Drosophila S2 cells led to a loss of promoter-proximal Pol II, without a release into productive elongation, suggesting increased levels of promoter-proximal transcription termination (Henriques *et al.*, 2018). This mirrors effects observed in NELF-depleted cells, where turnover of promoter-proximal Pol II was more rapid (Gilchrist *et al.*, 2010; Henriques et al., 2013; Shao and Zeitlinger, 2017). Thus, DSIF and NELF are central to regulating the stability of paused Pol II. Recent studies using rapid inducible protein depletion have provided an even more fine-grained view of the roles of DSIF and NELF. Acute SPT5 depletion led to destabilization and degradation of promoter-proximal Pol II (Aoi *et al.*, 2021; Hu et al., 2021). In contrast, acute NELF depletion triggered premature termination of promoter-proximally paused Pol II (Aoi *et al.*, 2020). Both of these distinct pathways result in removal of Pol II from chromatin. These lines of evidence

suggest that our results could be explained by a reduced stability of paused Pol II with age. It is currently actively debated on how much of the paused Pol II complex proceeds into productive elongation versus promoter-proximal termination (Core and Adelman, 2019; Price, 2018). Our results suggest an age-related shift of the balance towards promoter-proximal termination. Identifying the specific termination- and/or degradation-regulating factors was, however, beyond the scope of this work. Future work will elucidate the magnitude with which these contribute to the observed age-related decrease in promoter-proximal Pol II pausing. Of particular interest is the Integrator complex, whose RNA endonuclease activity has been implicated in promoter-proximal transcription termination (Elrod et al., 2019; Skaar et al., 2015). Notably, both NELF and DSIF can associate with the Integrator complex (Yamamoto et al., 2014).

What is the effect of promoter-flanking nucleosomes on promoter-proximal Pol II pausing? Intriguingly, we observed an increased nucleosome occupancy downstream of the TSSs of tNET genes. The +1 nucleosome has been reported to play a role in regulating Pol II pausing (Jimeno-Gonzalez *et al.*, 2015) by creating a second barrier downstream of the promoter-proximal pause site (Aoi *et al.*, 2020; Weber *et al.*, 2014). Pausing at this second pause site has been termed “intrinsic pausing” to distinguish it from the “regulated pausing” controlled by DSIF and NELF that occurs further upstream (Core and Adelman, 2019). Currently, it is not clear if and how the nucleosome-dependent, intrinsic pausing is regulated. However, the presence of the histone variant H2A.Z in the +1 nucleosomes correlates with decreased Pol II pausing, suggesting that H2A.Z decreases the nucleosomal barrier (Weber *et al.*, 2014). Furthermore, the promoter-flanking nucleosomes of highly paused genes are generally less stable, suggesting that paused Pol II destabilizes nucleosomes and/or causes partial histone exchange (Deal et al., 2010; Li and Gilmour, 2013; Teves and Henikoff, 2014). Consistent with our nucleoATAC results, we can envision a scenario in which the age-related decrease in promoter-proximally paused Pol II alters downstream nucleosome occupancy. Alternatively or in synergy, an increased nucleosome deposition with age might contribute to the destabilization of promoter-proximal Pol II. This could be further aggravated by age-related changes in the recruitment of histone chaperones that aid in Pol II passage through nucleosomes.

Overall, to explain the age-related decrease in pausing, we propose the following working model (Figure 27): With age, chromatin accessibility at promoters of protein-coding genes increases. This increase in chromatin accessibility could lead to an initial increase in transcription initiation and thus transcriptional output that we did not detect as it may have occurred at time points not assessed in our experiments. Such increase in transcriptional

output, when passing a threshold, might then trigger a negative feedback loop that impinges on the stability of the pausing complex to prevent further aberrant transcription and maintain transcription fidelity.

5. Conclusions and future directions

In this study, we characterize age-related changes in the local chromatin landscape of murine liver tissue and their link to transcriptional regulation. To the best of our knowledge, this is the first systematic inventory of the connection between aging, chromatin accessibility and transcriptional regulation directly *in vivo*, in a whole tissue. Addressing our initially posed research questions, we can conclude that:

How does aging affect the local chromatin landscape?

Aging of murine liver is accompanied by an increase in chromatin accessibility at promoter regions.

How do age-related chromatin changes influence transcriptional output?

While promoter accessibility is a requirement for transcription, increased accessibility does not automatically increase transcriptional output.

Age-related changes of the nascent and steady-state transcriptome are not unidirectional, suggesting that there is no global up- or down-regulation of transcription programs.

Age-related changes of the nascent transcriptome do not directly reflect the steady-state mRNA levels, highlighting the additional contribution of post-transcriptional regulation.

How does aging affect transcriptional regulation?

Aging is accompanied by a decrease in promoter-proximal Pol II pausing at protein-coding genes.

We propose that the decreased promoter-proximal Pol II pausing is due to a reduced stability of the pausing complex and may represent a mechanism to compensate for the age-related increase in accessibility in order to prevent aberrant transcription (Figure 27).

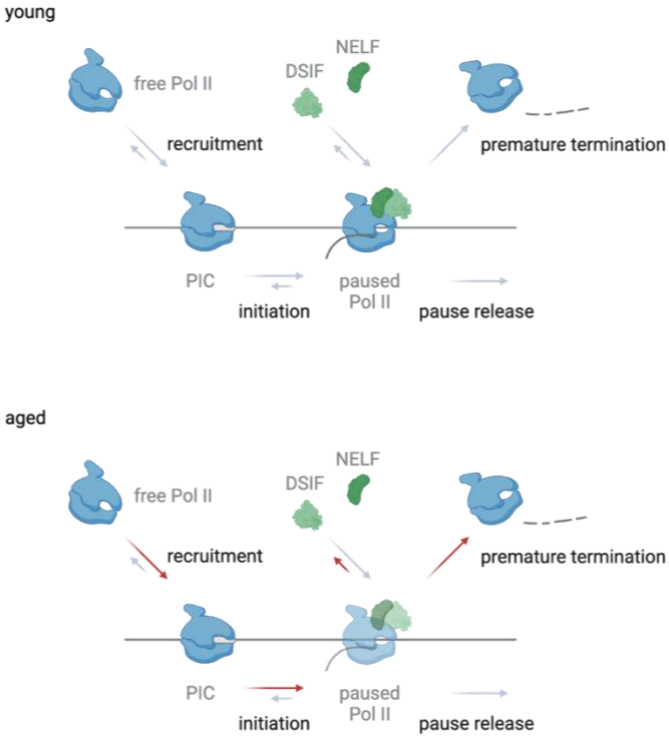

Figure 27. Model of age-related changes in promoter-proximal Pol II pausing in murine liver tissue. With age, chromatin accessibility at promoters of protein-coding genes increases, while promoter-proximal Pol II pausing decreases. We propose that a reduced stability of paused Pol II and increased rates of promoter-proximal termination maintain transcription fidelity and prevent aberrant transcription. Figure created with Biorender.

These intriguing findings raise exciting new questions:

Is the observed effect tissue-specific? Liver is a highly metabolic organ that is relatively resistant to age-related changes in transcription programs (Zhang *et al.*, 2021). Like hepatocytes, cardiomyocytes are also characterized by low turnover rates (Bergmann et al., 2015) and low aging scores (Zhang *et al.*, 2021). Thus, it would be interesting to characterize age-related changes in transcriptional regulation in another tissue, e.g. the heart, to address similarities and dissimilarities between two organs with similar aging scores.

How is Pol II recruitment to and transcription initiation at promoters affected by age? Given that (t)NET-seq does not provide a direct readout on transcription initiation, alternative methods (Start-seq, PRO-cap, ChIP-nexus) would be necessary to address this.

How is the shift in paused Pol II turnover regulated? Future experiments aimed at identifying these regulators should aid in better understanding the triggers of the age-related decrease in promoter-proximal Pol II pausing.

Do alterations in enhancer-promoter interactions contribute to the age-related decrease in Pol II pausing? Aging is accompanied by changes in enhancer-promoter interactions (Koohy *et al.*, 2018). Furthermore, eRNAs have been implicated in regulating promoter-proximal Pol II pausing (Gorbovytska *et al.*, 2021; Schaukowitch *et al.*, 2014; Shii *et al.*, 2017; Zhao *et al.*, 2016). Although we did not observe an age-related change in eRNA production, their delivery to and action at promoters might be altered with age.

Pharmacological inhibitors, which are widely used for mechanistic studies of transcription regulation, are not suitable for *in vivo* studies due to their toxicity and off-target effects. Additionally, metabolic RNA labeling approaches do not provide an immediate readout of nascent transcription. Future studies using CRISPR/Cas9 or the auxin-degron system to deplete pausing factors or other regulators will allow for dissecting causality of the observed effects. Complementing the *in vivo* work, alternative models (e.g. liver organoids) could be used to facilitate a faster manipulation.

6. Materials and Methods

6.1 Animals

Young (3-month-old), middle-aged (12-month-old) and aged (18-month-old) male C57BL/6N mice were used. Mice were provided with *ad libitum* standard rodent diet and water. Mice were bred and maintained in the mouse facility of the Max Planck Institute for Biology of Ageing according to ethical regulations and animal licenses of the State Office North Rhine-Westphalia, Germany (LANUV). Sacrificing and harvesting of tissue was performed by Dr. Peter Tessarz.

6.2 ATAC-seq

ATAC-seq libraries were prepared by Dr. Chrysa Nikopoulou following the Omni-ATAC protocol (Corces *et al.*, 2017), which employs an optimized transposition reaction to reduce the number of mitochondrial reads and improve the overall quality of the dataset. ATAC-seq libraries were prepared from liver tissue of three young and four aged biological replicates. Unless otherwise stated, the entire procedure was performed at 4°C or on ice.

Table 1. Buffers and reaction mixes for ATAC-seq. Nuclei EZ lysis buffer was purchased from Sigma-Aldrich (NUC101), Invitrogen™ Digitonin (5 %) from Thermo Fischer (BN2006), DNase I (RNase-free, 2,0000 U/ml) from NEB (M0303), NEBNext® High-Fidelity 2x PCR Master Mix from NEB (M0541), TD buffer and Tn5 transposase from Illumina (20034197), SYBR™ Green I from Thermo Fischer (S7563). For PCR primer sequences see Table 2.

Reaction mix/buffer	**Components**	
nuclei isolation buffer I	494 µl 55 µl 1 µl	nuclei EZ lysis buffer DNAseI buffer (10x) DNAse I
nuclei isolation buffer II	246.5 µl 27.5 µl 1 µl	nuclei EZ lysis buffer DNAseI buffer (10x) DNAse I
transposition reaction mix	25 µl 5 µl 5 µl 2.5 µl 12.5 µl	tagment DNA (TD) buffer (2x) digitonin (0.1 %) Tween-20 (1 %) Tn5 transposase 1x PBS
PCR mix	10 µl 10 µl 2.5 µl 2.5 µl 25 µl	transposed DNA nuclease-free water barcoded forward PCR primer (25 µM) barcoded reverse PCR primer (25 µM) NEBNext® High-Fidelity PCR Master Mix (2x)

qPCR mix	5 µl	PCR-amplified DNA
	4.41 µl	nuclease-free H2O
	0.25 µl	barcoded forward PCR primer (25 µM)
	0.25 µl	barcoded reverse PCR primer (25 µM)
	0.09 µl	SYBR™ Green I (100 x)
	5 µl	NEBNext® High-Fidelity PCR Master Mix (2x)

Nuclei were isolated from 50-100 mg of liver tissue. For this, samples were incubated with 500 µl of nuclei isolation buffer I (Table 1) for 15 min on ice. Then, 250 µl of nuclei EZ lysis buffer (Sigma-Aldrich) were added and samples were vortexed vigorously (4 cycles of 2 seconds “on” and 1 second “off”). After centrifuging the samples at 500 x g for 5 min, the pellets were incubated with 250 µl of nuclei isolation buffer II (Table 1) for 10 min on ice. Then, 500 µl of nuclei EZ lysis buffer (Sigma-Aldrich) were added and samples were vortexed vigorously as described above. After centrifuging the samples at 500 x g for 5 min, the pellets were incubated in 500 µl of nuclei EZ lysis buffer (Sigma-Aldrich) for 20 min on ice. Residual debris was removed by filtration through a 40-µm cell strainer followed by centrifugation at 500 x g for 5 min.

After washing the nuclei pellet with 1x PBS, nuclei were counted using a hemocytometer. 50-100 mg of liver tissue typically yielded 2-5 million nuclei. 50,000 nuclei were pelleted at 500 x g for 5 min. The permeabilized nuclei were resuspended in the transposition reaction mix (Table 1) and incubated at 37°C for 30 min. DNA was immediately purified using the DNA Clean & Concentrator™-5 kit (Zymo Research, catalog number D4013) and eluted in 10 µl sterile water. Transposed and purified DNA was PCR-amplified (Table 1) using barcoded PCR primers (Table 2) and the following program: 5 min at 72°C and 30 seconds at 98°C, followed by five cycles of 10 seconds at 98°C, 30 seconds at 63°C and 1 minute at 72°C.

To reduce GC and size bias in the final ATAC-seq libraries, the PCR amplification was stopped before saturation. For this, libraries were initially amplified for five cycles, after which a 5-µl aliquot of the PCR reaction (10 %) was used for qPCR (Table 1) using the following conditions: 30 seconds at 98°C, followed by 20 cycles of 10 seconds at 98°C, 30 seconds at 63°C and 1 minute at 72°C. After determining the optimal cycle number, the remaining 45 µl of the initial PCR reaction were amplified to the cycle number determined by qPCR. The number of additional cycles ranged from 5 to 7 cycles (i.e. 10 to 12 cycles in total).

Libraries were purified using the DNA Clean & Concentrator™-5 kit (Zymo Research, catalog number D4013) and eluted in 21 µl sterile water. Library quality was assessed on a 2200 TapeStation (Agilent Technologies). Libraries were sequenced in paired-end mode on an Illumina HiSeq 2500 platform. Following the initial sequencing (100-bp read length), an additional sequencing run (50-bp read length) was performed.

Table 2. Sequences of PCR primers used for ATAC-seq. Barcode sequence in the reverse primers is underlined.

Oligo name	**Sequence (5' to 3')**
Forward primer Ad1_noMX	AATGATACGGCGACCACCGAGATCTACACTCGTCGG CAGCGTCAGATGTG
Reverse primer Ad2.3	CAAGCAGAAGACGGCATACGAGATTTCTGCCTGTCTC GTGGGCTCGGAGATGT
Reverse primer Ad2.4	CAAGCAGAAGACGGCATACGAGATGCTCAGGAGTCT CGTGGGCTCGGAGATGT
Reverse primer Ad2.5	CAAGCAGAAGACGGCATACGAGATAGGAGTCCGTCT CGTGGGCTCGGAGATGT
Reverse primer Ad2.6	CAAGCAGAAGACGGCATACGAGATCATGCCTAGTCT CGTGGGCTCGGAGATGT
Reverse primer Ad2.7	CAAGCAGAAGACGGCATACGAGATGTAGAGAGGTCT CGTGGGCTCGGAGATGT
Reverse primer Ad2.8	CAAGCAGAAGACGGCATACGAGATCCTCTCTGGTCT CGTGGGCTCGGAGATGT
Reverse primer Ad2.9	CAAGCAGAAGACGGCATACGAGATAGCGTAGCGTCT CGTGGGCTCGGAGATGT

6.3 Tissue NET-seq (tNET-seq)

We modified the original NET-seq protocol (Mayer and Churchman, 2016) for application in murine liver tissue and named this new adaptation of the protocol tissue NET-seq (tNET-seq). In the following, our modifications are embedded in the original protocol from (Mayer and Churchman, 2016). Modified steps are highlighted in **yellow**. The entire procedure was performed on ice or at 4°C using RNase-free equipment.

Whole livers from 9 mice (3 per age group: young, middle-aged and aged) were processed immediately after sacrifice. The livers from young mice weighed between 1 and 1.5 g, while those from middle-aged and aged mice were heavier with 2-2.5 g.

tNET-seq reagents

Table 3. Buffers used for tNET-seq. All buffers were freshly prepared and pre-chilled on ice. Nuclei EZ lysis buffer and α-amanitin were purchased from Sigma-Aldrich, Halt™ protease inhibitor cocktail (100x) from Thermo Scientific and Recombinant RNasin® from Promega.

Buffer	**Components**
nuclei isolation buffer	nuclei EZ lysis buffer 1x Halt™ protease inhibitor cocktail 40 U RNasin® 25 μM α-amanitin
nuclei wash buffer	0.1 % (v/v) Triton X-100 1 mM EDTA 25 μM α-amanitin 40 U RNasin® 1x Halt™ protease inhibitor cocktail 1x PBS
glycerol buffer	20 mM Tris-HCl (pH 8.0) 75 mM NaCl 0.5 mM EDTA 50 % (v/v) glycerol 0.85 mM DTT 25 μM α-amanitin 10 U RNasin® 1x Halt™ protease inhibitor cocktail RNase-free H_2O
nuclei lysis buffer	1 % (v/v) NP-40 20 mM HEPES (pH 7.5) 300 mM NaCl 1 M urea 0.2 mM EDTA 1 mM DTT 25 μM α-amanitin 10 U RNasin® Halt™ protease inhibitor cocktail RNase-free H_2O
chromatin resuspension solution	25 μM α-amanitin 20 U RNasin® 1x Halt™ protease inhibitor cocktail 1x PBS
bind/wash buffer (2x)	5 mM Tris-HCl (pH 7.0) 2 M NaCl 1 mM EDTA 0.2 % (v/v) Triton X-100 RNase-free H_2O

Table 4. Oligonucleotide sequences used for tNET-seq library preparation. Illumina barcode sequences are underlined. rApp: 5'-adenylated ribonucleotide. $(N)_6$: random hexameric sequence. 3ddC: 3'dideoxycytosine. 5Phos: 5'-phosphate. iSp18: internal 18-atom hexa-ethylenglycol spacers.

Name	**Sequence (5' to 3')**
DNA linker	rApp$(N)_6$CTGTAGGCACCATCAAT3ddC
oGAB11 (RNA control oligo)	AGUCACUUAGCGAUGUACACUGACUGUG-OH
RT primer oLSC007	5Phos/ATCTCGTATGCCGTCTTCTGCTTG/iSp18/CACTCA/iSp18/TCCGACGATCATTGATGGTGCCTACAG
PCR forward primer MHL001	AATGATACGGCGACCACCGAGATCGGAAGAGCACACGTCTGAACTCCAGTCAC<u>TGCATC</u>TCCGACGATCATTGATGG
PCR forward primer MHL002	AATGATACGGCGACCACCGAGATCGGAAGAGCACACGTCTGAACTCCAGTCAC<u>ATGCCA</u>TCCGACGATCATTGATGG
PCR reverse primer (oNTI231)	CAAGCAGAAGACGGCATACGA
Sequencing primer (oLSC006)	TCCGACGATCATTGATGGTGCCTACAG

Tissue homogenization and cell fractionation

1-19| Place the fresh liver tissue in ice-cold PBS, cut into smaller pieces and homogenize in 3 ml of nuclei isolation buffer using a Dounce tissue homogenizer (Wheaton). After complete homogenization, transfer the sample to a Falcon tube. Add 3 ml of nuclei isolation buffer to the remaining pieces in the tissue homogenizer, homogenize further and transfer the remnants also to the tube. Following an incubation on ice for 5 min, pass the samples through a 70-μm cell strainer and collect the nuclei by centrifuging at 500 x g for 20 min.

Resuspend the nuclei pellet in 4 ml of nuclei isolation buffer. After incubation on ice for 5 min, collect the nuclei by centrifuging at 500 x g for 5 min. To remove cytoplasmic remnants, wash the nuclei pellet with 1600 μl nuclei wash buffer and centrifuge at 1,150 x g for 5 min. Repeat the washing with 800 μl nuclei wash buffer. Then, gently resuspend the pellet in 200 µl of glycerol buffer using a cut 1,000-µl tip and transfer the suspension to a new 1.5-ml RNase-free microcentrifuge tube. To lyse nuclei, add 400 µl of nuclei lysis buffer, mix samples by pulsed vortexing and incubate on ice for 20 min. After assessing nuclei lysis of a small aliquot under a light microscope, centrifuge the samples at 18,500 x g for 2 min. Completely remove the supernatant (nucleoplasmic fraction) and resuspend the chromatin pellet in 50 µl chromatin resuspension solution.

Preparation of nascent RNA

20| Add 700 µl of QIAzol lysis reagent (part of miRNeasy mini kit, Qiagen) to the resuspended chromatin from Step 19.

21| Mix thoroughly by slowly pipetting up and down using a 1-ml syringe with a 22G needle. Alternatively, the chromatin pellet can also be solubilized by gentle vortexing.

Caution: Be aware that the QIAzol lysis reagent contains phenol. Handle solutions with care and according to institutional regulations.

Critical step. Mix very carefully until the solution is homogeneous. Mix it slowly to avoid spilling the sample.

22| Prepare RNA using the miRNeasy mini kit according to the manufacturer's instructions, including the optional on-column DNase treatment using the RNase-free DNase set (Qiagen).

23| Elute the nascent RNA in 25 µl RNase-free H_2O. Assess the quantity and quality of the prepared RNA using NanoDrop 2000 (Thermo Scientific). RNA yield from one whole liver typically ranged from 10 to 56 µg. The absorbance A260/A280 ratios were around 2.1.

Barcode DNA linker ligation

24| Denature the RNA sample from Step 23 and 5 µl of the ligation control oligonucleotide oGAB11 (10 µM) for 2 min at 80 °C in a Thermomixer.

25| Prepare DNA linker ligation mix for each RNA sample and for oGAB11 in 0.2-ml RNase-free PCR tubes (Table 5). Prepare three ligation reactions per RNA sample and for the oGAB11 ligation control; the RNA input per ligation reaction is 1 µg.

Critical step. Before adding the truncated T4 RNA ligase 2, it is important to mix the ligation reaction until it is homogeneous. Next, add the ligase and mix again. Incompletely mixed samples will negatively affect the ligation efficiency.

26| Incubate the ligation mixes for 15 min at 37°C and then overnight at 16°C.

27| Add 0.7 µl of EDTA (0.5 M) to each ligation mix to stop the ligation reaction. Merge the 3 RNA ligation reactions.

Table 5. Composition of the DNA linker ligation reactions.

Component	Amount per reaction (µl)		Final
	RNA sample	oGAB11 control	
PEG8000 (50% v/v)	8.0	8.0	20% (v/v)
DMSO	2.0	2.0	10 % (v/v)
T4 RNA ligase buffer (10x)	2.0	2.0	1x
Barcode DNA linker (1 µg)	1.0	1.0	
RNA sample (1 µg)	6.0	-	
oGAB11 (10 µM)	-	1.0	0.5 µM
RNase-free H_2O	-	5.0	
Truncated T4 RNA ligase 2	1.0	1.0	200 U

RNA fragmentation

28| Prior to RNA fragmentation, precipitate the RNA to remove PEG, which can affect the fragmentation reaction.

1. To each sample, add 60 µl of 3 M sodium acetate, 2 µl GlycoBlue (15 mg/ml) and 600 µl of 100 % ethanol.
2. Incubate the samples at -80°C for 45 min.
   Pause point. The precipitations can be left at −80°C overnight.
3. Centrifuge the samples for 30 min at full speed.
4. Wash the samples twice with 500 µl of each 100 % ethanol and 70 % ethanol.
5. Air-dry the pellets for 5 min and resuspend in 20 µl sterile water (10 µl for oGAB11 ligation control).

Following precipitation, add 20 µl of 2× alkaline fragmentation solution to each sample and mix. Please note that Steps 28 and 29 are not performed for the oGAB11 ligation control.

29| Fragment the RNA at 95 °C in a thermal cycler for 20 min.

Critical step. The fragmentation time needs to be adjusted whenever a new batch of alkaline fragmentation solution is applied. An over-fragmentation or under-fragmentation of the nascent RNA pool can lead to systematic biases. In a typical experiment RNA is fragmented

between 10 and 40 min at 95 °C. The optimal fragmentation time is when most RNA molecules are in the required size range, usually between 35 and 100 nt.

30-35| Following fragmentation, precipitate the RNA and the oGAB11 ligation control as described above (step 28).

36| Add 20 µl of 2× TBE-urea denaturing sample buffer to each RNA sample and mix it.

37| Prepare the RNA control ladder and the oGAB11 control. Add 1.0 µl 0.5 µl of RNA control ladder or 1 µl oGAB11 to 9 µl of RNase-free H_2O. Add 10 µl of 2× TBU denaturing sample buffer to each control sample and mix it.

38| Denature the RNA sample and RNA control samples (oGAB11 ligation control, ladder and oGAB11) for 2 min at 80°C. Cool the samples on ice for 3 min.

39| Pre-run a 15% (wt/vol) polyacrylamide TBE-urea gel at 200 V for 15 min in 1× TBE.

40| Separate the fragmented RNA samples and the RNA control samples (including the oGAB11 ligation control) by PAGE at 200 V for 65 min.

41| Stain the gel in 50 ml of gel staining solution for 5 min at room temperature on a shaker. Protect the gel from light during staining by the use of a black gel box.

42| Visualize the fragmented RNA and the oGAB11 ligation control under blue light. For the fragmented RNA, excise the region between 35 (in the middle of the dye front) and 100 nt. For the oGAB11 ligation control, excise the narrow band at ~55 nt.

43| Extract the RNA from the gel slice by rapid gel extraction:

1. Pierce the bottom of a 0.5-ml RNase-free microcentrifuge tube with a 23G needle.
2. Put the pierced 0.5-ml tube in a 1.5-ml RNase-free microcentrifuge tube.
3. Combine and place the gel slices for each sample into the inner pierced 0.5-ml tube.
4. Centrifuge the mixture at 20,000g for 4 min at room temperature.
5. Add 200 µl RNA recovery buffer (Zymo Research, R1070-1-10) to the excised gel slices.
6. Incubate the sample for 15 min at 70°C in a Thermomixer (1500 rpm).
7. Vortex the mixture for 30 s at a medium intensity setting.
8. Cut the tip off of a 1,000-µl pipette tip and transfer the gel slurry into a Zymo-Spin IV Column (Zymo Research, C1007-50).
9. Freeze for 2 min at -80°C and subsequently thaw by placing at 70°C for 1 min.
10. Centrifuge the mixture at 20,000g for 30 sec at room temperature.
11. The expected eluate volume is ~200 µl.

44-45| Precipitate the RNA by adding 90 µl of 3 M sodium acetate, 2 µl GlycoBlue (15 mg/ml) and 900 µl of 100 % ethanol. Proceed as described above (step 28).

46| Re-suspend the size-selected RNA and the oGAB11 ligation control in 10 µl of pre-cooled RNase-free H_2O.

cDNA synthesis by reverse transcription

47-51| Synthesize cDNA using the SuperScript™ III First-Strand Synthesis System (Thermo Fischer) following the manufacturer's instructions. In brief, add 0.8 µl dNTPs (10 mM) and 0.5 µl of the reverse primer oLSC007 (10 µM, Table 4) to 10 µl of RNA sample and to the oGAB11 control. After incubating at 80°C in a thermal cycler for 2 min and cooling on ice for 3 min, add 10 µl of cDNA synthesis mix consisting of 2 µl of 10x RT buffer, 4 µl of 25 mM $MgCl_2$, 2 µl of 0.1 M DTT, 1 µl of RNaseOUT™ (40 U/µl) and 1 µl of SuperScript® III RT (200 U/µl) to each sample.

52| Incubate the mixture for 30 min at 48°C in a thermal cycler.

53| Add 1.8 µl of 1 N NaOH, mix well and incubate the reaction for 20 min at 98°C.

54| Neutralize the reaction by adding 1.8 µl of 1 N HCl; mix well and put the reaction on ice.

55| Add 20 µl of 2× TBU denaturing sample buffer to each cDNA sample and the oGAB11 cDNA control, and then mix.

56| Prepare the DNA control ladder. Add 1.0 µl of DNA control ladder to 9 µl of RNase-free H_2O. Add 10 µl of 2× TBU denaturing sample buffer to the ladder and mix.

57| Denature the cDNA sample, oGAB11 cDNA control and DNA control ladder for 3 min at 95°C in a Thermomixer. Cool the samples on ice for 3 min.

58| Pre-run a 10% (wt/vol) polyacrylamide TBE-urea gel at 200 V for 15 min in 1× TBE.

59| Separate the cDNA sample, the oGAB11 cDNA control and the DNA ladder by PAGE at 200 V for 65 min.

60| Stain the gel in 50 ml of gel staining solution for 5 min at room temperature on a shaker. Protect the gel from light during staining by the use of a black gel box.

61| Visualize the gel under blue/UV light and excise the cDNA between 85 and 160 nt.

62| Extract the cDNA from the gel slice by rapid gel extraction (see step 43). To 200 µl eluate, add 25 µl of 5 M NaCl and mix.

63-65| Precipitate the cDNA by adding 2 µl GlycoBlue (15 mg/ml) and 750 µl of 100 % ethanol. Proceed as described above (step 28). Resuspend cDNA and oGAB11 control cDNA in 15 µl of pre-cooled RNase-free H_2O each.

Pause point. The cDNA can be stored indefinitely at −20°C.

Circularization of cDNA

66| Prepare circularization mix (Table 6) and store it on ice.

67| Add 4 µl of circularization mix to 15 µl of cDNA sample and the oGAB11 cDNA control sample in a 0.2-ml RNase-free PCR tube, and then mix well.

68| Add 1 µl of CircLigase (100 U/µl) and mix.

Table 6. Composition of the cDNA circularization reactions.

Component	Amount per reaction (µl)	Final
CircLigase reaction buffer (10x)	2.0	1x
ATP (1 mM)	1.0	50 µM
$MnCl_2$ (50 mM)	1.0	2.5 mM

69| Incubate the CircLigase reaction for 60 min at 60°C and for 10 min at 80°C in a thermal cycler.

Pause point. Circularized cDNA can be stored indefinitely at −20°C.

Specific depletion of highly abundant mature RNAs

70| For depletion of the 20 most abundant chromatin-associated mature RNAs (Table 7), prepare one specific depletion reaction per sample in 0.2-ml DNase-free PCR tubes (Table 8). Please note that the oGAB11 control sample is not subjected to the depletion procedure.

71| Perform subtractive hybridization in a thermal cycler (Table 9).

72| Prepare Dynabeads MyOne streptavidin C1 (10 mg/ml) at room temperature.

1. Re-suspend the beads by gentle vortexing.
2. Transfer 100 µl of beads per depletion reaction to a DNase-free 1.5-ml microcentrifuge tube.
3. Place the tube on a magnetic rack for 1 min and withdraw all of the supernatant from the tube.
4. Remove the tube from the magnetic rack and re-suspend beads in 100 µl of bind/wash buffer.
5. Repeat this washing procedure (steps 3 and 4) two more times.
6. Place the tube on a magnetic rack for 1 min and withdraw the supernatant from the tube.
7. Remove the tube from the magnetic rack and re-suspend the beads in 30 µl of bind/wash buffer.
8. Transfer 25 µl of the re-suspended and washed beads to a new tube.
9. Place the tube in a Thermomixer at 37°C to equilibrate for 15–30 min.

73| Transfer 40 µl of depletion reaction directly from the 0.2-ml PCR tube in the thermal cycler (from Step 71) to the washed and equilibrated beads in the Thermomixer. Immediately mix by pipetting.

Table 7. Depletion oligonucleotides for the 20 most abundant chromatin-associated mature RNAs captured in NET-seq libraries from mESCs cells. Biotinylated oligonucleotides were purchased from Sigma Aldrich in HPLC quality.

Gene	Transcript type	DNA sequence (5' to 3')
Snord49a	snoRNA	AGTCAGCCAGGAGCAGTTATCGTCAGTTATCGAC
Rn45s	rRNA	GAGAGCCGCCCGAACGACCGACTTCCCTACGGGCCC
Snord65	snoRNA	CTTCAGAAAACCATAGGCTCACCACTACCAATCT
Snord82	snoRNA	GAACCATGGGGTTGAAATGAAATATGCTGATGTGCT
Snord49b	snoRNA	GTCAGCTAACTAGGGATGTCGTCAGTTGTCGCAT
Snord2	snoRNA	AGTGATCAGCAAGAGTATTCTCTTCATTTCAGGTCA
Snord99	snoRNA	TCTCAGTCCCATATCCGCATTTCTCATCCATAGA
Snord95	snoRNA	CAGCTCAGAAACAGCCTCTGGATTTCAGCAAAGCAA
Snord55	snoRNA	CGTGGGGAAGCCAACCTTGGAGAGCTGAGCGTGC
Snord68	snoRNA	CATCAGATGGAAAAGGGTTCAAAAGTACTTTCAT
Snord32a	snoRNA	GACTGTGAGATCAACCCATGCACCGCTCTGAGACTC
Snord87	snoRNA	GTTTCTTTGAAGAGAGAATCTTAAAAGACTGAGA
Rmrp	ncRNA	CGCACCAACCACACGGGGCTCATTCTCAGCGCGGCTAC
Snord100	snoRNA	CTCGCTGAGGAAACTGCACGTCACCCTCCTGAAA
Snora68	snoRNA	GTGCAGTGCCCCCCAGAGTGAATCAGTAGGCTCTACAGAA
Rnu3a	snRNA	AACCACTCAGACTGTGTCCTCTCCCTCTCAACCCTCAA
Snord42b	snoRNA	GAGACCTGTGATGTCTTCAAAGGAACCACTGATG
Snord83b	snoRNA	TGAGGAATTATTCCCTGTTGCCTTCCTTCTGAGA
Snord110	snoRNA	TTGCTCAGACACATGGAGTCGTCAGTGATCTCTCAGGG
Snord47	snoRNA	CCTCAGAAATAAAATGGAACGGTTTAAAGGTGAT

Table 8. Composition of the depletion reactions.

Component	**Amount per reaction (µl)**	**Final**
Circularization reaction (from step 69)	20	
Depletion DNA oligo pool	4.0	1 µM
SSC, 20x	4.0	2x
DNase-free H_2O	12.0	

Table 9. Parameters for depletion of highly abundant mature RNAs.

	Temperature	**Time**
Denature	99°C	90 s
Annealing	99-37°C in 0.1°C steps	1s (per 0.1°C step)
Final annealing	37°C	15 min

74| Incubate the mixture in the Thermomixer for 15 min at 37°C with mixing at 1,000 rpm.

75| Transfer the tubes from the Thermomixer into a magnetic rack and leave them for 1 min. Transfer the supernatant into a new 1.5-ml microcentrifuge tube.

Critical step. The supernatant needs to be transferred carefully. Any remaining magnetic beads in the supernatant will have a negative impact on subsequent steps.

76-79| Precipitate the oligo-depleted, circularized cDNA by adding 6 µl of 5 M sodium chloride, 2 µl GlycoBlue (15 mg/ml) and 250 µl of 100 % ethanol. Proceed as described above (step 28). Resuspend the cDNA in 10 µl sterile water.

Pause point. DNA can be stored indefinitely at −20°C.

PCR amplification of the cDNA sequencing library

80| Prepare PCR mix for four pilot PCR amplification reactions for both the cDNA sample and the oGAB11 control cDNA sample (Table 10). Mix well and store it on ice.

81| For each PCR, put 19 µl of PCR master mix in a 0.2-ml RNase-free PCR tube.

82| Add 1 µl of circularized cDNA and mix it well.

83| Perform PCR pilot amplifications (Table 11). Remove one PCR tube for each sample at the end of the extension step after 6, 8, 10 and 12 cycles.

Table 10. Composition of PCR amplification reactions.

Component	**Amount for 4 reactions (µl)**	**Final**
Phusion HF buffer (5x)	15.2	1x
dNTPs (10 mM)	1.5	0.2 mM
Forward primer (Ilumina index primer, 100 µM)	0.4	0.5 µM
oNTI231 (reverse primer, 100 µM)	0.4	0.5 µM
DNase-free H_2O	57.6	
Phusion DNA polymerase (2 U/µl)	0.9	1.8 U

Table 11. Parameters for PCR amplification.

Cycle number	**Denature**	**Anneal**	**Extend**
1	98°C, 30s		
2-14	98°C, 10 s	60°C, 10 s	72°C, 5 s

84| Add 3.4 µl of 6× DNA loading dye to each tube and mix well.

85| Prepare DNA control ladder. Add 1.0 µl of DNA control ladder to 9 µl of DNase-free H_2O. Add 2 µl of 6× DNA loading dye and mix well.

86| Separate the PCR products and the DNA control ladder by TBE gel electrophoresis on an 8% (wt/vol) TBE gel at 180 V for 55 min.

87| Stain the gel in 50 ml of gel staining solution for 5 min at room temperature on a shaker. Protect the gel from light during staining by the use of a black gel box.

88| Visualize the gel under blue/UV light and identify the optimal PCR amplification cycle for each cDNA sequencing library. The NET-seq library runs at ~150 nt. The optimal PCR amplification cycle is characterized by a clear band at ~150 nt and the absence of PCR products at the higher-molecular-weight range.

89| Perform four PCR amplification reactions per sample with the optimal amplification cycle. The oGAB11 control sample is not subjected to amplification. Add 6 µl of 6× DNA loading dye to each sample and mix well. Separate the PCR products by TBE gel electrophoresis on a 4% (wt/vol) low melt agarose gel at 80 V for 2 h.

90| For each sample, excise the band that contains the PCR product from the gel.

Critical step. Excise the broad band at ~150 nt. Avoid contamination from the lower band that runs at ~120 nt, representing PCR product from empty circles. Empty circles are circularized

cDNA molecules that arise from unextended RT primers, and hence they do not contain any information about the original nascent RNA.

91-101| Purify the final NET-seq library using the Nucleospin™ Gel and PCR Clean-up kit (Macherey-Nagel) according to the manufacturer's instructions. Elute in 10 µl of Tris-HCl (10 mM, pH 8.0).

Pause point. The DNA sequencing library can be stored indefinitely at −20°C.

Quantification and characterization of the NET-seq library

102| Prepare a 1:5 dilution of the NET-seq library by adding 1 µl of the NET-seq library to 4 µl of Tris-HCl (10 mM, pH 8.0); mix well.

103| Use 1 µl of the diluted NET-seq library for quantification with the Qubit fluorometer using the Qubit dsDNA HS assay kit. Prepare the sample and perform the measurement according to the manufacturer's protocol.

104| Use 1 µl of the diluted NET-seq library for characterization on the Agilent Bioanalyzer; use the high-sensitivity DNA analysis kit according to the manufacturer's instructions.

105| Sequence the human NET-seq library from the 3′ end on the Illumina platform using oLSC006 (Table 4) as a custom sequencing primer.

tNET-seq libraries were sequenced on an Illumina HiSeq 2500 platform (75-bp single-end reads).

6.4 ChIP-seq

The ChIP-seq procedure was optimized for application in murine liver tissue by Dora Grbavac. ChIP-seq libraries were prepared from two independent biological replicates per age group (young and aged). Unless otherwise stated, the entire procedure was performed at 4°C or on ice.

ChIP buffers

Table 12. Composition of ChIP buffers. Protease inhibitors (leupeptin, pepstatin, PMSF) and HDAC inhibitors (sodium butyrate) were freshly added.

Buffer	**Composition**
lysis buffer	50 mM Hepes pH 7.9 140 mM NaCl 1 mM EDTA 10 % glycerol 0.5 % NP-40 0.25 % Triton x-100 0.5 µg/ml leupeptin 0.7 µg/ml pepstatin A 0.5 mM PMSF 5 mM sodium butyrate
wash buffer	10 mM Tris pH 8.1 200 mM NaCl 1mM EDTA 0.5mM EGTA 0.5 µg/ml leupeptin 0.7 µg/ml pepstatin A 0.5 mM PMSF 5 mM sodium butyrate
shearing buffer	0.1 % SDS 1 mM EDTA 10 mM Tris pH 8.0 0.5 µg/ml leupeptin 0.7 µg/ml pepstatin A 0.5 mM PMSF 5 mM sodium butyrate
IP buffer	1 % Triton 0.1 % SDS 1 mM EDTA 10 mM Tris pH 8.0 150 mM NaCl
TSE-150 buffer	1 % Triton 0.1 % SDS 2 mM EDTA 20 mM Tris pH 8.0 150 mM NaCl

TSE-500 buffer	1% Triton 0.1% SDS 2 mM EDTA 20 mM Tris 8.0 500 mM NaCl
LiCl buffer	0.25 M LiCl 1 % NP-40 1 % sodium deoxycholate 1 mM EDTA 10 mM Tris pH 8.0
TE buffer	1mM EDTA 10 mM Tris pH 8.0
PK digestion buffer	20 mM Hepes pH 7.5 1 mM EDTA pH 8.0 0.5 % SDS

Tissue crosslinking

Freshly harvested liver tissue was washed four times with ice-cold 1x PBS (Gibco), cut on ice into small pieces and washed three more times with 1x PBS. The tissue was then crosslinked with 1 % formaldehyde (Carl Roth) and homogenized in a pre-chilled Dounce tissue homogenizer (Wheaton) using a loose pestle (15 strokes). After incubation for 10 minutes rocking at room temperature, the crosslinking reaction was quenched with the addition of glycine to a final concentration of 0.125 M. After incubation for 5 minutes rocking at room temperature, the samples were centrifuged at 3,260 x g for 5 minutes and the supernatant was discarded.

Cell lysis, chromatin extraction and sonication

300 mg of cross-linked tissue were lysed in 2 ml lysis buffer (Table 12) and homogenized in a pre-chilled Dounce tissue homogenizer (Wheaton) using both a loose and tight pestle (15 strokes each). After addition of 10 ml of lysis buffer (Table 12), the samples were incubated on ice for 20 minutes and centrifuged at 3,260 x g for 5 minutes. Nuclei pellets were washed by resuspending twice in 10 ml wash buffer (Table 12) and centrifuging at 3,260 x g for 5 min, and then washing with 4 ml shearing buffer (Table 12) without disturbing the pellet. Then, pellets were resuspended in 2 ml shearing buffer and sonicated using a Focused Ultrasonicator M220 (Covaris). Sonication was performed in two rounds using both mild and intense sonication conditions (Table 13). Between sonication rounds, samples were centrifuged at 1,500 x g for 5 minutes.

Table 13. Sonication parameters used for ChIP experiments.

Program	Peak power	Duty Factor	Cycles/Burst	Average Power	Temperature Range
Mild	75	10.0	200	10.0	5-7°C
Intense	75	25.4	200	19.1	5-7°C

After sonication, cellular debris was precipitated by centrifugation at 14,000 x g for 20 minutes. Aliquots of clear supernatant were taken as sonication quality control (100-µL aliquot) as well as ChIP input control (10 µg of chromatin).

Sonication efficiency was assessed by reverse crosslinking a 100-µl aliquot of sonicated chromatin. For this, RNA remnants were first degraded by incubating with 3 µl of RNase A (1 mg/ml stock, DNase-free, Thermo Fischer Scientific) at 37°C for 30 min. Then, proteins were digested by incubating with 5 µl proteinase K (1 mg/ml stock, Thermo Fischer Scientific) at 50°C for 30 minutes. After addition of NaCl to a final concentration of 0.3 M, samples were incubated at 65°C overnight. DNA was then purified using the Nucleospin Gel and PCR Clean up kit (Macherey-Nagel) by following the manufacturer's instructions with slight modifications. After adding 5 volumes of buffer NTB, samples were centrifuged at 11,000 x g for 30 seconds and washed twice with 650 µl NT3 buffer. Buffer remnants were removed by centrifuging at 11,000 x g for 1 minute. DNA was eluted by adding 25 µl UltraPure water (Gibco), incubating for 1 min at room temperature and centrifuging at 11,000 x g for 1 minute. DNA concentrations were measured on a NanoPhotometer N60/50 (Implen) using UltraPure water as a blank. The size distribution of sheared chromatin was visualized on a 2200 TapeStation (Agilent Technologies).

Immunoprecipitation

After confirming efficient sonication, crosslinked samples were immunoprecipitated. For this, 25 µg of DNA were combined with 1 % Triton X-100 and 150 mM NaCl (final concentrations). SPT4 antibody (Cell Signaling Technology, catalog number: 64828, lot number: 1) was then added according to the manufacturer's recommendations (1:100 dilution). For spike-in normalization, 40 ng of *Drosophila melanogaster* spike-in chromatin and 2 µg spike-in antibody (Active motif, catalog number: 616886, lot number: 00419007) were added to the IP reactions, along with the experimental chromatin and antibody. Samples were incubated rotating at 4°C overnight.

Magnetic protein G Dynabeads (Invitrogen) were equilibrated by washing three times with IP buffer. The immunoprecipitation reactions were then incubated with the beads at 4 °C for 90 minutes. The beads were subsequently washed twice with each TSE-150 and TSE-500 buffer and once with each LiCl and TE buffer. The beads were then incubated in 45 µl PK digestion buffer supplemented with 3 µl RNAse A (1 mg/ml stock, DNAse free, Thermo Fischer Scientific) at 37°C for 30 minutes. After addition of 5 µl proteinase K (1 mg/ml stock, Thermo Fischer Scientific), samples were incubated at 50°C for 30 minutes with periodic vortexing. Reverse crosslinking for both input control and ChIP samples was performed by adding NaCl to a final concentration of 0.3 M to the supernatant and incubating at 65°C overnight. DNA was purified using the Nucleospin Gel and PCR Clean up kit (Macherey-Nagel) as described above and eluted in 45 µl UltraPure water (Gibco).

Library preparation

Library preparation was performed as previously described (Ford et al., 2014) with slight modifications. In brief, 20 µl of ChIP DNA were incubated with end-repair mix (Table 14) at 20°C for 30 min. Reactions were purified by incubating with 90 µl (per 50-µl reaction, i.e. 1.8x) AMPure XP beads (Beckman Coulter) at room temperature for 5 min. Using a magnetic rack, beads were washed twice with 200 µl of 70 % EtOH and air-dried at room temperature for 3 minutes. Fragments were eluted by incubating with 22 µl of UltraPure water (Gibco) at room temperature for 5 minutes. End-repaired DNA was then incubated with A-tailing mix (Table 14) at 37°C for 30 minutes. After terminating the reaction at 70°C for 5 minutes, adapters were ligated to the A-tailed DNA by incubating with adapter ligation mix (Table 14) at 30°C for 15 minutes. 5.5 µl of 0.5 M EDTA (pH 8.0, Invitrogen) were added to terminate the ligation reaction. DNA fragments were purified by adding 108 µL AMPure XP beads (per 60-µl reaction, i.e. 1.8x), washing twice as described above and eluting in 24 µl UltraPure water. Adapter-ligated DNA was PCR-amplified according to the following program: 45 seconds at 98°C, followed by 17 cycles of 15 seconds at 98°C, 30 sec at 63°C and 30 sec at 72°C and a final extension for 60 seconds at 72°C. Subsequently, double-sided size selection (~200-650 bp) was performed by adding 20 µl AMPure XP beads (per 40-µl PCR reaction, i.e. 0.5x) and incubating for 5 minutes. After placing samples on a magnetic rack, the supernatant was transferred to a new 1.5-ml tube and 12 µl AMPure XP beads (i.e. 0.3x) were added to the supernatant. After a 5-minute incubation, beads were washed twice with 200 µL of 85 % EtOH and air-dried. DNA was eluted in 24 µl UltraPure water. After assessing fragment size distribution on a 2200 TapeStation (Agilent Technologies), libraries were pooled together to a final concentration of 3 ng/µl each and sequenced on an Illumina Hi-Seq 2500 platform (paired-end, 50-bp reads).

Table 14. Composition of reaction mixes used for ChIP-seq library preparation. All components were purchased from NEB: T4 DNA polymerase (catalog number: M0203S), Klenow fragment (3' → 5' exo-) (catalog number: M0212S), T4 Polynucleotide Kinase (PNK, catalog number: M0201S), Quick Ligation™ Kit (catalog number: M2200S), Deoxynucleotide Solution Set (catalog number: N0446S).

Buffer	**Components**	
end-repair mix	20 µl 5 µl 5 µl 2 µl 0.5 µl 17.5 µl	ChIP DNA NEB T4 DNA ligase buffer (without ATP) ATP (10 mM) dNTPs (10 mM) end repair enzyme mix (5 µl T4 DNA polymerase, 1 µl Klenow fragment, 5 µl T4 PNK) H_2O
A-tailing mix	16.5 µl 2 µl 1 µl 0.5 µl	end-repaired DNA NEB buffer 2 (10x) dATP (4 mM) Klenow fragment (5 U/ µl)
adapter ligation mix	20 µl 27.25 µl 2.5 µl 1 µl 3.75 µl	A-tailed DNA Quick ligase reaction buffer (2x) NEXTflex™ adapters (1:10) Quick ligase (2000 U/ µl) H_2O
library amplification PCR mix	19 µl 1 µl 20 µl	DNA PCR primer mix HiFi HotStart Kapa Mix (2x)

Table 15. Oligonucleotide sequences used for ChIP-seq library preparation. Barcode sequence is underlined. For details on the barcode sequences see Table 16.

Name	**Primer sequence (5'-3')**
PCR Primer 1	AATGATACGGCGACCACCGAGATCTACAC
PCR Primer 2	CAAGCAGAAGACGGCATACGAGAT
NEXTflex™ DNA-seq adapter	AATGATACGGCGACCACCGAGATCTACACTCTTTCCCTACACGACGCTCTTCCGATCTGATCGGAAGAGCACACGTCTGAACTCCAGTCAC<u>XXXXXX</u>ATCTCGTATGCCGTCTTCTGCTTG

Table 16. Barcode sequences of the NEXTflex™ DNA-seq adapters used for multiplexing ChIP-seq libraries. These barcodes are compatible with Illumina® platforms.

Barcode adapter	**Index region of barcode adapter**
1	CGATGT
2	TGACCA
3	ACAGTG
4	GCCAAT
5	CAGATC
6	CTTGTA
7	ATCACG
8	TTAGGC
9	ACTTGA
10	GATCAG
11	TAGCTT
12	GGCTAC
13	AGTCAA
14	AGTTCC
15	ATGTCA
16	CCGTCC
17	GTAGAG
18	GTCCGC
19	GTGAAA
20	GTGGCC
21	GTTTCG
22	CGTACG
23	GAGTGG
24	GGTAGC

6.5 Computational analyses

Primary data processing

Primary sequencing data was quality controlled using FastQC (v 0.11.5).

Single-end tNET-seq reads were trimmed to 50-bp length using cutadapt (v 1.13) and the six 5'-end nucleotides corresponding to the random molecular barcode were removed from the sequencing reads. Note that the information of the barcode sequence remained associated with the sequencing read, which is crucial for identifying reads arising from reverse transcription mispriming and PCR duplication events (see below). Then, sequencing reads were aligned to the GRCm38 (Ensembl release 99) reference genome using STAR (v. 2.7.3a) (Dobin et al., 2013) with the following parameters: –clip3pAdapterSeq ATCTCGTATGCCGTCTTCTGCTTG –clip3pAdapterMMp 0.21 –clip3pAfterAdapterNbases 1 –outFilterMultimapNmax 101 –outSJfilterOverhangMin 3 1 1 1 –outSJfilterDistToOtherSJmin 0 0 0 0 –alignIntronMin 11 –alignEndsType EndToEnd. To avoid alignment biases in favor of annotated genomic regions, the alignment was performed without providing transcriptome annotation data. Using custom Python scripts (adapted from https://github.com/BradnerLab/netseq), the data was further processed to filter out reads from the following three categories: (i) reverse transcription mispriming events, identified as perfect matches between the molecular barcode sequence and the genomic sequence adjacent to the aligned read, (ii) PCR duplicates, i.e. reads with identical barcodes aligning to the same genomic position, and (iii) reads aligned precisely to the 3' ends of introns and exons, which originate from splicing intermediates that carry 3' hydroxyl groups and are thus susceptible to adapter ligation.

Paired-end ATAC-seq reads were trimmed to remove Tn5 transposase adapter sequence using cutadapt (v 1.13) with the parameter –minimum-length=20. Reads were then aligned to the GRCm38 reference genome (Ensembl release 99) using Bowtie2 (v 2.4.1) (Langmead and Salzberg, 2012) by enabling soft clipping (--local) and the alignment of fragments up to 2 kb (-X 2000). Aligned reads were then filtered for high-quality (MAPQ > 10) and properly paired (samtools flag 0x2) reads. Finally, reads arising from PCR duplicates and those aligned to the mitochondrial genome were removed using PicardTools (v 2.21.4) and samtools (v 1.10) in combination with grep, respectively.

ChIP-seq reads were aligned to the GRCm38 reference genome (Ensembl release 99) using Bowtie2 (v 2.4.1) (Langmead and Salzberg, 2012) by enabling soft clipping (--local). Where applicable, ChIP-seq data was also aligned to the *D.melanogaster* BDGP6 reference genome (Ensembl release 6) for downstream spike-in normalization (see below). Aligned reads were then filtered for high quality (MAPQ > 10). Reads arising from PCR duplicates and those

aligned to the mitochondrial genome were removed using PicardTools (v 2.21.4) and samtools (v 1.10) in combination with grep, respectively.
Using Rsamtools (v. 2.2.3), the quality of aligned reads was assessed using several parameters: (i) overall alignment rates, (ii) alignment statistics for individual chromosomes, and (iii) percentage of PCR duplicates. Additionally, fragment size distribution was assessed using ATACseqQC (v. 1.14.4).

Publicly available datasets

In addition to data sets generated for this study, we analyzed publicly available RNA-seq data from liver tissue of male mice aged 3, 12 and 18 months from the Tabula Muris Senis Consortium (Schaum *et al.*, 2020). Pre-processed data (raw count table) was retrieved from Figshare
(https://figshare.com/projects/The_murine_transcriptome_reveals_global_aging_nodes_with_organ-specific_phase_and_amplitude/65126).
Global aging genes were retrieved from a subsequent analysis of the Tabula Muris Senis data (Zhang *et al.*, 2021).
Additionally, we analyzed publicly available histone ChIP-seq data for H3, H3K27me3 and H3K4me3. Raw data originating liver tissue of 3, 12 and 29-month-old male mice was retrieved from the NCBI BioProject database (PRJNA281127) (Benayoun *et al.*, 2019) and processed as described above.

Spike-in normalization

Uniquely-mapped, non-duplicate reads were counted using samtools (v 1.10). To obtain the sample-specific normalization factors, the sample with the lowest number of reads aligned to the Drosophila reference genome was determined and divided by the reads counts for each sample. Aligned and filtered BAM files were then down-sampled proportional to the respective normalization factor.

Peak calling and annotation

ATAC-seq and ChIP-seq peaks were called on aligned and filtered BAM files using MACS2 (v. 2.2.7) (Zhang et al., 2008). Where applicable, peak calling was performed in paired-end mode (-f BAMPE). For TF and histone ChIP-seq, the corresponding input libraries and total

H3 ChIP-seq samples were used to determine the local background levels, respectively. Peaks displaying an FDR < 0.05 were considered as statistically significant.
The fraction of reads in peaks (FRiP) and fraction of reads in blacklisted regions (FRiBL) was determined using the R package ChIPQC (v. 1.21.0). Peaks falling in ENCODE blacklist regions (Amemiya et al., 2019) were subsequently removed. Peaks were annotated using the R packages ChIPseeker (v. 1.26.2) and ChIPpeakAnno (v 3.24.2). The promoter region was consistently defined as TSS +/- 200 bp.

Gene selection (“tNET genes”)

Annotation files for GRCm38 were retrieved from Ensembl (release 99). The genes included in the analysis were carefully selected to avoid contamination from transcription arising from other transcription units. Hence, only protein-coding genes were considered that are longer than 2 kb and non-overlapping within a region of 2.5 kb upstream of the TSS and downstream of the polyA site (n = 12,460). In case of multiple transcript isoforms, the most upstream annotated TSS and the most downstream annotated polyA sites were used. To ensure that only genes with sufficient coverage were included, the list was further filtered to contain only genes with RPKM > 1 (considering only uniquely aligned and filtered reads). The hereby generated gene list is referred to as tNET genes (n = 3,280).

Differential accessibility analysis with ATAC-seq

Overlapping peaks that were called in different ATAC-seq samples were resolved by defining a consensus peak set containing non-redundant peaks present in at least two biological replicates regardless of condition (i.e. age). Reads overlapping consensus peak regions were recorded using featureCounts from the R package Rsubread (v. 2.0.1). Differential accessibility analysis was performed using the R package DESeq2 (v. 1.26.0) (Love et al., 2014). Regions with an FDR < 5 % were considered to be statistically significant.

Differential expression analysis with RNA-seq

Differential expression analysis was performed using DESeq2 (v. 1.26.0) (Love *et al.*, 2014). Genes with an FDR < 5 % were considered to be statistically significant.

Recording Pol II density at nucleotide resolution

Pol II density was calculated by recording the genomic position of the 5' end of each tNET-seq read, which corresponds to the 3' end of the original nascent RNA and represents the exact genomic position of Pol II. For this, bedtools (v. 2.29.2) genomecov with the parameters -dz and -5 was used.

Differential transcription analysis with tNET-seq

Pol II density in gene bodies of tNET genes was retrieved using bedtools (v. 2.29.2) intersect and the read count matrix of genome-wide Pol II densities (see above). For this, the gene body was defined as 200 bp downstream of the TSS to 200 bp upstream of the TES. To identify differentially transcribed genes, differential analysis of Pol II density in gene bodies was performed using the R package DESeq2 (v. 1.26.0) (Love *et al.*, 2014). Here, only sense transcription was considered (i.e. tNET-seq reads sharing the same orientation as the annotation). Genes with an FDR < 5 % were considered to be statistically significant.

Trajectory analysis of nascent transcription with tNET-seq

To estimate nascent transcription trajectories during aging, we performed a likelihood-ratio test using the R package DESeq2 (v. 1.26.0) (Love *et al.*, 2014). Regions with an FDR < 5 % were considered to be statistically significant. Then, we identified common patterns using the R package DEGreport (v. 1.26.0). In brief, rlog-transformed counts of significantly differentially transcribed genes were used for calculating pair-wise gene expression among conditions using Kendall's rank. Divisive hierarchical clustering (DIANA) was then used on the gene-gene distance matrix for identifying groups of genes with similar trajectories. Z-scores of these genes were visualized.

Pol II pausing index

To quantify promoter-proximal pausing, we calculated the Pol II pausing index, which is defined as the ratio between the average Pol II density in the promoter-proximal region (defined here as TSS +/- 200 bp) over that in the gene body (defined here as TSS + 200 bp to TES - 200 bp) (Zeitlinger *et al.*, 2007) (Rahl *et al.*, 2010).
For computing the Pol II pausing index, RPM-normalized Pol II coverage files were generated using bedtools (v. 2.29.2) genomecov with the parameters -dz, -5 and -scale 1/number of

aligned reads in mio. The number of aligned reads after pre-processing was obtained using samtools view (v 1.10) with the flag -c and -F 260 to output the number of primary aligned reads only.

The RPM-normalized count matrices were intersected with annotation files for both promoter-proximal and gene body regions using bedtools (v. 2.29.2) intersect. After normalizing for region length, the pausing index was calculated by dividing the mean normalized Pol II density in the promoter-proximal region by the mean normalized Pol II density in the gene body region for each tNET gene. Here, only sense transcription was considered (i.e. tNET-seq reads sharing the same orientation as the annotation). Extreme data points were removed from the pausing analysis by retaining only genes with a pausing index $\leq$10 in all samples (n = 109 genes removed).

Pol II pausing index and promoter accessibility

To allow for a direct comparison between promoter accessibility and the Pol II pausing index, the ATAC-seq data was processed analogous to the tNET-seq data. In brief, RPM-normalized chromatin accessibility was calculated by recording the genomic position of the 5' end of each ATAC-seq read using bedtools (v. 2.29.2) genomecov as described above. We then computed chromatin accessibility in promoter-proximal regions (TSS +/- 200 bp) of tNET genes using bedtools (v. 2.29.2) intersect. After normalizing for region length, the $\log_2$ fold change in promoter accessibility in aged versus young mice was compared to the $\log_2$ fold change in pausing index in aged versus young mice.

Characterization of the nucleosome landscape

To analyze nucleosome positioning, we employed NucleoATAC (v. 0.3.4 with python v. 2.7.16) (Schep *et al.*, 2015), which relies on a model-based analysis of Tn5-tagmenation patterns to reflect the probability of nucleosome occupancy at a given locus. Importantly, this method is independent of accessibility (i.e. total coverage of ATAC-seq fragments). To achieve the sequencing depth recommended for the software, we merged ATAC-seq reads from independent biological replicates. Then, we performed nucleosome analysis using a consensus peak set of non-redundant ATAC-seq peaks present in at least two biological replicates regardless of condition (i.e. age).

For computing nucleosome occupancy scores and inter-dyad distances, we used the combined nucleosome position track (nucmap_combined.bed.gz) from our NucleoATAC analysis, which provides the most comprehensive map of both low and high-resolution

nucleosome calls. To visualize nucleosome occupancy, we used the occ.bedgraph.gz track to calculate average signal around TSSs using Deeptools (v. 3.5.1) (Ramirez et al., 2016). Finally, we calculated nucleosome fuzziness scores from NucleoATAC-derived nucpos.bed.gz files.

Identification of active enhancers in murine liver tissue

For identifying active enhancers in murine liver tissue, we combined our accessibility data (ATAC-seq) with publicly available histone modification data (H3K27ac and H3K4me3 ChIP-seq, (Benayoun *et al.*, 2019)). For each dataset, we defined a consensus peak set containing peaks present in all samples regardless of biological condition (i.e. age). Enhancers were then identified as H3K27ac peaks that (i) do not overlap H3K4me3 peaks, (ii) do not fall within TSS +/- 1 kb, and (iii) overlap accessible sites identified through ATAC-seq. This resulted in the identification of 8,855 enhancer regions active in murine liver tissue.

Functional enrichment analysis

GO databases were queried using the R package clusterProfiler (v. 3.18.1) (Yu et al., 2012). To test for over-representation, the complete gene list of the mouse database (Mm.eg.db, v. 3.12.0) served as background. After removing semantic redundancy, GO terms were ranked by adjusted p-value (Benjamini-Hochberg procedure, FDR < 0.05).

Visualization

For visualization purposes, aligned and filtered BAM files were converted to bigwig coverage tracks using Deeptools (v. 3.5.1) (Ramirez *et al.*, 2016). For ATAC-seq and tNET-seq, a bin size of 1 bp was used, while ChIP-seq reads were extended and counted in 10-bp bins. Bigwig files were normalized to 1x coverage (--normalizeUsing RPGC). For tNET-seq, only the position of the 5’ end of the sequencing read was recorded (--Offset 1).
Metagene profiles and heatmaps of mean signal enrichment were generated using Deeptools (v 3.5.1) (Ramirez *et al.*, 2016) and files normalized to 1x coverage as input. For tNET-seq, reads sharing the same or opposite orientation with the annotation were assigned as sense or antisense, respectively. Biological replicates were visualized either separately or merged prior to visualization.

Sample-by-sample correlation and principal component analyses were performed using rlog-transformed read counts via DESeq2 (v. 1.26.0) (Love *et al.*, 2014).
Single-gene sequencing tracks were visualized with Integrative Genomics Viewer (v. 2.8.0)

Reproducibility and statistical analysis

The R versions used for analyses were v. 3.6.3 and 4.0.3. Python version 3.9.0 (v. 2.7.16 for nucleoATAC) was used.
Statistical parameters and significance are reported in the figures and figure legends. Whenever possible, we used non-parametric statistical tests to avoid assuming normality of data distributions. In cases where a test for normally distributed data was used, normal distribution was first confirmed using a Shapiro-Wilk test.

7. References

Adelman, K., and Lis, J.T. (2012). Promoter-proximal pausing of RNA polymerase II: emerging roles in metazoans. Nat Rev Genet *13*, 720-731. 10.1038/nrg3293.

Amemiya, H.M., Kundaje, A., and Boyle, A.P. (2019). The ENCODE Blacklist: Identification of Problematic Regions of the Genome. Sci Rep *9*, 9354. 10.1038/s41598-019-45839-z.

Andersson, R., Gebhard, C., Miguel-Escalada, I., Hoof, I., Bornholdt, J., Boyd, M., Chen, Y., Zhao, X., Schmidl, C., Suzuki, T., et al. (2014). An atlas of active enhancers across human cell types and tissues. Nature *507*, 455-461. 10.1038/nature12787.

Aoi, Y., Smith, E.R., Shah, A.P., Rendleman, E.J., Marshall, S.A., Woodfin, A.R., Chen, F.X., Shiekhattar, R., and Shilatifard, A. (2020). NELF Regulates a Promoter-Proximal Step Distinct from RNA Pol II Pause-Release. Mol Cell *78*, 261-274 e265. 10.1016/j.molcel.2020.02.014.

Aoi, Y., Takahashi, Y.H., Shah, A.P., Iwanaszko, M., Rendleman, E.J., Khan, N.H., Cho, B.K., Goo, Y.A., Ganesan, S., Kelleher, N.L., and Shilatifard, A. (2021). SPT5 stabilization of promoter-proximal RNA polymerase II. Mol Cell. 10.1016/j.molcel.2021.08.006.

Baluapuri, A., Hofstetter, J., Dudvarski Stankovic, N., Endres, T., Bhandare, P., Vos, S.M., Adhikari, B., Schwarz, J.D., Narain, A., Vogt, M., et al. (2019). MYC Recruits SPT5 to RNA Polymerase II to Promote Processive Transcription Elongation. Mol Cell *74*, 674-687 e611. 10.1016/j.molcel.2019.02.031.

Baumgart, M., Groth, M., Priebe, S., Savino, A., Testa, G., Dix, A., Ripa, R., Spallotta, F., Gaetano, C., Ori, M., et al. (2014). RNA-seq of the aging brain in the short-lived fish N. furzeri - conserved pathways and novel genes associated with neurogenesis. Aging Cell *13*, 965-974. 10.1111/acel.12257.

Benayoun, B.A., Pollina, E.A., Singh, P.P., Mahmoudi, S., Harel, I., Casey, K.M., Dulken, B.W., Kundaje, A., and Brunet, A. (2019). Remodeling of epigenome and transcriptome landscapes with aging in mice reveals widespread induction of inflammatory responses. Genome Res *29*, 697-709. 10.1101/gr.240093.118.

Bentley, D.L., and Groudine, M. (1986). A block to elongation is largely responsible for decreased transcription of c-myc in differentiated HL60 cells. Nature *321*, 702-706. 10.1038/321702a0.

Bergmann, O., Zdunek, S., Felker, A., Salehpour, M., Alkass, K., Bernard, S., Sjostrom, S.L., Szewczykowska, M., Jackowska, T., Dos Remedios, C., et al. (2015). Dynamics of Cell Generation and Turnover in the Human Heart. Cell *161*, 1566-1575. 10.1016/j.cell.2015.05.026.

Bernecky, C., Plitzko, J.M., and Cramer, P. (2017). Structure of a transcribing RNA polymerase II-DSIF complex reveals a multidentate DNA-RNA clamp. Nat Struct Mol Biol *24*, 809-815. 10.1038/nsmb.3465.

Bintu, L., Kopaczynska, M., Hodges, C., Lubkowska, L., Kashlev, M., and Bustamante, C. (2011). The elongation rate of RNA polymerase determines the fate of transcribed nucleosomes. Nat Struct Mol Biol *18*, 1394-1399. 10.1038/nsmb.2164.

Bochkis, I.M., Przybylski, D., Chen, J., and Regev, A. (2014). Changes in nucleosome occupancy associated with metabolic alterations in aged mammalian liver. Cell Rep *9*, 996-1006. 10.1016/j.celrep.2014.09.048.

Boija, A., Mahat, D.B., Zare, A., Holmqvist, P.H., Philip, P., Meyers, D.J., Cole, P.A., Lis, J.T., Stenberg, P., and Mannervik, M. (2017). CBP Regulates Recruitment and Release of Promoter-Proximal RNA Polymerase II. Mol Cell *68*, 491-503 e495. 10.1016/j.molcel.2017.09.031.

Booth, L.N., and Brunet, A. (2016). The Aging Epigenome. Mol Cell *62*, 728-744. 10.1016/j.molcel.2016.05.013.

Borsari, B., Villegas-Miron, P., Perez-Lluch, S., Turpin, I., Laayouni, H., Segarra-Casas, A., Bertranpetit, J., Guigo, R., and Acosta, S. (2021). Enhancers with tissue-specific activity are enriched in intronic regions. Genome Res *31*, 1325-1336. 10.1101/gr.270371.120.

Bose, D.A., Donahue, G., Reinberg, D., Shiekhattar, R., Bonasio, R., and Berger, S.L. (2017). RNA Binding to CBP Stimulates Histone Acetylation and Transcription. Cell *168*, 135-149 e122. 10.1016/j.cell.2016.12.020.

Brueckner, F., and Cramer, P. (2008). Structural basis of transcription inhibition by alpha-amanitin and implications for RNA polymerase II translocation. Nat Struct Mol Biol *15*, 811-818. 10.1038/nsmb.1458.

Buenrostro, J.D., Giresi, P.G., Zaba, L.C., Chang, H.Y., and Greenleaf, W.J. (2013). Transposition of native chromatin for fast and sensitive epigenomic profiling of open chromatin, DNA-binding proteins and nucleosome position. Nat Methods *10*, 1213-1218. 10.1038/nmeth.2688.

Buratowski, S., Hahn, S., Guarente, L., and Sharp, P.A. (1989). Five intermediate complexes in transcription initiation by RNA polymerase II. Cell *56*, 549-561. 10.1016/0092-8674(89)90578-3.

Burlingame, R.W., Love, W.E., Wang, B.C., Hamlin, R., Nguyen, H.X., and Moudrianakis, E.N. (1985). Crystallographic structure of the octameric histone core of the nucleosome at a resolution of 3.3 A. Science *228*, 546-553. 10.1126/science.3983639.

Buschbeck, M., and Hake, S.B. (2017). Variants of core histones and their roles in cell fate decisions, development and cancer. Nat Rev Mol Cell Biol *18*, 299-314. 10.1038/nrm.2016.166.

Cajigas, I., Chakraborty, A., Swyter, K.R., Luo, H., Bastidas, M., Nigro, M., Morris, E.R., Chen, S., VanGompel, M.J.W., Leib, D., et al. (2018). The Evf2 Ultraconserved Enhancer lncRNA Functionally and Spatially Organizes Megabase Distant Genes in the Developing Forebrain. Mol Cell *71*, 956-972 e959. 10.1016/j.molcel.2018.07.024.

Chandra, T., Ewels, P.A., Schoenfelder, S., Furlan-Magaril, M., Wingett, S.W., Kirschner, K., Thuret, J.Y., Andrews, S., Fraser, P., and Reik, W. (2015). Global reorganization of the nuclear landscape in senescent cells. Cell Rep *10*, 471-483. 10.1016/j.celrep.2014.12.055.

Chandra, T., Kirschner, K., Thuret, J.Y., Pope, B.D., Ryba, T., Newman, S., Ahmed, K., Samarajiwa, S.A., Salama, R., Carroll, T., et al. (2012). Independence of repressive histone marks and chromatin compaction during senescent heterochromatic layer formation. Mol Cell *47*, 203-214. 10.1016/j.molcel.2012.06.010.

Chen, F.X., Smith, E.R., and Shilatifard, A. (2018). Born to run: control of transcription elongation by RNA polymerase II. Nat Rev Mol Cell Biol *19*, 464-478. 10.1038/s41580-018-0010-5.

Chen, F.X., Xie, P., Collings, C.K., Cao, K., Aoi, Y., Marshall, S.A., Rendleman, E.J., Ugarenko, M., Ozark, P.A., Zhang, A., et al. (2017). PAF1 regulation of promoter-proximal pause release via enhancer activation. Science *357*, 1294-1298. 10.1126/science.aan3269.

Chen, Y., Bravo, J.I., Son, J.M., Lee, C., and Benayoun, B.A. (2020). Remodeling of the H3 nucleosomal landscape during mouse aging. Transl Med Aging *4*, 22-31. 10.1016/j.tma.2019.12.003.

Chereji, R.V., Eriksson, P.R., Ocampo, J., Prajapati, H.K., and Clark, D.J. (2019). Accessibility of promoter DNA is not the primary determinant of chromatin-mediated gene regulation. Genome Res *29*, 1985-1995. 10.1101/gr.249326.119.

Chereji, R.V., Kan, T.W., Grudniewska, M.K., Romashchenko, A.V., Berezikov, E., Zhimulev, I.F., Guryev, V., Morozov, A.V., and Moshkin, Y.M. (2016). Genome-wide profiling of nucleosome sensitivity and chromatin accessibility in Drosophila melanogaster. Nucleic Acids Res *44*, 1036-1051. 10.1093/nar/gkv978.

Chereji, R.V., Ocampo, J., and Clark, D.J. (2017). MNase-Sensitive Complexes in Yeast: Nucleosomes and Non-histone Barriers. Mol Cell *65*, 565-577 e563. 10.1016/j.molcel.2016.12.009.

Ciccarone, F., Tagliatesta, S., Caiafa, P., and Zampieri, M. (2018). DNA methylation dynamics in aging: how far are we from understanding the mechanisms? Mech Ageing Dev *174*, 3-17. 10.1016/j.mad.2017.12.002.

Corces, M.R., Trevino, A.E., Hamilton, E.G., Greenside, P.G., Sinnott-Armstrong, N.A., Vesuna, S., Satpathy, A.T., Rubin, A.J., Montine, K.S., Wu, B., et al. (2017). An improved ATAC-seq protocol reduces background and enables interrogation of frozen tissues. Nat Methods *14*, 959-962. 10.1038/nmeth.4396.

Core, L., and Adelman, K. (2019). Promoter-proximal pausing of RNA polymerase II: a nexus of gene regulation. Genes Dev *33*, 960-982. 10.1101/gad.325142.119.

Core, L.J., Waterfall, J.J., and Lis, J.T. (2008). Nascent RNA sequencing reveals widespread pausing and divergent initiation at human promoters. Science *322*, 1845-1848. 10.1126/science.1162228.

Creyghton, M.P., Cheng, A.W., Welstead, G.G., Kooistra, T., Carey, B.W., Steine, E.J., Hanna, J., Lodato, M.A., Frampton, G.M., Sharp, P.A., et al. (2010). Histone H3K27ac separates active from poised enhancers and predicts developmental state. Proc Natl Acad Sci U S A *107*, 21931-21936. 10.1073/pnas.1016071107.

Cruickshanks, H.A., McBryan, T., Nelson, D.M., Vanderkraats, N.D., Shah, P.P., van Tuyn, J., Singh Rai, T., Brock, C., Donahue, G., Dunican, D.S., et al. (2013). Senescent cells harbour features of the cancer epigenome. Nat Cell Biol *15*, 1495-1506. 10.1038/ncb2879.

Cruz, C., Della Rosa, M., Krueger, C., Gao, Q., Horkai, D., King, M., Field, L., and Houseley, J. (2018). Tri-methylation of histone H3 lysine 4 facilitates gene expression in ageing cells. Elife *7*. 10.7554/eLife.34081.

Dang, W., Steffen, K.K., Perry, R., Dorsey, J.A., Johnson, F.B., Shilatifard, A., Kaeberlein, M., Kennedy, B.K., and Berger, S.L. (2009). Histone H4 lysine 16 acetylation regulates cellular lifespan. Nature *459*, 802-807. 10.1038/nature08085.

De Santa, F., Barozzi, I., Mietton, F., Ghisletti, S., Polletti, S., Tusi, B.K., Muller, H., Ragoussis, J., Wei, C.L., and Natoli, G. (2010). A large fraction of extragenic RNA pol II transcription sites overlap enhancers. PLoS Biol *8*, e1000384. 10.1371/journal.pbio.1000384.

Deal, R.B., Henikoff, J.G., and Henikoff, S. (2010). Genome-wide kinetics of nucleosome turnover determined by metabolic labeling of histones. Science *328*, 1161-1164. 10.1126/science.1186777.

Deng, W., Lee, J., Wang, H., Miller, J., Reik, A., Gregory, P.D., Dean, A., and Blobel, G.A. (2012). Controlling long-range genomic interactions at a native locus by targeted tethering of a looping factor. Cell *149*, 1233-1244. 10.1016/j.cell.2012.03.051.

Dobin, A., Davis, C.A., Schlesinger, F., Drenkow, J., Zaleski, C., Jha, S., Batut, P., Chaisson, M., and Gingeras, T.R. (2013). STAR: ultrafast universal RNA-seq aligner. Bioinformatics *29*, 15-21. 10.1093/bioinformatics/bts635.

Elrod, N.D., Henriques, T., Huang, K.L., Tatomer, D.C., Wilusz, J.E., Wagner, E.J., and Adelman, K. (2019). The Integrator Complex Attenuates Promoter-Proximal Transcription at Protein-Coding Genes. Mol Cell *76*, 738-752 e737. 10.1016/j.molcel.2019.10.034.

ENCODE (2021). ATAC-seq Data Standards and Processing Pipeline. https://www.encodeproject.org/atac-seq/.

Eychenne, T., Novikova, E., Barrault, M.B., Alibert, O., Boschiero, C., Peixeiro, N., Cornu, D., Redeker, V., Kuras, L., Nicolas, P., et al. (2016). Functional interplay between Mediator and TFIIB in preinitiation complex assembly in relation to promoter architecture. Genes Dev *30*, 2119-2132. 10.1101/gad.285775.116.

Farnung, L., Vos, S.M., and Cramer, P. (2018). Structure of transcribing RNA polymerase II-nucleosome complex. Nat Commun *9*, 5432. 10.1038/s41467-018-07870-y.

Feser, J., Truong, D., Das, C., Carson, J.J., Kieft, J., Harkness, T., and Tyler, J.K. (2010). Elevated histone expression promotes life span extension. Mol Cell *39*, 724-735. 10.1016/j.molcel.2010.08.015.

Fitz, J., Neumann, T., and Pavri, R. (2018). Regulation of RNA polymerase II processivity by Spt5 is restricted to a narrow window during elongation. EMBO J *37*. 10.15252/embj.201797965.

Ford, E., Nikopoulou, C., Kokkalis, A., and Thanos, D. (2014). A method for generating highly multiplexed ChIP-seq libraries. BMC Res Notes *7*, 312. 10.1186/1756-0500-7-312.

Franceschi, C., and Campisi, J. (2014). Chronic inflammation (inflammaging) and its potential contribution to age-associated diseases. J Gerontol A Biol Sci Med Sci *69 Suppl 1*, S4-9. 10.1093/gerona/glu057.

Gao, T., and Qian, J. (2020). EnhancerAtlas 2.0: an updated resource with enhancer annotation in 586 tissue/cell types across nine species. Nucleic Acids Res *48*, D58-D64. 10.1093/nar/gkz980.

Gariglio, P., Bellard, M., and Chambon, P. (1981). Clustering of RNA polymerase B molecules in the 5' moiety of the adult beta-globin gene of hen erythrocytes. Nucleic Acids Res *9*, 2589-2598. 10.1093/nar/9.11.2589.

Gaykalova, D.A., Kulaeva, O.I., Volokh, O., Shaytan, A.K., Hsieh, F.K., Kirpichnikov, M.P., Sokolova, O.S., and Studitsky, V.M. (2015). Structural analysis of nucleosomal barrier to transcription. Proc Natl Acad Sci U S A *112*, E5787-5795. 10.1073/pnas.1508371112.

Gilchrist, D.A., Dos Santos, G., Fargo, D.C., Xie, B., Gao, Y., Li, L., and Adelman, K. (2010). Pausing of RNA polymerase II disrupts DNA-specified nucleosome organization to enable precise gene regulation. Cell *143*, 540-551. 10.1016/j.cell.2010.10.004.

Gilmour, D.S., and Lis, J.T. (1986). RNA polymerase II interacts with the promoter region of the noninduced hsp70 gene in Drosophila melanogaster cells. Mol Cell Biol *6*, 3984-3989. 10.1128/mcb.6.11.3984-3989.1986.

Gorbovytska, V., Kim, S., Kuybu, F., Götze, M., Um, D., Kang, K., Pittroff, A., Schneider, L., Leitner, A., Kim, T., and Kuhn, C. (2021). Enhancer RNAs stimulate Pol II pause release by harnessing multivalent interactions to NELF. bioRxiv *2021.04.25.441328*. 10.1101/2021.04.25.441328.

Gorisch, S.M., Wachsmuth, M., Toth, K.F., Lichter, P., and Rippe, K. (2005). Histone acetylation increases chromatin accessibility. J Cell Sci *118*, 5825-5834. 10.1242/jcs.02689.

Greer, E.L., Maures, T.J., Hauswirth, A.G., Green, E.M., Leeman, D.S., Maro, G.S., Han, S., Banko, M.R., Gozani, O., and Brunet, A. (2010). Members of the H3K4 trimethylation complex regulate lifespan in a germline-dependent manner in C. elegans. Nature *466*, 383-387. 10.1038/nature09195.

Greten, F.R., and Grivennikov, S.I. (2019). Inflammation and Cancer: Triggers, Mechanisms, and Consequences. Immunity *51*, 27-41. 10.1016/j.immuni.2019.06.025.

Gutierrez, G., Millan-Zambrano, G., Medina, D.A., Jordan-Pla, A., Perez-Ortin, J.E., Penate, X., and Chavez, S. (2017). Subtracting the sequence bias from partially digested MNase-seq data reveals a general contribution of TFIIS to nucleosome positioning. Epigenetics Chromatin *10*, 58. 10.1186/s13072-017-0165-x.

Harabula, I., and Pombo, A. (2021). The dynamics of chromatin architecture in brain development and function. Curr Opin Genet Dev *67*, 84-93. 10.1016/j.gde.2020.12.008.

Heintzman, N.D., Stuart, R.K., Hon, G., Fu, Y., Ching, C.W., Hawkins, R.D., Barrera, L.O., Van Calcar, S., Qu, C., Ching, K.A., et al. (2007). Distinct and predictive chromatin signatures of transcriptional promoters and enhancers in the human genome. Nat Genet *39*, 311-318. 10.1038/ng1966.

Henriques, T., Gilchrist, D.A., Nechaev, S., Bern, M., Muse, G.W., Burkholder, A., Fargo, D.C., and Adelman, K. (2013). Stable pausing by RNA polymerase II provides an opportunity to target and integrate regulatory signals. Mol Cell *52*, 517-528. 10.1016/j.molcel.2013.10.001.

Henriques, T., Scruggs, B.S., Inouye, M.O., Muse, G.W., Williams, L.H., Burkholder, A.B., Lavender, C.A., Fargo, D.C., and Adelman, K. (2018). Widespread transcriptional pausing and elongation control at enhancers. Genes Dev *32*, 26-41. 10.1101/gad.309351.117.

Holstege, F.C., van der Vliet, P.C., and Timmers, H.T. (1996). Opening of an RNA polymerase II promoter occurs in two distinct steps and requires the basal transcription factors IIE and IIH. EMBO J *15*, 1666-1677.

Horvath, S. (2013). DNA methylation age of human tissues and cell types. Genome Biol *14*, R115. 10.1186/gb-2013-14-10-r115.

Hsieh, C.L., Fei, T., Chen, Y., Li, T., Gao, Y., Wang, X., Sun, T., Sweeney, C.J., Lee, G.S., Chen, S., et al. (2014). Enhancer RNAs participate in androgen receptor-driven looping that selectively enhances gene activation. Proc Natl Acad Sci U S A *111*, 7319-7324. 10.1073/pnas.1324151111.

Hu, S., Peng, L., Xu, C., Wang, Z., Song, A., and Chen, F.X. (2021). SPT5 stabilizes RNA polymerase II , orchestrates transcription cycles , and maintains the enhancer landscape SPT5 stabilizes RNA polymerase II , orchestrates transcription cycles , and maintains the enhancer landscape. Mol Cell. 10.1016/j.molcel.20a21.08.029.

Hu, Z., Chen, K., Xia, Z., Chavez, M., Pal, S., Seol, J.H., Chen, C.C., Li, W., and Tyler, J.K. (2014). Nucleosome loss leads to global transcriptional up-regulation and genomic instability during yeast aging. Genes Dev *28*, 396-408. 10.1101/gad.233221.113.

Huang, Z., Du, G., Huang, X., Han, L., Han, X., Xu, B., Zhang, Y., Yu, M., Qin, Y., Xia, Y., et al. (2018). The enhancer RNA lnc-SLC4A1-1 epigenetically regulates unexplained recurrent pregnancy loss (URPL) by activating CXCL8 and NF-kB pathway. EBioMedicine *38*, 162-170. 10.1016/j.ebiom.2018.11.015.

Ivanov, A., Pawlikowski, J., Manoharan, I., van Tuyn, J., Nelson, D.M., Rai, T.S., Shah, P.P., Hewitt, G., Korolchuk, V.I., Passos, J.F., et al. (2013). Lysosome-mediated processing of chromatin in senescence. J Cell Biol *202*, 129-143. 10.1083/jcb.201212110.

Jeronimo, C., Poitras, C., and Robert, F. (2019). Histone Recycling by FACT and Spt6 during Transcription Prevents the Scrambling of Histone Modifications. Cell Rep *28*, 1206-1218 e1208. 10.1016/j.celrep.2019.06.097.

Jimeno-Gonzalez, S., Ceballos-Chavez, M., and Reyes, J.C. (2015). A positioned +1 nucleosome enhances promoter-proximal pausing. Nucleic Acids Res *43*, 3068-3078. 10.1093/nar/gkv149.

Jin, C., and Felsenfeld, G. (2007). Nucleosome stability mediated by histone variants H3.3 and H2A.Z. Genes Dev *21*, 1519-1529. 10.1101/gad.1547707.

Jin, C., Li, J., Green, C.D., Yu, X., Tang, X., Han, D., Xian, B., Wang, D., Huang, X., Cao, X., et al. (2011). Histone demethylase UTX-1 regulates C. elegans life span by targeting the insulin/IGF-1 signaling pathway. Cell Metab *14*, 161-172. 10.1016/j.cmet.2011.07.001.

Kaeberlein, M., McVey, M., and Guarente, L. (1999). The SIR2/3/4 complex and SIR2 alone promote longevity in Saccharomyces cerevisiae by two different mechanisms. Genes Dev *13*, 2570-2580. 10.1101/gad.13.19.2570.

Kaikkonen, M.U., Spann, N.J., Heinz, S., Romanoski, C.E., Allison, K.A., Stender, J.D., Chun, H.B., Tough, D.F., Prinjha, R.K., Benner, C., and Glass, C.K. (2013). Remodeling of the enhancer landscape during macrophage activation is coupled to enhancer transcription. Mol Cell *51*, 310-325. 10.1016/j.molcel.2013.07.010.

Kanfi, Y., Naiman, S., Amir, G., Peshti, V., Zinman, G., Nahum, L., Bar-Joseph, Z., and Cohen, H.Y. (2012). The sirtuin SIRT6 regulates lifespan in male mice. Nature *483*, 218-221. 10.1038/nature10815.

Kao, S.Y., Calman, A.F., Luciw, P.A., and Peterlin, B.M. (1987). Anti-termination of transcription within the long terminal repeat of HIV-1 by tat gene product. Nature *330*, 489-493. 10.1038/330489a0.

Kaplan, C.D., Larsson, K.M., and Kornberg, R.D. (2008). The RNA polymerase II trigger loop functions in substrate selection and is directly targeted by alpha-amanitin. Mol Cell *30*, 547-556. 10.1016/j.molcel.2008.04.023.

Kaplan, N., Moore, I.K., Fondufe-Mittendorf, Y., Gossett, A.J., Tillo, D., Field, Y., LeProust, E.M., Hughes, T.R., Lieb, J.D., Widom, J., and Segal, E. (2009). The DNA-encoded nucleosome organization of a eukaryotic genome. Nature *458*, 362-366. 10.1038/nature07667.

Kim, T.K., Hemberg, M., Gray, J.M., Costa, A.M., Bear, D.M., Wu, J., Harmin, D.A., Laptewicz, M., Barbara-Haley, K., Kuersten, S., et al. (2010). Widespread transcription at neuronal activity-regulated enhancers. Nature *465*, 182-187. 10.1038/nature09033.

Kim, Y.W., Lee, S., Yun, J., and Kim, A. (2015). Chromatin looping and eRNA transcription precede the transcriptional activation of gene in the beta-globin locus. Biosci Rep *35*. 10.1042/BSR20140126.

Kimmel, J.C., Penland, L., Rubinstein, N.D., Hendrickson, D.G., Kelley, D.R., and Rosenthal, A.Z. (2019). Murine single-cell RNA-seq reveals cell-identity- and tissue-specific trajectories of aging. Genome Res *29*, 2088-2103. 10.1101/gr.253880.119.

King, H.W., Fursova, N.A., Blackledge, N.P., and Klose, R.J. (2018). Polycomb repressive complex 1 shapes the nucleosome landscape but not accessibility at target genes. Genome Res *28*, 1494-1507. 10.1101/gr.237180.118.

Koohy, H., Bolland, D.J., Matheson, L.S., Schoenfelder, S., Stellato, C., Dimond, A., Varnai, C., Chovanec, P., Chessa, T., Denizot, J., et al. (2018). Genome organization and chromatin analysis identify transcriptional downregulation of insulin-like growth factor signaling as a hallmark of aging in developing B cells. Genome Biol *19*, 126. 10.1186/s13059-018-1489-y.

Kreiling, J.A., Tamamori-Adachi, M., Sexton, A.N., Jeyapalan, J.C., Munoz-Najar, U., Peterson, A.L., Manivannan, J., Rogers, E.S., Pchelintsev, N.A., Adams, P.D., and Sedivy, J.M. (2011). Age-associated increase in heterochromatic marks in murine and primate tissues. Aging Cell *10*, 292-304. 10.1111/j.1474-9726.2010.00666.x.

Kubik, S., Bruzzone, M.J., Albert, B., and Shore, D. (2017). A Reply to "MNase-Sensitive Complexes in Yeast: Nucleosomes and Non-histone Barriers," by Chereji et al. Mol Cell *65*, 578-580. 10.1016/j.molcel.2017.01.010.

Kubik, S., Bruzzone, M.J., Jacquet, P., Falcone, J.L., Rougemont, J., and Shore, D. (2015). Nucleosome Stability Distinguishes Two Different Promoter Types at All Protein-Coding Genes in Yeast. Mol Cell *60*, 422-434. 10.1016/j.molcel.2015.10.002.

Kubik, S., O'Duibhir, E., de Jonge, W.J., Mattarocci, S., Albert, B., Falcone, J.L., Bruzzone, M.J., Holstege, F.C.P., and Shore, D. (2018). Sequence-Directed Action of RSC Remodeler and General Regulatory Factors Modulates +1 Nucleosome Position to Facilitate Transcription. Mol Cell *71*, 89-102 e105. 10.1016/j.molcel.2018.05.030.

Kuryan, B.G., Kim, J., Tran, N.N., Lombardo, S.R., Venkatesh, S., Workman, J.L., and Carey, M. (2012). Histone density is maintained during transcription mediated by the chromatin remodeler RSC and histone chaperone NAP1 in vitro. Proc Natl Acad Sci U S A *109*, 1931-1936. 10.1073/pnas.1109994109.

Kwak, Y.T., Guo, J., Prajapati, S., Park, K.J., Surabhi, R.M., Miller, B., Gehrig, P., and Gaynor, R.B. (2003). Methylation of SPT5 regulates its interaction with RNA polymerase II and transcriptional elongation properties. Mol Cell *11*, 1055-1066. 10.1016/s1097-2765(03)00101-1.

Landt, S.G., Marinov, G.K., Kundaje, A., Kheradpour, P., Pauli, F., Batzoglou, S., Bernstein, B.E., Bickel, P., Brown, J.B., Cayting, P., et al. (2012). ChIP-seq guidelines and practices of the ENCODE and modENCODE consortia. Genome Res *22*, 1813-1831. 10.1101/gr.136184.111.

Langmead, B., and Salzberg, S.L. (2012). Fast gapped-read alignment with Bowtie 2. Nat Methods *9*, 357-359. 10.1038/nmeth.1923.

Larke, M.S.C., Schwessinger, R., Nojima, T., Telenius, J., Beagrie, R.A., Downes, D.J., Oudelaar, A.M., Truch, J., Graham, B., Bender, M.A., et al. (2021). Enhancers predominantly regulate gene expression during differentiation via transcription initiation. Mol Cell *81*, 983-997 e987. 10.1016/j.molcel.2021.01.002.

Lee, C., Li, X., Hechmer, A., Eisen, M., Biggin, M.D., Venters, B.J., Jiang, C., Li, J., Pugh, B.F., and Gilmour, D.S. (2008). NELF and GAGA factor are linked to promoter-proximal pausing at many genes in Drosophila. Mol Cell Biol *28*, 3290-3300. 10.1128/MCB.02224-07.

Lee, C.K., Shibata, Y., Rao, B., Strahl, B.D., and Lieb, J.D. (2004). Evidence for nucleosome depletion at active regulatory regions genome-wide. Nat Genet *36*, 900-905. 10.1038/ng1400.

Lee, S.H., Lee, J.H., Lee, H.Y., and Min, K.J. (2019). Sirtuin signaling in cellular senescence and aging. BMB Rep *52*, 24-34.

Li, J., and Gilmour, D.S. (2013). Distinct mechanisms of transcriptional pausing orchestrated by GAGA factor and M1BP, a novel transcription factor. EMBO J *32*, 1829-1841. 10.1038/emboj.2013.111.

Li, W., Notani, D., Ma, Q., Tanasa, B., Nunez, E., Chen, A.Y., Merkurjev, D., Zhang, J., Ohgi, K., Song, X., et al. (2013). Functional roles of enhancer RNAs for oestrogen-dependent transcriptional activation. Nature *498*, 516-520. 10.1038/nature12210.

Liu, L., Cheung, T.H., Charville, G.W., Hurgo, B.M., Leavitt, T., Shih, J., Brunet, A., and Rando, T.A. (2013). Chromatin modifications as determinants of muscle stem cell quiescence and chronological aging. Cell Rep *4*, 189-204. 10.1016/j.celrep.2013.05.043.

Lopez-Otin, C., Blasco, M.A., Partridge, L., Serrano, M., and Kroemer, G. (2013). The hallmarks of aging. Cell *153*, 1194-1217. 10.1016/j.cell.2013.05.039.

Love, M.I., Huber, W., and Anders, S. (2014). Moderated estimation of fold change and dispersion for RNA-seq data with DESeq2. Genome Biol *15*, 550. 10.1186/s13059-014-0550-8.

Lu, R.J., Taylor, S., Contrepois, K., Kim, M., Bravo, J.I., Ellenberger, M., Sampathkumar, N.K., and Benayoun, B.A. (2021). Multi-omic profiling of primary mouse neutrophils predicts a

pattern of sex- and age-related functional regulation. Nature Aging *1*, 715-733. 10.1038/s43587-021-00086-8.

Luger, K., Mader, A.W., Richmond, R.K., Sargent, D.F., and Richmond, T.J. (1997). Crystal structure of the nucleosome core particle at 2.8 A resolution. Nature *389*, 251-260. 10.1038/38444.

Marshall, N.F., and Price, D.H. (1995). Purification of P-TEFb, a transcription factor required for the transition into productive elongation. J Biol Chem *270*, 12335-12338. 10.1074/jbc.270.21.12335.

Maures, T.J., Greer, E.L., Hauswirth, A.G., and Brunet, A. (2011). The H3K27 demethylase UTX-1 regulates C. elegans lifespan in a germline-independent, insulin-dependent manner. Aging Cell *10*, 980-990. 10.1111/j.1474-9726.2011.00738.x.

Mayer, A., and Churchman, L.S. (2016). Genome-wide profiling of RNA polymerase transcription at nucleotide resolution in human cells with native elongating transcript sequencing. Nat Protoc *11*, 813-833. 10.1038/nprot.2016.047.

Mayer, A., di Iulio, J., Maleri, S., Eser, U., Vierstra, J., Reynolds, A., Sandstrom, R., Stamatoyannopoulos, J.A., and Churchman, L.S. (2015). Native elongating transcript sequencing reveals human transcriptional activity at nucleotide resolution. Cell *161*, 541-554. 10.1016/j.cell.2015.03.010.

McCauley, B.S., Sun, L., Yu, R., Lee, M., Liu, H., Leeman, D.S., Huang, Y., Webb, A.E., and Dang, W. (2021). Altered chromatin states drive cryptic transcription in aging mammalian stem cells. Nat Aging *1*, 684-697. 10.1038/s43587-021-00091-x.

Michishita, E., McCord, R.A., Berber, E., Kioi, M., Padilla-Nash, H., Damian, M., Cheung, P., Kusumoto, R., Kawahara, T.L., Barrett, J.C., et al. (2008). SIRT6 is a histone H3 lysine 9 deacetylase that modulates telomeric chromatin. Nature *452*, 492-496. 10.1038/nature06736.

Mieczkowski, J., Cook, A., Bowman, S.K., Mueller, B., Alver, B.H., Kundu, S., Deaton, A.M., Urban, J.A., Larschan, E., Park, P.J., et al. (2016). MNase titration reveals differences between nucleosome occupancy and chromatin accessibility. Nat Commun *7*, 11485. 10.1038/ncomms11485.

Missra, A., and Gilmour, D.S. (2010). Interactions between DSIF (DRB sensitivity inducing factor), NELF (negative elongation factor), and the Drosophila RNA polymerase II transcription elongation complex. Proc Natl Acad Sci U S A *107*, 11301-11306. 10.1073/pnas.1000681107.

Moskowitz, D.M., Zhang, D.W., Hu, B., Le Saux, S., Yanes, R.E., Ye, Z., Buenrostro, J.D., Weyand, C.M., Greenleaf, W.J., and Goronzy, J.J. (2017). Epigenomics of human CD8 T cell differentiation and aging. Sci Immunol *2*. 10.1126/sciimmunol.aag0192.

Mostoslavsky, R., Chua, K.F., Lombard, D.B., Pang, W.W., Fischer, M.R., Gellon, L., Liu, P., Mostoslavsky, G., Franco, S., Murphy, M.M., et al. (2006). Genomic instability and aging-like phenotype in the absence of mammalian SIRT6. Cell *124*, 315-329. 10.1016/j.cell.2005.11.044.

Mousavi, K., Zare, H., Dell'orso, S., Grontved, L., Gutierrez-Cruz, G., Derfoul, A., Hager, G.L., and Sartorelli, V. (2013). eRNAs promote transcription by establishing chromatin accessibility at defined genomic loci. Mol Cell *51*, 606-617. 10.1016/j.molcel.2013.07.022.

Mueller, B., Mieczkowski, J., Kundu, S., Wang, P., Sadreyev, R., Tolstorukov, M.Y., and Kingston, R.E. (2017). Widespread changes in nucleosome accessibility without changes in nucleosome occupancy during a rapid transcriptional induction. Genes Dev *31*, 451-462. 10.1101/gad.293118.116.

Muhlbacher, W., Sainsbury, S., Hemann, M., Hantsche, M., Neyer, S., Herzog, F., and Cramer, P. (2014). Conserved architecture of the core RNA polymerase II initiation complex. Nat Commun *5*, 4310. 10.1038/ncomms5310.

Muse, G.W., Gilchrist, D.A., Nechaev, S., Shah, R., Parker, J.S., Grissom, S.F., Zeitlinger, J., and Adelman, K. (2007). RNA polymerase is poised for activation across the genome. Nat Genet *39*, 1507-1511. 10.1038/ng.2007.21.

Mylonas, C., and Tessarz, P. (2018). Transcriptional repression by FACT is linked to regulation of chromatin accessibility at the promoter of ES cells. Life Sci Alliance *1*, e201800085. 10.26508/lsa.201800085.

Nagarajavel, V., Iben, J.R., Howard, B.H., Maraia, R.J., and Clark, D.J. (2013). Global 'bootprinting' reveals the elastic architecture of the yeast TFIIIB-TFIIIC transcription complex in vivo. Nucleic Acids Res *41*, 8135-8143. 10.1093/nar/gkt611.

Nogales, E., Patel, A.B., and Louder, R.K. (2017). Towards a mechanistic understanding of core promoter recognition from cryo-EM studies of human TFIID. Curr Opin Struct Biol *47*, 60-66. 10.1016/j.sbi.2017.05.015.

O'Sullivan, R.J., Kubicek, S., Schreiber, S.L., and Karlseder, J. (2010). Reduced histone biosynthesis and chromatin changes arising from a damage signal at telomeres. Nat Struct Mol Biol *17*, 1218-1225. 10.1038/nsmb.1897.

Pavri, R., Zhu, B., Li, G., Trojer, P., Mandal, S., Shilatifard, A., and Reinberg, D. (2006). Histone H2B monoubiquitination functions cooperatively with FACT to regulate elongation by RNA polymerase II. Cell *125*, 703-717. 10.1016/j.cell.2006.04.029.

Pezone, A., Zuchegna, C., Tramontano, A., Romano, A., Russo, G., de Rosa, M., Vinciguerra, M., Porcellini, A., Gottesman, M.E., and Avvedimento, E.V. (2019). RNA Stabilizes Transcription-Dependent Chromatin Loops Induced By Nuclear Hormones. Sci Rep *9*, 3925. 10.1038/s41598-019-40123-6.

Price, D.H. (2018). Transient pausing by RNA polymerase II. Proc Natl Acad Sci U S A *115*, 4810-4812. 10.1073/pnas.1805129115.

Pu, M., Ni, Z., Wang, M., Wang, X., Wood, J.G., Helfand, S.L., Yu, H., and Lee, S.S. (2015). Trimethylation of Lys36 on H3 restricts gene expression change during aging and impacts life span. Genes Dev *29*, 718-731. 10.1101/gad.254144.114.

Qiu, Y., and Gilmour, D.S. (2017). Identification of Regions in the Spt5 Subunit of DRB Sensitivity-inducing Factor (DSIF) That Are Involved in Promoter-proximal Pausing. J Biol Chem *292*, 5555-5570. 10.1074/jbc.M116.760751.

Rahl, P.B., Lin, C.Y., Seila, A.C., Flynn, R.A., McCuine, S., Burge, C.B., Sharp, P.A., and Young, R.A. (2010). c-Myc regulates transcriptional pause release. Cell *141*, 432-445. 10.1016/j.cell.2010.03.030.

Rahnamoun, H., Lee, J., Sun, Z., Lu, H., Ramsey, K.M., Komives, E.A., and Lauberth, S.M. (2018). RNAs interact with BRD4 to promote enhanced chromatin engagement and transcription activation. Nat Struct Mol Biol *25*, 687-697. 10.1038/s41594-018-0102-0.

Ramachandran, S., Ahmad, K., and Henikoff, S. (2017). Transcription and Remodeling Produce Asymmetrically Unwrapped Nucleosomal Intermediates. Mol Cell *68*, 1038-1053 e1034. 10.1016/j.molcel.2017.11.015.

Ramirez, F., Ryan, D.P., Gruning, B., Bhardwaj, V., Kilpert, F., Richter, A.S., Heyne, S., Dundar, F., and Manke, T. (2016). deepTools2: a next generation web server for deep-sequencing data analysis. Nucleic Acids Res *44*, W160-165. 10.1093/nar/gkw257.

Rhee, H.S., Bataille, A.R., Zhang, L., and Pugh, B.F. (2014). Subnucleosomal structures and nucleosome asymmetry across a genome. Cell *159*, 1377-1388. 10.1016/j.cell.2014.10.054.

Roeder, R.G., and Rutter, W.J. (1969). Multiple forms of DNA-dependent RNA polymerase in eukaryotic organisms. Nature *224*, 234-237. 10.1038/224234a0.

Rougvie, A.E., and Lis, J.T. (1988). The RNA polymerase II molecule at the 5' end of the uninduced hsp70 gene of D. melanogaster is transcriptionally engaged. Cell *54*, 795-804. 10.1016/s0092-8674(88)91087-2.

Sartorelli, V., and Lauberth, S.M. (2020). Enhancer RNAs are an important regulatory layer of the epigenome. Nat Struct Mol Biol *27*, 521-528. 10.1038/s41594-020-0446-0.

Schaukowitch, K., Joo, J.Y., Liu, X., Watts, J.K., Martinez, C., and Kim, T.K. (2014). Enhancer RNA facilitates NELF release from immediate early genes. Mol Cell *56*, 29-42. 10.1016/j.molcel.2014.08.023.

Schaum, N., Lehallier, B., Hahn, O., Palovics, R., Hosseinzadeh, S., Lee, S.E., Sit, R., Lee, D.P., Losada, P.M., Zardeneta, M.E., et al. (2020). Ageing hallmarks exhibit organ-specific temporal signatures. Nature *583*, 596-602. 10.1038/s41586-020-2499-y.

Schep, A.N., Buenrostro, J.D., Denny, S.K., Schwartz, K., Sherlock, G., and Greenleaf, W.J. (2015). Structured nucleosome fingerprints enable high-resolution mapping of chromatin architecture within regulatory regions. Genome Res *25*, 1757-1770. 10.1101/gr.192294.115.

Schwabish, M.A., and Struhl, K. (2004). Evidence for eviction and rapid deposition of histones upon transcriptional elongation by RNA polymerase II. Mol Cell Biol *24*, 10111-10117. 10.1128/MCB.24.23.10111-10117.2004.

Scruggs, B.S., Gilchrist, D.A., Nechaev, S., Muse, G.W., Burkholder, A., Fargo, D.C., and Adelman, K. (2015). Bidirectional Transcription Arises from Two Distinct Hubs of Transcription Factor Binding and Active Chromatin. Mol Cell *58*, 1101-1112. 10.1016/j.molcel.2015.04.006.

Sen, P., Dang, W., Donahue, G., Dai, J., Dorsey, J., Cao, X., Liu, W., Cao, K., Perry, R., Lee, J.Y., et al. (2015). H3K36 methylation promotes longevity by enhancing transcriptional fidelity. Genes Dev *29*, 1362-1376. 10.1101/gad.263707.115.

Sen, P., Shah, P.P., Nativio, R., and Berger, S.L. (2016). Epigenetic Mechanisms of Longevity and Aging. Cell *166*, 822-839. 10.1016/j.cell.2016.07.050.

Shao, W., and Zeitlinger, J. (2017). Paused RNA polymerase II inhibits new transcriptional initiation. Nat Genet *49*, 1045-1051. 10.1038/ng.3867.

Shetty, A., Kallgren, S.P., Demel, C., Maier, K.C., Spatt, D., Alver, B.H., Cramer, P., Park, P.J., and Winston, F. (2017). Spt5 Plays Vital Roles in the Control of Sense and Antisense Transcription Elongation. Mol Cell *66*, 77-88 e75. 10.1016/j.molcel.2017.02.023.

Shii, L., Song, L., Maurer, K., Zhang, Z., and Sullivan, K.E. (2017). SERPINB2 is regulated by dynamic interactions with pause-release proteins and enhancer RNAs. Mol Immunol *88*, 20-31. 10.1016/j.molimm.2017.05.005.

Siebold, A.P., Banerjee, R., Tie, F., Kiss, D.L., Moskowitz, J., and Harte, P.J. (2010). Polycomb Repressive Complex 2 and Trithorax modulate Drosophila longevity and stress resistance. Proc Natl Acad Sci U S A *107*, 169-174. 10.1073/pnas.0907739107.

Sigova, A.A., Abraham, B.J., Ji, X., Molinie, B., Hannett, N.M., Guo, Y.E., Jangi, M., Giallourakis, C.C., Sharp, P.A., and Young, R.A. (2015). Transcription factor trapping by RNA in gene regulatory elements. Science *350*, 978-981. 10.1126/science.aad3346.

Skaar, J.R., Ferris, A.L., Wu, X., Saraf, A., Khanna, K.K., Florens, L., Washburn, M.P., Hughes, S.H., and Pagano, M. (2015). The Integrator complex controls the termination of transcription at diverse classes of gene targets. Cell Res *25*, 288-305. 10.1038/cr.2015.19.

Soutourina, J. (2018). Transcription regulation by the Mediator complex. Nat Rev Mol Cell Biol *19*, 262-274. 10.1038/nrm.2017.115.

Spurlock, C.F., 3rd, Shaginurova, G., Tossberg, J.T., Hester, J.D., Chapman, N., Guo, Y., Crooke, P.S., 3rd, and Aune, T.M. (2017). Profiles of Long Noncoding RNAs in Human Naive and Memory T Cells. J Immunol *199*, 547-558. 10.4049/jimmunol.1700232.

Stefanelli, G., Azam, A.B., Walters, B.J., Brimble, M.A., Gettens, C.P., Bouchard-Cannon, P., Cheng, H.M., Davidoff, A.M., Narkaj, K., Day, J.J., et al. (2018). Learning and Age-Related Changes in Genome-wide H2A.Z Binding in the Mouse Hippocampus. Cell Rep *22*, 1124-1131. 10.1016/j.celrep.2018.01.020.

Stegeman, R., and Weake, V.M. (2017). Transcriptional Signatures of Aging. J Mol Biol *429*, 2427-2437. 10.1016/j.jmb.2017.06.019.

Sun, D., Luo, M., Jeong, M., Rodriguez, B., Xia, Z., Hannah, R., Wang, H., Le, T., Faull, K.F., Chen, R., et al. (2014). Epigenomic profiling of young and aged HSCs reveals concerted changes during aging that reinforce self-renewal. Cell Stem Cell *14*, 673-688. 10.1016/j.stem.2014.03.002.

Tabula Muris, C. (2020). A single-cell transcriptomic atlas characterizes ageing tissues in the mouse. Nature *583*, 590-595. 10.1038/s41586-020-2496-1.

Tettey, T.T., Gao, X., Shao, W., Li, H., Story, B.A., Chitsazan, A.D., Glaser, R.L., Goode, Z.H., Seidel, C.W., Conaway, R.C., et al. (2019). A Role for FACT in RNA Polymerase II Promoter-Proximal Pausing. Cell Rep *27*, 3770-3779 e3777. 10.1016/j.celrep.2019.05.099.

Teves, S.S., and Henikoff, S. (2014). Transcription-generated torsional stress destabilizes nucleosomes. Nat Struct Mol Biol *21*, 88-94. 10.1038/nsmb.2723.

Tsai, P.F., Dell'Orso, S., Rodriguez, J., Vivanco, K.O., Ko, K.D., Jiang, K., Juan, A.H., Sarshad, A.A., Vian, L., Tran, M., et al. (2018). A Muscle-Specific Enhancer RNA Mediates Cohesin Recruitment and Regulates Transcription In trans. Mol Cell *71*, 129-141 e128. 10.1016/j.molcel.2018.06.008.

Tvardovskiy, A., Schwammle, V., Kempf, S.J., Rogowska-Wrzesinska, A., and Jensen, O.N. (2017). Accumulation of histone variant H3.3 with age is associated with profound changes in the histone methylation landscape. Nucleic Acids Res *45*, 9272-9289. 10.1093/nar/gkx696.

Ucar, D., Marquez, E.J., Chung, C.H., Marches, R., Rossi, R.J., Uyar, A., Wu, T.C., George, J., Stitzel, M.L., Palucka, A.K., et al. (2017). The chromatin accessibility signature of human immune aging stems from CD8(+) T cells. J Exp Med *214*, 3123-3144. 10.1084/jem.20170416.

Venkatesh, S., and Workman, J.L. (2015). Histone exchange, chromatin structure and the regulation of transcription. Nat Rev Mol Cell Biol *16*, 178-189. 10.1038/nrm3941.

Villeponteau, B. (1997). The heterochromatin loss model of aging. Exp Gerontol *32*, 383-394. 10.1016/s0531-5565(96)00155-6.

Voong, L.N., Xi, L., Sebeson, A.C., Xiong, B., Wang, J.P., and Wang, X. (2016). Insights into Nucleosome Organization in Mouse Embryonic Stem Cells through Chemical Mapping. Cell *167*, 1555-1570 e1515. 10.1016/j.cell.2016.10.049.

Vos, S.M., Farnung, L., Boehning, M., Wigge, C., Linden, A., Urlaub, H., and Cramer, P. (2018a). Structure of activated transcription complex Pol II-DSIF-PAF-SPT6. Nature *560*, 607-612. 10.1038/s41586-018-0440-4.

Vos, S.M., Farnung, L., Linden, A., Urlaub, H., and Cramer, P. (2020). Structure of complete Pol II-DSIF-PAF-SPT6 transcription complex reveals RTF1 allosteric activation. Nat Struct Mol Biol *27*, 668-677. 10.1038/s41594-020-0437-1.

Vos, S.M., Farnung, L., Urlaub, H., and Cramer, P. (2018b). Structure of paused transcription complex Pol II-DSIF-NELF. Nature *560*, 601-606. 10.1038/s41586-018-0442-2.

Wada, T., Takagi, T., Yamaguchi, Y., Ferdous, A., Imai, T., Hirose, S., Sugimoto, S., Yano, K., Hartzog, G.A., Winston, F., et al. (1998). DSIF, a novel transcription elongation factor that regulates RNA polymerase II processivity, is composed of human Spt4 and Spt5 homologs. Genes Dev *12*, 343-356. 10.1101/gad.12.3.343.

Weber, C.M., Ramachandran, S., and Henikoff, S. (2014). Nucleosomes are context-specific, H2A.Z-modulated barriers to RNA polymerase. Mol Cell *53*, 819-830. 10.1016/j.molcel.2014.02.014.

Wong, K.H., Jin, Y., and Struhl, K. (2014). TFIIH phosphorylation of the Pol II CTD stimulates mediator dissociation from the preinitiation complex and promoter escape. Mol Cell *54*, 601-612. 10.1016/j.molcel.2014.03.024.

Wu, C.H., Yamaguchi, Y., Benjamin, L.R., Horvat-Gordon, M., Washinsky, J., Enerly, E., Larsson, J., Lambertsson, A., Handa, H., and Gilmour, D. (2003). NELF and DSIF cause promoter proximal pausing on the hsp70 promoter in Drosophila. Genes Dev *17*, 1402-1414. 10.1101/gad.1091403.

Yamamoto, J., Hagiwara, Y., Chiba, K., Isobe, T., Narita, T., Handa, H., and Yamaguchi, Y. (2014). DSIF and NELF interact with Integrator to specify the correct post-transcriptional fate of snRNA genes. Nat Commun *5*, 4263. 10.1038/ncomms5263.

Yu, G., Wang, L.G., Han, Y., and He, Q.Y. (2012). clusterProfiler: an R package for comparing biological themes among gene clusters. OMICS *16*, 284-287. 10.1089/omi.2011.0118.

Zeitlinger, J., Stark, A., Kellis, M., Hong, J.W., Nechaev, S., Adelman, K., Levine, M., and Young, R.A. (2007). RNA polymerase stalling at developmental control genes in the Drosophila melanogaster embryo. Nat Genet *39*, 1512-1516. 10.1038/ng.2007.26.

Zentner, G.E., and Henikoff, S. (2013). Regulation of nucleosome dynamics by histone modifications. Nat Struct Mol Biol *20*, 259-266. 10.1038/nsmb.2470.

Zhang, M.J., Pisco, A.O., Darmanis, S., and Zou, J. (2021). Mouse aging cell atlas analysis reveals global and cell type-specific aging signatures. Elife *10*. 10.7554/eLife.62293.

Zhang, Y., Liu, T., Meyer, C.A., Eeckhoute, J., Johnson, D.S., Bernstein, B.E., Nusbaum, C., Myers, R.M., Brown, M., Li, W., and Liu, X.S. (2008). Model-based analysis of ChIP-Seq (MACS). Genome Biol *9*, R137. 10.1186/gb-2008-9-9-r137.

Zhao, Y., Wang, L., Ren, S., Wang, L., Blackburn, P.R., McNulty, M.S., Gao, X., Qiao, M., Vessella, R.L., Kohli, M., et al. (2016). Activation of P-TEFb by Androgen Receptor-Regulated Enhancer RNAs in Castration-Resistant Prostate Cancer. Cell Rep *15*, 599-610. 10.1016/j.celrep.2016.03.038.

Zhou, V.W., Goren, A., and Bernstein, B.E. (2011). Charting histone modifications and the functional organization of mammalian genomes. Nat Rev Genet *12*, 7-18. 10.1038/nrg2905.

Zumer, K., Maier, K.C., Farnung, L., Jaeger, M.G., Rus, P., Winter, G., and Cramer, P. (2021). Two distinct mechanisms of RNA polymerase II elongation stimulation in vivo. Mol Cell *81*, 3096-3109 e3098. 10.1016/j.molcel.2021.05.028.

8. Eidesstattliche Erklärung

Erklärung zur Dissertation

gemäß der Promotionsordnung vom 12. März 2020

Hiermit versichere ich an Eides statt, dass ich die vorliegende Dissertation selbstständig und ohne die Benutzung anderer als der angegebenen Hilfsmittel und Literatur angefertigt habe. Alle Stellen, die wörtlich oder sinngemäß aus veröffentlichten und nicht veröffentlichten Werken dem Wortlaut oder dem Sinn nach entnommen wurden, sind als solche kenntlich gemacht. Ich versichere an Eides statt, dass diese Dissertation noch keiner anderen Fakultät oder Universität zur Prüfung vorgelegen hat; dass sie - abgesehen von unten angegebenen Teilpublikationen und eingebundenen Artikeln und Manuskripten - noch nicht veröffentlicht worden ist sowie, dass ich eine Veröffentlichung der Dissertation vor Abschluss der Promotion nicht ohne Genehmigung des Promotionsausschusses vornehmen werde. Die Bestimmungen dieser Ordnung sind mir bekannt. Darüber hinaus erkläre ich hiermit, dass ich die Ordnung zur Sicherung guter wissenschaftlicher Praxis und zum Umgang mit wissenschaftlichem Fehlverhalten der Universität zu Köln gelesen und sie bei der Durchführung der Dissertation zugrundeliegenden Arbeiten und der schriftlich verfassten Dissertation beachtet habe und verpflichte mich hiermit, die dort genannten Vorgaben bei allen wissenschaftlichen Tätigkeiten zu beachten und umzusetzen. Ich versichere, dass die eingereichte elektronische Fassung der eingereichten Druckfassung vollständig entspricht

Teilpublikationen:

Bozukova, M., Nikopoulou, C., Kleinenkuhnen, N., Grbavac, D., Goetsch, K., Tessarz, P. (2022). Aging is associated with increased chromatin accessibility and reduced polymerase pausing in liver. Mol Syst Biol. 18: e11002. 10.15252/msb.202211002.

Datum, Name und Unterschrift